Anexo:

Close approaches of the trans-Neptunian objects to Pluto have left observable signatures on their orbital distribution

THE ASTRONOMICAL JOURNAL, 119:953–969, 2000 February

CLOSE APPROACHES OF TRANS-NEPTUNIAN OBJECTS TO PLUTO HAVE LEFT OBSERVABLE SIGNATURES ON THEIR ORBITAL DISTRIBUTION

D. NESVORNÝ AND F. ROIG
Institute of Astronomy and Geophysics, São Paulo University, Av. Miguel Stefano 4200, 04301 São Paulo, Brazil; david@orion.iagusp.usp.br
AND
S. FERRAZ-MELLO
National Observatory, Rio de Janeiro, Brazil
Received 1999 July 21; accepted 1999 November 3

ABSTRACT

It is shown that in addition to four outer planets (Jupiter to Neptune) Pluto should be also taken into account in studies of the orbital dynamics in the trans-Neptunian region. Pluto's effect is particularly large on the orbits in the 2:3 Neptune mean motion resonance. The trajectories found stable over the age of the solar system when only the gravitational effect of four outer planets is considered are often destabilized there in the effect of close Pluto approaches. We estimate that many dynamically primordial bodies moving initially with low to moderate amplitudes in the 2:3 Neptune resonance (semimajor axis 39.45 AU) have been removed from their respective, otherwise stable, locations, when their resonant amplitudes increased in the course of close encounters with Pluto. At large libration amplitude, the orbits became exposed to chaotic changes, and objects were ejected from the 2:3 resonance to Neptune-crossing trajectories. The process of the resonant amplitude excitation was especially efficient for orbits with moderate and large inclinations ($i > 8°$), where more than 50% of the population has been removed in 4×10^9 yr. We estimate that the remaining part of the primordial resonant population at these inclinations should have had its resonant amplitude excited to about 80°. The effect of Pluto on low-inclination orbits is smaller. We have examined the distribution of 33 objects observed on the 2:3 resonant orbits (Plutinos) and found that there could actually exist indications of the above mechanism. The resonant amplitudes of Plutinos are unusually high for $0.15 < e < 0.3$ when compared with randomly generated distribution, and, also, there is only one object (1997 QJ4) on an orbit similar to that of Pluto. In fact, a certain gap may be noticed in the distribution of Plutinos at Pluto's inclination and eccentricity, which, if confirmed by future observations, may be the consequence of Pluto's sweeping effect.

Key words: celestial mechanics, stellar dynamics — Kuiper belt, Oort cloud

1. INTRODUCTION

The existence of a belt of small bodies beyond Neptune has been independently suggested by Edgeworth (1949) and Kuiper (1951)—hereafter we refer to the belt as the Edgeworth-Kuiper belt (EKB). Fernández (1980) proposed that such a belt could be a reservoir of short-period comets whose low inclinations, as was later shown by Duncan, Quinn, & Tremaine (1988), cannot be explained assuming their origin in the isotropic Oort cloud. The first direct observational evidence of the EKB was the discovery of 1992 QB1 by Jewitt & Luu (1993).

The first results on the stability of the trans-Neptunian region were obtained by Levison & Duncan (1993) and Holman & Wisdom (1993) by means of numeric simulations. In later work, Duncan, Levison, & Budd (1995) numerically computed the evolution of four outer planets (Jupiter to Neptune) and 1300 test particles (with initial inclination equal to 1°) over 4×10^9 yr and mapped the stability of orbits in the 32–50 AU semimajor axis interval with the following findings: (1) the stable orbits with perihelion distances q less than 35 AU were found to be associated with the first-order mean motion resonances with Neptune, where the phase-protection mechanism (as in the case of Pluto in the 2:3 resonance; Cohen & Hubbard 1965) and the absence of overlapping inner secular resonances (Morbidelli, Thomas, & Moons 1995) both contribute to orbit preservation; and (2) the unstable orbits with $q > 35$ AU were found to be related to the perihelion and node secular resonances (mainly ν_8, ν_{17}, and ν_{18} located at $40 < a < 42$ AU, according to Knežević et al. 1991).

There are currently registered about 120 EKB objects in the Minor Planet Center catalog.[1] Their orbital distribution is well correlated with the results of Duncan et al. (1995) in the sense that most of them have orbits characterized by long-term stability. Thirty-three of the known EKB objects and Pluto happen to fall in the region of the 2:3 mean motion resonance with Neptune at the semimajor axis $a = 39.45$ AU.

Pluto has a peculiar orbit. It is highly eccentric ($e = 0.25$) with large inclination ($i = 17°$). Its resonant argument $\sigma = 2\lambda_N - 3\lambda + \varpi$, where λ_N is the mean Neptune longitude and λ and ϖ are the mean and perihelion longitudes of Pluto, librates around 180° with $\sim 80°$ amplitude (A_σ) and $\sim 20{,}000$ yr period. In addition to the 2:3 commensurability, Pluto's argument of perihelion (ω) librates about 90° (Williams & Benson 1971). Its amplitude A_ω is approximately 23°, and its period is about 3.8×10^6 yr. The libration of ω is a consequence of Pluto being located in Kozai's secular resonance (Kozai 1962). In addition to the 2:3 and Kozai resonances, there is a commensurability of 1:1 between libration of ω and the circulation of the angle $\Omega - \Omega_N$ (Milani, Nobili, & Carpino 1989), where Ω and Ω_N are the nodal longitudes of Pluto and Neptune, respectively.

[1] At: http://cfa-www.harvard.edu/cfa/ps/lists/TNOs.html.

The long-term stability of Pluto's orbit has been confirmed by Kinoshita & Nakai (1984) and Sussman & Wisdom (1988). It turned out that in spite of the positive maximum Lyapunov exponent ($\sim 10^{-7}$ yr^{-1}) its orbit is stable over the age of the solar system.

The 33 Plutinos sharing the 2:3 resonance with Pluto have eccentricities in the range from 0.08 to 0.35 and inclinations smaller than 20° (only one known resonant object—1996 KY1—has the inclination of about 30°). The orbits of most Plutinos are expected to be stable on long time intervals. The orbital elements of Plutinos are, however, usually not determined with sufficient precision to make the long-term simulations of their orbits meaningful.

Concerning the global stability of the 2:3 Neptune resonance, the works based on averaged circular (Morbidelli et al. 1995) and circular (Malhotra 1996) models indicated that the central resonant space is stable over the age of the solar system, but both were missing an important ingredient—the complete perturbations of outer planets other than Neptune—in order to provide sufficiently reliable stability boundaries. The stability boundaries were as a function of the resonant amplitudes A_σ and A_ω computed for the orbits with Pluto-like inclinations by Levison & Stern (1995). They have found that the orbits starting with $A_\sigma < 50°$ are stable and the orbits with $A_\sigma > 120°$ are unstable over 4×10^9 yr. For intermediate resonant amplitudes A_σ, usually a small amplitude of ω-libration is needed for stabilization of the orbit. The stability of the 2:3 resonance was further investigated by Morbidelli (1997) with the emphasis on a number of escaping objects and their relation to the short-period comets.

We analyze the orbital distribution of Plutinos in § 2 and show that there can actually exist some uncommon features that could have resulted only with difficulty from the secular evolution under the perturbations of four outer planets. Although this observational evidence is based on a small number of known 2:3 resonant objects and their frequently inaccurate orbital elements, we believe that it is worth of examining the possible causes.

Although a number of primordial and collision mechanisms that complicate the matter could had been involved, some of the features of Plutino orbital distribution may be a result of the interaction with Pluto in the past 4×10^9 yr. We conjecture that the small Pluto mass (the total mass of the Pluto-Charon binary is estimated to be $1/1.35 \times 10^8$ of the Sun's mass) can be compensated both by the length of the time interval in question and by the similarity of the orbital parameters of Pluto and Plutinos (§ 3). In order to test this hypothesis we have performed several numeric simulations considering Pluto as the fifth massive body in addition to the four outer planets. The setup and results of our main experiment, in which we place the test particles in the 2:3 and Kozai resonances, are explained in § 3. A simple classification of orbits based on their interaction with Pluto is given in § 4.

We analyze the effect of Pluto on 2:3 resonant orbits and show that it results in an important excitation of the resonant amplitude A_σ. Pluto's effect is especially important on the inclined orbits, and we show that a large number of objects have been removed from the 2:3 resonance in consequence of the excitation of A_σ beyond the stability limits. The surviving part of the 2:3 resonant population should have had the mean A_σ of about 80° (§ 5). The dependence of these results on the eccentricity is studied in § 6.

As this paper was being revised, we learned about the work of Yu & Tremaine (1999). The authors develop a simplified model of Plutino dynamics under the joint effect of Neptune and Pluto. As this work is closely related to the subject of our paper, we will comment on the results of Yu & Tremaine whenever we find it appropriate.

2. PLUTO AND THE ORBITAL DISTRIBUTION OF PLUTINOS

There are Pluto and 33 trans-Neptunian objects (Plutinos) located in the 2:3 mean motion resonance with Neptune that are registered in the Minor Planet Center Catalog at the time of writing of this paper (1999 March). Thirteen (39%) of the Plutinos are objects observed in more than one opposition with the orbital elements determined with good precision. The other 20 Plutinos (61%) are single-opposition objects for which it was assumed in order to allow for the computation of the orbital elements that they were observed at perihelion (i.e., assumed mean anomaly $M = 0$). The mean anomaly computed for the multi-opposition Plutinos is generally nonzero (but usually within $\pm 40°$—with the exception of 1996 RR20, which is far from perihelion with $M = 112°.3$). This means, as the distribution of Plutinos in the mean anomaly should be the same for single- and multiopposition objects, that the orbital elements of single-opposition Plutinos are generally imprecise, and for some of them the determination of the orbital elements may be wrong as the assumption on their present M can turn out to be invalid. The sizes of known Plutinos range between 50 and 300 km in diameter and are fairly uncertain owing to unknown albedos.

Jewitt, Luu, & Trujillo (1998) estimate on the basis of the current discovery rate that there are between 7000 and 14,000 objects larger than 100 km in diameter in the 2:3 Neptune mean motion resonance. The observations are providing new EKB objects with an increasing discovery rate, and it is clear that there will be soon available an extensive database of Plutinos' orbital and physical characteristics. The question is, however, whether there is something that can be inferred on the orbital distribution of Plutinos at present, from the orbital properties of the 33 observed bodies. We will show in the following that the population of 2:3 resonant objects really differs in several aspects from what would be expected to be an initially random distribution shaped by the long-term gravitation effect of four outer planets.

We have started our analysis by advancing Pluto and 33 Plutinos to the same date: 1999 January 22 (MJD 2,451,200.5). First, the four outer planets (Jupiter to Neptune) were propagated to the catalog date of each object, and then, each object was individually integrated as a massless particle with four outer planets up to the destination time. Even if the integration time was at most only 1960 days, this procedure cannot be substituted by a shift of M according to the mean motion because the short periodic perturbations of Jupiter cause variations of semimajor axis of some Plutinos as large as 0.08 AU with a periodicity of 11.8 yr.

In order to suppress the short periodic variations of Plutino trajectories and retain the resonant and secular variations, we have applied the digital filter of Quinn, Tremaine, & Duncan (1991) in the following experiment. In this experiment, Pluto and Plutinos were integrated with four outer planets for 10^7 yr using the symmetric multistep inte-

grator of Quinlan & Tremaine (1990). The time step for the integration was less than 0.1% of the orbital period so that no spurious instabilities should have been created by low-order resonances between the time step and the dynamical frequencies. Tests have also been done changing the time step. The filtering procedure was sequentially applied 3 times on the integration output increasing the sampling interval at each step from the initial 2 to the final 200 yr. All periods shorter than 1200 yr were suppressed by a factor of 10^5 in amplitude, and the periods larger than 2000 yr were retained in the filtered signal. The filtered elements were $a \exp \imath\sigma$, $e \exp \imath\varpi$, and $i \exp \imath\Omega$ (i is the orbital inclination and $\imath = \sqrt{-1}$).

The purpose of this integration was in numeric determination of the orbital elements that would characterize the properties of the resonant and secular motions of Plutinos. The instantaneous (osculating) orbital elements a, e, and i on 1999 January 22 were not suitable for this purpose because of the following reason. Assume a Plutino to have the same amplitudes A_σ, A_ω and the same "mean" inclination as Pluto, but a phase difference in σ and ω from Pluto's resonant angle and perihelion argument on 1999 January 22. Plutino's instantaneous orbital elements a, e, and i on 1999 January 22 were then considerably different from the orbital elements of Pluto on this date, in spite of both orbits having the same resonant and secular evolutions.

There are a number of different approaches to this problem. In the case of a motion in the mean motion resonance, the *proper* orbital elements can be defined as the values of instantaneous a, e, and i at intersections of a trajectory with some phase space manifold (Nesvorný & Ferraz-Mello 1997), as the maximum or minimum values of instantaneous a, e, and i over a long time interval (Morbidelli 1997) or as amplitudes of resonant angles computed as the maximum excursion of the resonant angles from the libration centers (Levison & Stern 1995).

Following the approach of Nesvorný & Ferraz-Mello (1997) the natural choice of the manifold is $\sigma = 180°$ and $\omega = 90°$ as these values correspond to the libration centers of the 2:3 and Kozai resonances. The behavior of trajectories in the 2:3 and Kozai resonances (Morbidelli et al. 1995) is such that the instantaneous orbital elements a and e oscillate with σ while the e and i change is correlated with ω. When $\sigma = 180°$ both a and e are at the extrema of their resonant oscillations, a having the value corresponding to the maximum excursion from the center of the 2:3 resonance. When $\omega = 90°$, i is also at the maximum excursion from the center of the Kozai resonance.

In Figure 1 we show the semimajor axis, eccentricity, and inclination of Pluto and Plutinos at the first intersection of their trajectories with $\sigma = 180°$ and $\omega = 90°$ (or $\omega = 270°$—the value corresponding to the second libration center of the Kozai resonance; see Morbidelli et al. 1995—if there is no intersection with $\omega = 90°$ within 10^7 yr). The open circles in Figure 1 are the multiopposition Plutinos, the dots are the single-opposition objects, and the circled plus sign marks the position of Pluto. As we consider the first intersection, there is one symbol per object in Figure 1. Owing to the symmetry of the 2:3 resonance with respect to the libration centers, the next intersection of an orbit with $\sigma = 180°$ would be symmetrically placed in the opposite half-plane of the 2:3 resonance in Figure 1*a*. A similar symmetry holds for the orbits with the libration of ω for which the next intersection of $\omega = 90°$ would occur in the opposite half-plane of the Kozai resonance in Figure 1*b*.

The bold lines in Figure 1*a* are the separatrices and libration centers of the 2:3 resonance. Other lines in the figure show the positions of the secular resonances (ν_8, ν_{18}, and Kozai resonance denoted by ω) and the secondary resonance 5:1, where the resonant frequency is a factor of 5 larger than the frequency of the perihelion longitude. Other secondary resonances, where the integer ratios of the resonant and perihelion frequencies are smaller, are located at lower eccentricities under the dotted line of the 5:1 secondary resonance. The bold lines in Figure 1*b* are separatrices of the Kozai resonance, and the dotted line shows the libration centers of ω. Locations of the resonances and their separatrices have been computed by Thomas (1998) following the seminumeric method of Henrard (1990).

Most of the Plutinos are located at $39.25 < a < 39.7$ AU and $0.08 < e < 0.35$ in Figure 1*a*. In this central area of the 2:3 resonance, the orbits are stable over the age of the solar system (Morbidelli 1997). This is in agreement with the presumption that the observed Plutinos are long-lived 2:3

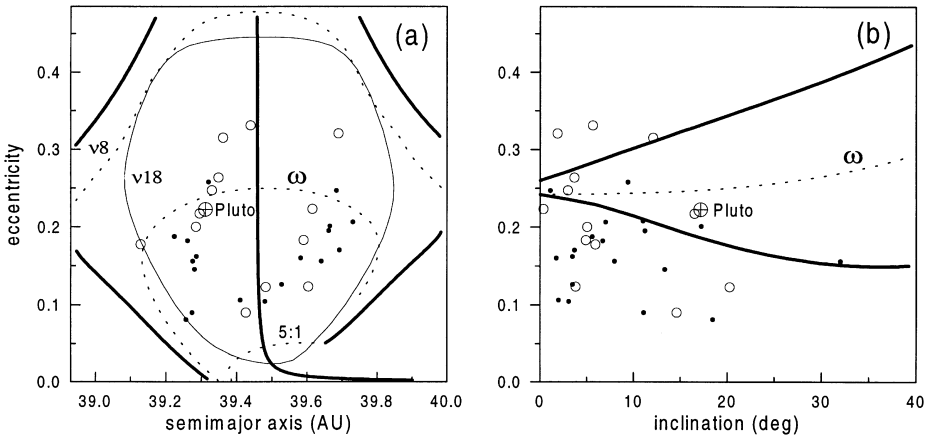

FIG. 1.—Orbital elements of Pluto (*circled plus sign*), multiopposition (*open circles*) and single-opposition Plutinos (*dots*) at the time when their $\sigma = 180°$ and $\omega = 90°$. The separatrices and libration centers of the 2:3 Neptune resonance are shown by bold lines in (*a*). The other lines denote the locations of the secular (ω-libration in Kozai resonance, ν_8 and ν_{18}) and secondary resonances (5:1). The bold lines in (*b*) show the location of the separatrices of the Kozai resonance; the dashed line denoted by ω is its libration center. In (*a*), note the lack of objects near the libration centers of the 2:3 resonance ($a = 39.45$ AU) for $0.15 < e < 0.3$. In (*b*), there are few objects with orbital characteristics similar to Pluto's orbit, and among them only 1997 QJ4 has a well-determined and stable orbit.

resonant objects. The resonant orbits are unstable outside the above semimajor axis limits owing to the simultaneous presence of the ν_{18}, ν_8, and Kozai secular resonances at large libration amplitudes $A_\sigma > 130°$. According to Nesvorný & Roig (2000) there exists another instability under the line of the 5:1 secondary resonance owing to the overlap of the 2:1, 3:1, and 4:1 secondary resonances. No resonant objects are known with $e < 0.08$ (Fig. 1*a*). The orbits with eccentricities larger than 0.35 are also unstable. There are the overlapping ν_8 and ν_{18} secular resonances that destabilize motion there, and moreover, the orbital perihelion is already close to the orbit of Uranus ($a_U = 19.22$ AU) for these eccentricities. No resonant objects with $e > 0.35$ have been discovered until now.

What is surprising concerning the Plutino distribution in Figure 1*a* is that in the interval $0.15 < e < 0.3$ there are no objects close to the libration centers (bold vertical line at $a = 39.5$ AU). The orbits of such objects would be characterized by small resonant amplitudes $A_\sigma < 50°$ and the stability over the age of the solar system according to the results of Morbidelli (1997).

The inclinations of most Plutinos are lower than 10°, and there is only one object, 1996 RR20 (observed in one opposition), with an inclination larger than 20° (Fig. 1*b*). According to Nesvorný & Roig (2000) the resonant orbits with large inclinations $20° < i < 30°$ are stable over the age of the solar system. There is, however, a large observational incompleteness at these inclinations, which means that how fast the real density of Plutinos decreases with inclination can only be shown by future observational searches specifically directed to this subject.

The resonant object, the symbol for which overlaps the symbol of Pluto in both panels of Figure 1, is the multiopposition Plutino 1997 QJ4. Its orbital evolution is apparently very similar to that of Pluto. The absolute magnitude of this body is 7.5, which means a diameter between 85 km (for 0.25 albedo) and 200 km (for 0.05 albedo). The other object that appears close to Pluto's position in Figure 1*b* is 1998 WW24 (the point at $e = 0.2$ and $i = 17°$). This is a single-opposition object with large resonant amplitude $A_\sigma = 115°$ and is actually not in the Kozai resonance (the separatrices of the Kozai resonance in Fig. 1*b* were computed for $A_\sigma = 0$). Another object, the single-opposition 1997 TX8 with $i \sim 10°$ close to the libration center of the Kozai resonance (dotted line in Fig. 1*b*), was found unstable in our integration owing to its initially large A_σ. The fact that this objects escapes from the 2:3 resonance in less than 10^7 yr suggests that the orbital elements of this body were not correctly determined from the observation (otherwise the flux of escaping bodies from the 2:3 resonance would be unacceptably large).

Consequently, among 33 known Plutinos, only 1997 QJ4 has an orbit with characteristics similar to Pluto's orbit. In fact, a gap may be noted around Pluto in the distribution of Plutinos in Figure 1*b*. This gap roughly coincides with the area of Kozai resonance for $i > 5°$ and is probably somewhat larger for the inclinations comparable with Pluto's inclination ($i = 17°$). Levison & Stern (1995) computed that with four outer planets, the orbits at low resonant amplitudes A_σ and A_ω are stable, so that, if real, this gap could be attributed to Pluto's own gravitational effect rather than to the effect of four outer planets.

We show in Table 1 the amplitudes A_σ and A_ω of four Plutinos (and Pluto) found with stable ω-libration in 10^7 yr.

TABLE 1

PLUTO AND FOUR PLUTINOS WITH STABLE LIBRATIONS OF THE ARGUMENT OF PERIHELION IN 10^7 YR

Object (1)	$\langle i \rangle$ (deg) (2)	A_σ (deg) (3)	A_ω (deg) (4)
Pluto	15.9	84.9	22.9
1997 QJ4	15.8	98.5	27.6
1998 UU43	11.6	80.6	47.9
1994 TB	16.7	55.2	73.1
1996 SZ4	6.4	90.6	79.2

NOTE.—Col. (2): Mean inclination. Col. (3): Amplitude of σ (A_σ). Col. (4): Amplitude of ω.

All but 1998 UU43 have the center of ω-libration at 90°. 1998 UU43 oscillates about 270°.

The perihelion argument of Pluto and 1997 QJ4 oscillates around 90° with low amplitude, while ω of 1998 UU43 oscillates about 270°. 1994 TB and 1996 SZ4 are very close to separatrices (their ω starts to alternate between libration and circulation soon after 10^7 yr). All these Plutinos were observed in more than one opposition.

The maximum eccentricity versus A_σ, the latter being computed as the maximum excursion of σ from 180° on a 10^7 yr interval, is shown in Figure 2*a*. Triangles are the Plutinos with inclination smaller than 10°, and plus signs are the Plutinos with $i > 10°$. Two single-opposition objects (1996 KY1 and 1997 TX8) escaped from the 2:3 resonance on this interval, probably owing to the imprecise determination of their initial orbital elements from few observations. Two multiopposition objects (1993 RO and 1996 RR20) have A_σ larger than 120° (128° and 124°, respectively) and are probably unstable in the long run.

For $0.15 < e < 0.3$ in Figure 2*a* there is only one Plutino with $A_\sigma < 70°$ (no such object for $0.2 < e < 0.3$), which is, as already noted in Figure 1*a*, a rather surprising underpopulation of stable low-A_σ orbits. To assure that the lack of resonant objects at low A_σ is significant, we have performed the following test.

The initial orbital elements of 150 test particles have been randomly chosen with $39 < a < 39.8$ AU, $0.1 < e < 0.35$, and $i < 20°$, and A_σ was determined for them by the same procedure as for the real resonant objects (i.e., as the maximum excursion from 180° in 10^7 yr). In Figure 2*b*, we compare the cumulative number of real ($0.15 < e < 0.3$) and randomly generated bodies versus A_σ. The number of test particles was rescaled to 20 objects with $A_\sigma < 130°$, which is the cumulative number of real Plutinos at this limit.

The cumulative number of test particles linearly increases with the libration amplitude with a characteristic slope. We have verified that this slope is a robust feature of random distributions of orbits in the 2:3 resonance. The real distribution considerably differs from the random one. While for $A_\sigma < 70°$ the cumulative number of real Plutinos increases less steeply with increasing A_σ, for $A_\sigma > 70°$, the slope is steeper than the random one owing e to a relative surplus of real Plutinos with these libration amplitudes. In contrast to the distribution of real Plutinos, the random distribution indicates that about 25% of objects (five of 20 objects) with $A_\sigma < 130°$ should have $A_\sigma < 70°$.

Even if the final conclusion is due to a fairly uncertain small sample of known resonant objects, we believe that there actually exist indications in the observed orbital

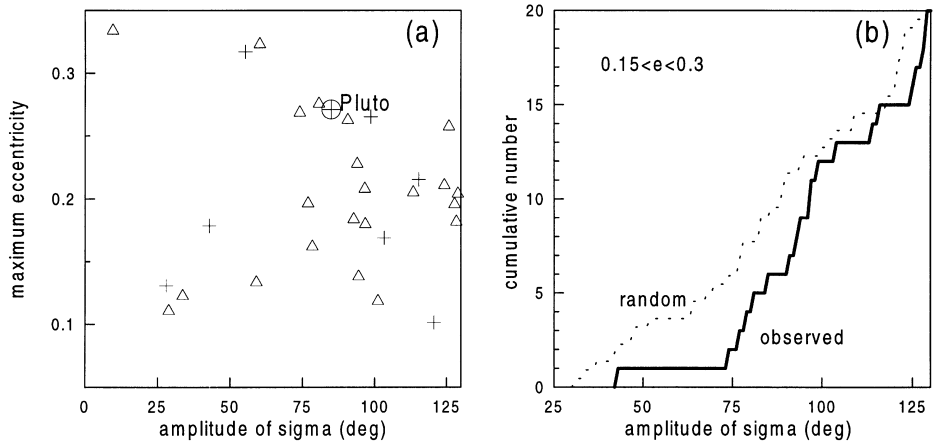

FIG. 2.—(*a*) Maximum eccentricity vs. the amplitude of the resonant angle A_σ, both being computed on 10^7 yr interval. Plutinos with $i < 10°$ are denoted by triangles and those with $i > 10°$ by plus signs. Pluto's orbit is marked by a circled plus sign. There is an apparent lack of objects with $A_\sigma < 70°$ for $0.15 < e < 0.3$. In (*b*) we compare the cumulative number of known Plutionos having the resonant amplitude smaller than A_σ (*solid line*) with a randomly generated distribution (*dotted line*). For $A_\sigma < 70°$ there are 5 times fewer Plutinos than the randomly generated bodies. This difference is interesting as it cannot be explained by the dynamical clearing of low-A_σ region under the effect of four outer planets.

distribution of Plutinos that suggest that their resonant amplitudes were excited to values larger than 70° in the past. This fact, together with the lack of the 2:3 resonant objects with orbits similar to Pluto in the Kozai resonance, are the two observational results we would like to address in the following.

3. PLUTO'S INTERACTION WITH THE 2:3 RESONANT OBJECTS

We assume that Pluto's orbit is ancient. Although how its elongated and inclined orbit were formed is a debatable question (Malhotra 1993; Levison, Stern, & Duncan 1999; Petit, Morbidelli, & Valsecchi 1999), it is agreed that this happened at least some 4×10^9 yr ago. We also assume that the gravitational pull of this planet was in the past 4×10^9 yr proportional to the mass of $1/1.35 \times 10^8$ fraction of the Sun's mass, which is about the best estimate of the total mass of Pluto-Charon binary based on *Hubble Space Telescope* (*HST*) observations (see Stern & Yelle 1999). The question is then what are the possible consequences of Pluto's sweeping through the 2:3 resonant region.

A question related to this subject was addressed by Levison & Stern (1995). They studied the early dynamical evolution of the Pluto-Charon binary under the effect of other 2:3 resonant bodies and suggested the possible origin of Pluto's uncommon heliocentric orbit. Here, however, we are more interested in the opposite case of Pluto's interaction with the resonant objects as a possible effect of Pluto's gravitational scattering on the 2:3 resonant population.

According to Morbidelli (1997), the low-amplitude 2:3 resonant orbits are stable for $0.1 < e < 0.3$ in the model with four outer planets (Jupiter to Neptune) in the sense that they do not leave the resonance in 4×10^9 yr. Even if the range of stable resonant orbits spans a slightly larger interval in eccentricities, for $0.1 < e < 0.3$ and $A_\sigma < 50$, the orbits are not only stable against ejection by four outer planets, but moreover, as their proper elements are almost constant on 4×10^9 yr (Morbidelli 1997), the orbits do not chaotically evolve with time. This moderate eccentricity and low-A_σ resonant region is an ideal testing place for Pluto's hypothetical effect. The secular changes of proper orbital elements in the model with the gravitational perturbations of four outer planets and Pluto must be attributed to Pluto's own effect there.

Moreover, according to the previous section there exists a strong motivation for a study of Pluto's effect on the resonant low-A_σ orbits, which is the lack of objects observed on such orbits. There should exist a mechanism other than the gravitational effect of the outer planets that removed the resonant objects from there, presumably by an excitation of their resonant amplitudes. Assuming that the lack of low-A_σ Plutinos is not dynamically primordial, we suspect two possible mechanisms of long-term excitation of A_σ: either the excitation in mutual encounters and collisions between the 2:3 resonant objects or the effect of close encounters between the resonant objects and Pluto. As the excitation happens mainly in $0.15 < e < 0.3$, we rather think the second mechanism to be at work. Indeed, Pluto has a mean eccentricity of 0.253, which places it close to the center of the above interval.

In order to estimate the possible long-term effect of Pluto on other 2:3 resonant objects, we have performed several simulations of different sets of initial conditions for time intervals ranging from 10^9 to 4×10^9 yr. Pluto has been included in these simulations as the fifth perturber (in addition to four outer planets) with a mass of $\mu = 1/1.35 \times 10^8$ solar masses. This mass is so low that the only expected effect on other resonant bodies presumably happens only when an object approaches Pluto at a small distance. The important quantity is then the radius of the Hill sphere of Pluto, which is given by

$$R_H = a_P \left(\frac{\mu}{3}\right)^{1/3} = 0.054 \text{ AU} , \quad (1)$$

where a_P is the semimajor axis of Pluto. This radius is equal to the distance from Pluto to the collinear stationary point in the circular model of the Sun–Pluto–test particle system. The sphere with Hill radius roughly delimits the space where Pluto's effect on the third body is important. In our case, the corresponding diameter of the zone of Pluto's influence is roughly the size of the central 2:3 resonant region, where $A_\sigma < 50°$.

The result of an encounter with Pluto depends on the mutual velocity V between the object and Pluto. According to Öpik (1976), a trajectory passing close to Pluto bends with an angle γ (deflection angle) between the asymptotes of the incoming and outgoing trajectories given by

$$\tan \frac{\gamma}{2} = (2\pi)^2 \frac{\mu}{bV^2}, \quad (2)$$

where $\mu = 1/1.35 \times 10^8$ and b is the minimum distance between the *unperturbed* path of the particle and Pluto, i.e., the path that would be followed if the planet had no mass (V is given in AU yr^{-1} and b in AU). The deflection angle scales as $1/V^2$. If V is small, then the deflection angle is large, and so is the expected change of the orbital elements. Owing to the large inclination of Pluto (17°), there exists a relatively large lower threshold of the mutual encounter velocity with the *low*-inclination orbits dictated by the mutual inclination of the intersecting trajectories. The changes of orbital elements and in particular of A_σ are expected to be small in this case. Indeed, our preliminary numerical simulation[2] of Pluto's effect on the low-inclination resonant orbits showed that the excitation of A_σ for the initially low-A_σ orbits is relatively small and accounts for at most 20° change of A_σ of individual test particles on 5×10^8 yr.

We have also noticed a weak dependence of $A_\sigma(t = 10^9$ yr) on the initial eccentricity in this experiment. The resonant amplitude excitation for the orbits initially with $e < 0.15$ was a factor 1.5 larger than the change of A_σ for $e > 0.2$. Yu & Tremaine (1999) suggested that Pluto's effect should be small for low-eccentricity orbits owing to larger mutual velocity between the test particles and Pluto. Indeed, the mutual velocity of two bodies at the encounter can be inferred from simple geometric considerations. Suppose Pluto's orbit is fixed with $a_P = 39.45$ AU, $e_P = 0.25$, $i_P = 17°$, and $\omega_P = 90°$. An object on a planar orbit of the same semimajor axis encounters Pluto at either the descending or ascending node of Pluto's orbit. Choosing the line between the Sun and Pluto's ascending node to be the reference axis, we have as a necessary condition for the intersection of both trajectories that object's perihelion longitude ϖ is

$$\varpi = \pm \frac{1}{e} \frac{e^2 - e_P^2}{1 - e_P^2}, \quad (3)$$

with the sign plus for the intersection in Pluto's ascending node and the sign minus for the intersection in Pluto's descending node. No intersection exist when $e < e_P^2 = 0.0625$ because in this case the perihelion distance of the object is larger than the heliocentric distances of Pluto's nodes. The mutual encounter velocity V is a function of the eccentricity e. For $e = 0.1$ the velocity is $V = 0.35$ AU yr^{-1}, and for $e = 0.25$ it is $V = 0.3$ AU yr^{-1}. The minimum encounter velocity of 0.3 AU yr^{-1} when both orbits have the same eccentricity is due to their mutual inclination.

Apart from the velocity the other important factor is the frequency of mutual encounters between test particles and Pluto. We have registered 5900 encounters within R_H to Pluto in 10^9 yr in our experiment. The number of encounters per particle varies with eccentricity. While at $e = 0.1$ it is about 40, at $e = 0.25$ it is only 20. This is probably the reason that the excitation of the libration amplitude is moderately larger at $e = 0.1$ than at $e = 0.25$ in our experiment, contrary to what would be expected from the encounter velocities. The cumulative deflection angle expected at $e = 0.1$ should be, according to the above results, a factor $40 \times 0.3^2/20 \times 0.35^2 = 1.5$ larger than the cumulative deflection angle at $e = 0.25$. The larger cumulative deflection angle translates to a larger excitation of A_σ at $e = 0.1$ observed in our experiment.

It may be inferred from the above considerations that the orbits with nonzero inclinations should suffer larger changes at encounters with Pluto's than the orbits with zero inclination. On the other hand, however, even an orbit with $i = i_P$ can have a large encounter velocity at the intersection if the nodes of both orbits are not aligned. There is an additional factor to be noted at this point.

Assuming the orbit of the Plutino with $a = 39.45$ AU and $e \sim e_P$, then this orbit is resonant both in the 2:3 mean motion resonance with Neptune and in the Kozai secular resonance. Assuming additionally that both libration amplitudes A_σ and A_ω of the Plutino orbit are zero and in an idealized case in which Pluto's orbit also has $A_\sigma^P = A_\omega^P = 0$, then $\sigma = \sigma_P = 180°$ and $\omega = \omega_P = 90°$, where the index P denotes the quantities of Pluto. These conditions result in the following relation between the mean longitudes and nodes:

$$\lambda - \lambda_P = \tfrac{1}{3}(\Omega - \Omega_P). \quad (4)$$

This means, as the arguments of perihelion are fixed at 90°, that the orbits intersect each other only if $\Omega = \Omega_P$. At such an instant, the close encounters become possible also as $\lambda = \lambda_P$. We therefore conclude that the only necessary (and sufficient) condition to be satisfied in order to have close and low-velocity encounters between Pluto and the resonant objects in the Kozai resonance is the alignment of nodes. The encounters at nodes are characterized by a velocity V proportional to $|\Delta i| = |i - i_P|$. Equation (4) will hold true on average even if the libration amplitudes are nonzero.

The motion of the nodal line of Pluto's orbit is retrograde and has a period of 3.8×10^6 yr. A Plutino on an orbit similar to that of Pluto naturally has a similar nodal period. Consequently, the differential rotation of nodes between Pluto and Plutino orbits will be very slow. The numeric integration shows that if there is no interaction between Pluto and Plutino, then $\Omega - \Omega_P$ has a period larger than 10^8 yr if $|\Delta i|$ is of order of a few degrees. The rotation of $\Omega - \Omega_P$ is prograde when $\Delta i > 0$ and retrograde when $\Delta i < 0$. Consequently, the period of many close encounters between Pluto and Plutino when $\Omega - \Omega_P = 0$ will be followed by a long period of time in which the Plutino orbit is protected from close encounters as $\lambda - \lambda_P \neq 0$.

4. ESCAPES FROM INITIALLY LOW-A_σ AND LOW-A_ω ORBITS

We have simulated the evolution of 101 test particles that were initially placed on the ω-librating orbits in the 2:3 mean motion resonance with Neptune. The initial elements were chosen so that both the libration amplitudes of ω and of σ of the particles were initially close to zero. The semi-

[2] The setup of this preliminary simulation was the same as for the experiment described in detail in the next section. Initially, $i = 2°$ for all test particles.

major axis and eccentricity were set to 39.2 AU and 0.25, and inclination was varied between 5° and 25° with a 0°.2 step. The initial angles were chosen so that $\sigma = 180°$, $\omega = 90°$, and $\Omega - \Omega_N = 0$, where Ω_N is the node longitude of Neptune.

As determined prior to the simulation, the initial osculating semimajor axis of 39.2 AU corresponds to the initial mean semimajor axis of 39.45 AU (the value of the 2:3 libration centers—Fig. 1*a*) for the configuration of planets on 1998 January 1 (MJD 2,450,814.5). The difference between the initial orbital and mean values of semimajor axes is a consequence of the short period variations of test particles orbits. Hence, the test particles were chosen within a small interval around the stable libration center of the 2:3 Neptune resonance with a corresponding libration amplitude of the resonant angle $\sigma = 2\lambda_N - 3\lambda + \varpi$ smaller than 20°.

The initial conditions of four major planets and Pluto were taken on 1998 January 1 (MJD 2,450,814.5) with respect to the invariant plane and equinox at epoch JD 2000. The orbits of five planets (massive bodies) and test particles (massless bodies) were followed forward in time using the swift_rmvs3 integrator of Levison & Duncan (1994) and a 1 yr time step. The total integration time span was 4×10^9 yr. The orbital elements were computed each 10^5 yr. For each test particle in the run we calculated the resonant amplitude A_σ at time t as the maximum excursion of σ from 180° in the interval $(t, t + 10^7)$ yr and the amplitude A_ω as the maximum excursion of ω from 90° on the same interval. We also calculated the proper eccentricities and inclinations at time t as the averages of orbital elements in the interval $(t, t + 10^7)$ yr (Morbidelli & Nesvorný 1999, their eq. [1]).

During the simulation we have monitored A_σ, and if this happened to exceed 175°, we classified the corresponding case as the escape from the 2:3 resonance. The test particle may then, however, survive a relatively long interval ($< 10^8$ yr) chaotically diffusing on the resonant border before the first important encounter with Neptune. The subsequent evolution under the effect of close encounters with giant planets was faster, and in an interval typically of order of 10^7 yr, the test particle was deactivated from the run. The test particle was deactivated when its orbit satisfied one of our stopping criteria: either too close an encounter to some giant planet or to the Sun, or ejection to a heliocentric distance larger than 100 AU. The behavior of bodies escaping from EKB and becoming giant-planet crossers was studied in detail by Levison & Duncan (1997).

Many test particles had escaped from the 2:3 Neptune resonance in the run (Fig. 3). The cumulative number of escapes is roughly a linear function of time with about 13 escapes per 10^9 yr. This resulted in total of 51 escaping particles in 4×10^9 yr.

While both the proper eccentricity and the proper inclination remained basically the same in the initial stages of evolution, the resonant amplitude A_σ of test particles increased. The final resonant amplitude $A_\sigma(4 \times 10^9$ yr) is shown in Figure 4*a* (*shadow bars*) versus the initial proper inclination (both computed on 10^7 yr interval). For the test particles escaping from the resonance before 4×10^9 yr, the quantity shown is 180°. The solid line denotes the initial resonant amplitude $A_\sigma(0)$. The horizontal line at $A_\sigma = 130°$ is given for reference, since for $A_\sigma > 130°$, the orbits are chaotic and diffuse quickly toward the borders of the 2:3

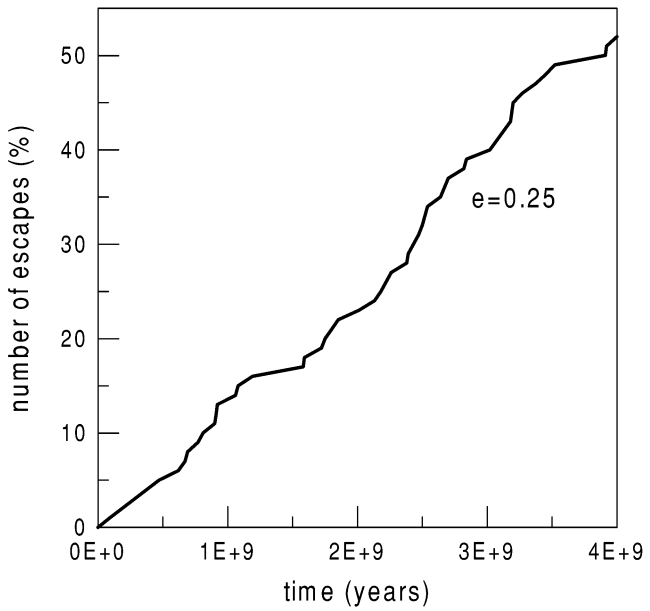

FIG. 3.—Cumulative number of escaping test particles from the 2:3 resonance. More than 50% of initially low-A_σ and low-A_ω ($e = 0.25$) test particles left the resonance before $t = 4 \times 10^9$ yr when their resonant amplitude increased beyond the instability limit.

resonance under the effect of four outer planets (Morbidelli 1997).

There is no strong dependence of $A_\sigma(4 \times 10^9$ yr) on the initial proper inclination observed in Figure 4*a*. Note, however, that the excitation of A_σ was moderately smaller

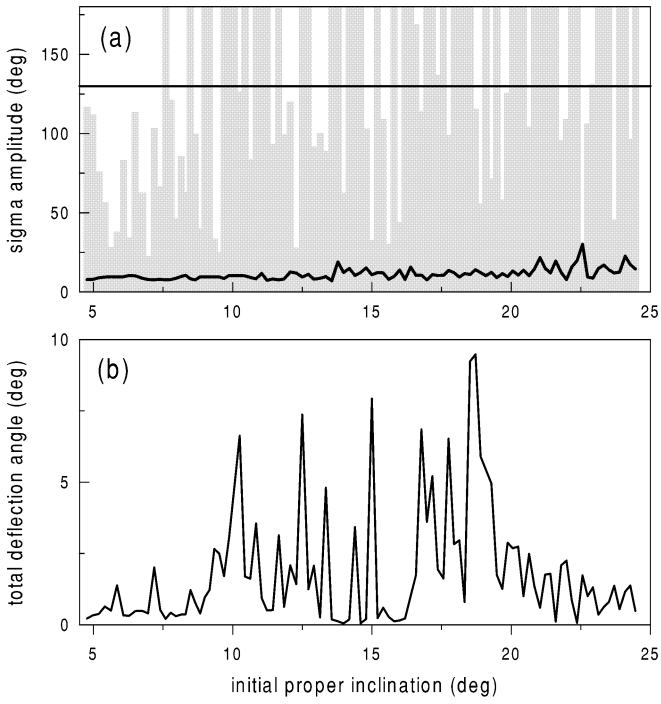

FIG. 4.—(*a*) Initial (*solid line*) and final (*shadow bars*) resonant amplitude A_σ observed in the simulation of test particles placed in the Kozai resonance with $e = 0.25$. The horizontal line at $A_\sigma = 130°$ shows an approximate limit where orbits are unstable owing to the effect of four outer planets. (*b*) Total deflection angle resulting from the encounters of test particles with Pluto in 4×10^9 yr. Öpik two-body approximation of encounters was used for its computation. See text for discussion.

at low inclinations. There were no escapes for $i < 7.^\circ5$, presumably because the mutual velocities of Pluto–test particle encounters were enhanced there by larger mutual inclination of their respective orbits, which rendered the encounters ineffective. Note on the other hand that only 12 (25%) of the test particles survived with $A_\sigma < 130^\circ$ for $16^\circ < i < 25^\circ$.

The excitation of A_σ observed in our simulation should be attributed to the gravitational effect of Pluto at close encounters. We have at least three reasons to believe this:

1. We have checked by a 10^9 yr integration that no excitation happened when only four outer planets (without Pluto) are considered in the integration. Initial and final A_σ were practically the same in this experiment for all test particles. Consequently, there is no A_σ enlargement without Pluto.

2. The swift_rmvs3 integrator was simulating the effect of the Pluto encounters correctly since the 5×10^8 yr integration with the Bulirsh-Stoer integrator gave roughly the same result. We have simulated the orbital evolution of 11 test particles at $9^\circ < i < 11^\circ$ and of 11 particles at $16^\circ < i < 18^\circ$. The mean excitation of A_σ on this time interval computed by Bulirsh-Stoer was 20% smaller than the one computed by Swift for $9^\circ < i < 11^\circ$ and was equal to the one computed by Swift for $16^\circ < i < 18^\circ$. The particle starting at $i = 9.^\circ2$ that escaped from the 2:3 resonance at $t = 3.5 \times 10^8$ yr in the simulation with swift_rmvs3, escaped also in the integration with Bulirsh-Stoer at $t = 3.2 \times 10^8$ yr. Considering the irreproducibility of a chaotic trajectory, such a coincidence is even surprising. The Bulirsh-Stoer routine treated close encounters with excellent precision, and we believe that the excitation of A_σ was correctly evaluated by this integration method. Consequently, the result of Swift was exact for $16^\circ < i < 18^\circ$ and the precision of this integration routine slightly degraded (within acceptable limits) for inclinations $\sim 10^\circ$. We have further checked that the precision of Swift worsened for initially zero inclinations. While the Bulirsh-Stoer integrator indicated a small ($\sim 10^\circ$) excitation of mean A_σ in 10^9 yr, the swift_rmvs3 method computed about double of this value. This presumably happened because of an inappropriate step size management of swift_rmvs3 at encounters and the consequent failure in energy conservation. Our tentative explanation of why Swift commits such a large error for low inclinations while being precise for the inclinations comparable to Pluto's is as follows. The physical effect of Pluto is, according to equation (2), proportional to $1/V^2$ and is large for large inclinations (low Pluto-particle mutual inclination). For low inclinations (large Pluto-particle mutual inclination), in a high-velocity regime of encounters, the physical effect of Pluto steeply decreases. From the above experience, we have reason to believe that swift_rmvs3 numerical errors at close encounters have different, less steep dependence on the mutual velocity than $1/V^2$ and are important only for high-velocity encounters.

3. For each encounter of a test particle with Pluto registered by the integrator, we compute the deflection angle and the change of orbital elements following equation (2) and a simple procedure described below, and these estimates are in qualitative agreement with the real simulation (we give an example of that later in Figs. 7 and 9 for the trajectory starting with $i = 11.^\circ8$).

The change of orbital elements due to the encounter may by computed in a two-body Öpik approximation. When a test particle is about the distance R_H from Pluto, we evaluate from the mutual velocity and position of the test particle and Pluto the energy and angular momentum of the Pluto-centric particle's orbit, neglecting the effect all other massive bodies. The particle's hyperbolic orbit is then uniquely defined as is the velocity of the outgoing trajectory at the intersection with the Hill sphere. The difference in heliocentric orbital elements computed at the points at which the incoming and outgoing trajectories intersect the Hill sphere is a measure of the orbital change at the close encounter. It is well known that the result of this computation strongly depends on the size of the sphere around a planet chosen for the computation, and as R_H is not the only choice, the real orbital change cannot be precisely computed. We use the two-body approximation for the interpretation of the results obtained by exact numeric simulations.

Figure 4*b* shows the cumulative deflection angle of the test particles that has been obtained by summing the deflection angles computed in the two-body approximations (eq. [2]) of all encounters of a test particle to Pluto during its lifetime (equal to 4×10^9 yr or the time when being deactivated). There is a rough correspondence between Figures 4*a* and 4*b*. First of all, the test particles starting at low inclinations have a small cumulative deflection of order of 1°. The effect of close encounters was apparently not sufficient for large excitation of their A_σ. Then there is the interval $9^\circ < i < 13^\circ$, where the cumulative deflection angle is as large as few degrees. The excitation of the resonant amplitude is larger for these inclinations, and many test particles initially falling into this interval of inclination escaped.

For the initial inclinations of about 15°, the situation is unclear as the cumulative deflection was less than 1° (with two exceptions). There were, however, several escapes at this interval in the exact simulation. The four surviving test particles in the range $13.^\circ5 < i < 16.^\circ5$ had been protected from close encounters with Pluto for most of the time of simulation. Their orbital dynamics resembled the motion near the leading and trailing Lagrangian points of the Sun–Pluto–test particle system (tadpole orbits—see Brown & Shook 1966). The test particles starting at larger inclination were with few exceptions ejected from the resonance. Their small relative orbital inclination with respect to the orbit of Pluto apparently enhanced the impact of close encounters.

5. TYPES OF ORBITAL BEHAVIOR

The graph of the cumulative deflection angle (Fig. 4*b*) may be interpreted in terms of the frequency and mutual velocity of encounters. In Figure 5*a* we show the number of encounters of test particles within R_H to Pluto in the first 3×10^8 yr of our simulation. Figure 5*b* shows the mean mutual velocity between the test particles and Pluto computed over the same time interval. There are on average 10 encounters within one Hill radius to Pluto in 3×10^8 yr.

Without much stress on precision we divide the integrated range of inclination into five intervals (Fig. 5), each of them being characterized by different dynamics and the interaction with Pluto.

5.1. $5^\circ < i < 9^\circ$

For $5^\circ < i < 9^\circ$, there were typically only five encounters per particle within one Hill radius to Pluto in 3×10^8 yr,

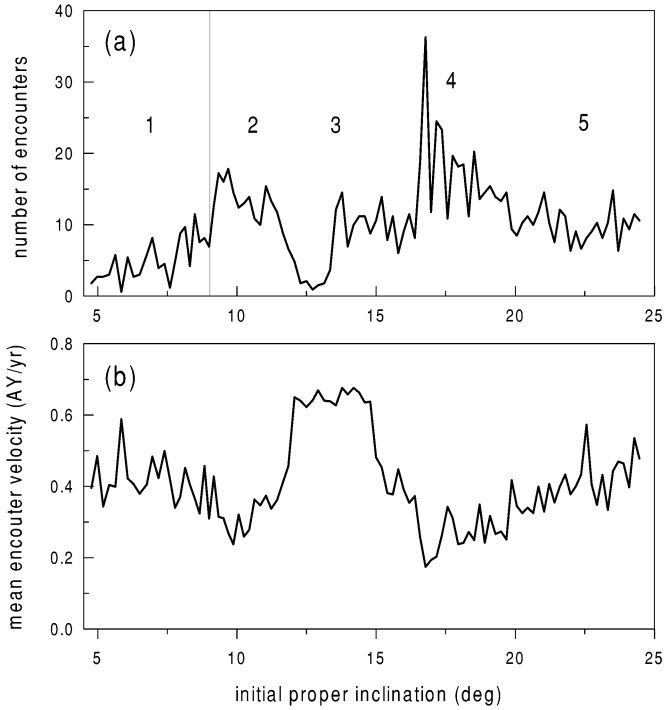

FIG. 5.—(*a*) For each test particle the number of its encounters within R_H to Pluto in the first 3×10^8 yr of simulation is shown. The simulated range of initial proper inclinations (*x*-axis) is roughly divided into five intervals with different evolutions of orbits. (*b*) The mean encounter velocity obtained by averaging over all approaches of a particle to Pluto in 3×10^8 yr. There were about 15 encounters for $15° < i < 20°$ where the mean encounter velocities were small. This is the region in which Pluto's effect is largest.

and the mean encounter velocity was about 0.4 AU yr^{-1}. This resulted in a small total deflection angle (Fig. 4*b*) and only a moderate excitation of A_σ (Fig. 4*a*). Typical evolution of orbits in this interval of inclinations is shown in Figure 6. The orbit of the test particle starting with the inclination of 7° initially exhibited motion typical for the Kozai resonance —oscillations of ω around 90°—for $t < 2.3 \times 10^8$ yr, where ω shortly moved retrogradely and then switched to the libration center at 270°. This alternation between the oscillation at 90° or 270° and the retrograde circulation of the perihelion argument is typical for the test particles at low inclinations where the size of the Kozai resonance is small. Amplitude of σ stayed small in Figure 6, and the particle survived the whole run in the 2:3 resonance. $\Delta\lambda = \lambda - \lambda_P$ showed circulation with a negative derivative and a large period in intervals of ω-libration.

5.2. $9° < i < 12°$

There were on average 15 encounters per 3×10^8 yr with the mean mutual velocity of 0.3 AU yr^{-1} for the particles starting with $9° < i < 12°$ (Fig. 5). This resulted in a relatively large total deflection angle that generally exceeded 2° in this interval. The dynamics of test particles was very interesting there and frequently resembled the pattern seen in Figure 7, where the orbital elements of the particle starting with $i = 11\overset{\circ}{.}8$ are shown. $\Delta\lambda$ initially evolved retrogradely, and when $\Delta\lambda \sim 0$, it reversed and advanced with a positive derivative up to 360° when it reversed once again and repeated the cycle. At the points of reversal, the inclination either increased or decreased. Such behavior calls to mind the horseshoe orbits of the 1:1 mean motion resonance. Here, however, probably owing to the high inclination of both the perturbed body and the perturber, the orbital element coupled with $\lambda - \lambda_P$ was the inclination and not the eccentricity or the semimajor axis. Note that the orbit in Figure 7 had its mean inclination somewhat smaller than the mean inclination of Pluto, which is also unlike the usual horseshoe pattern.

In Figure 8 we show the inclination and $\Delta\lambda$ of the same test particle ($i = 11\overset{\circ}{.}8$) in polar coordinates. Additional averaging of $\Delta\lambda$ and i over 5×10^8 yr has been performed in Figure 8. The horseshoe dynamics of the trajectory are now evident. It took about 7.5×10^8 yr for the test particle to complete one cycle.

The design of a perturbative treatment that would reproduce the orbit in Figure 8 is not a simple problem as there are two perturbers (Neptune and Pluto) and three resonances (2:3 with Neptune, Kozai, and 1:1 with Pluto) involved. The planar model of Yu & Tremaine (1999) does not apply here as the inclinations must be taken into account. In the next few paragraphs, we discuss a qualitative model based on the two-body approximation of encounters with Pluto.

We assume that if the distance of the test particle from Pluto (r) is larger than a small quantity R (of order of the radius of Pluto's Hill sphere: $R_H = 0.054$ AU) that the motion is determined by four outer planets (Jupiter to Neptune) and is characterized by constant proper actions, σ and ω libration, and a secular advance of the node longitude. Whenever $r < R$, we approximate the motion by the two-body (Pluto–test particle) dynamics and compute the resulting change of the heliocentric orbital elements according to the discussion earlier in this section.

The trajectory computed in this way (Fig. 9) for the same test particle as in Figure 7 ($i = 11\overset{\circ}{.}8$) approximates well the exact numeric simulation. While the eccentricity remained almost constant, both the semimajor axis and inclination were changing. The inclination pattern in Figure 9 is almost identical with the mean inclination in Figure 7. Concerning the angles, while $\lambda - \lambda_P$ remained on average constant, both ω and σ evolved, under the effect of close encounters with Pluto, several tens of degrees ahead.

The behavior of the orbit in Figure 7 may be also understood on the basis of simple geometric arguments. Initially $i < i_P$ so that according to what was noted in the last paragraph of § 3, $\Omega - \Omega_P$ advances with a negative derivative, and so does $\lambda - \lambda_P$ according to equation (4). This is what happened for $t < 2 \times 10^8$ yr in Figure 7. The effect of Pluto was unimportant in this interval because the planet was angularly distant from the test particle. At $t = 2.3 \times 10^8$ yr, the difference in mean longitudes $\lambda - \lambda_P$ was small and on average positive. As $\Delta\Omega = \Omega - \Omega_P$ was also small and positive at this moment and if we suppose that $a = a_P$, $e = e_P$, and $\omega = \omega_P = 90°$, close encounters between the test particle and Pluto occurred at each revolution of their orbits in both the descending and ascending nodes. Define a fixed reference frame in the tangential plane of Pluto's node (perpendicular to Pluto's heliocentric position vector when Pluto is at node) so that the *x*-axis is parallel to Pluto's velocity vector and another reference frame in the same plane whose origin moves with Pluto's velocity at node

$$v = na\sqrt{\frac{1+e^2}{1-e^2}} \tag{5}$$

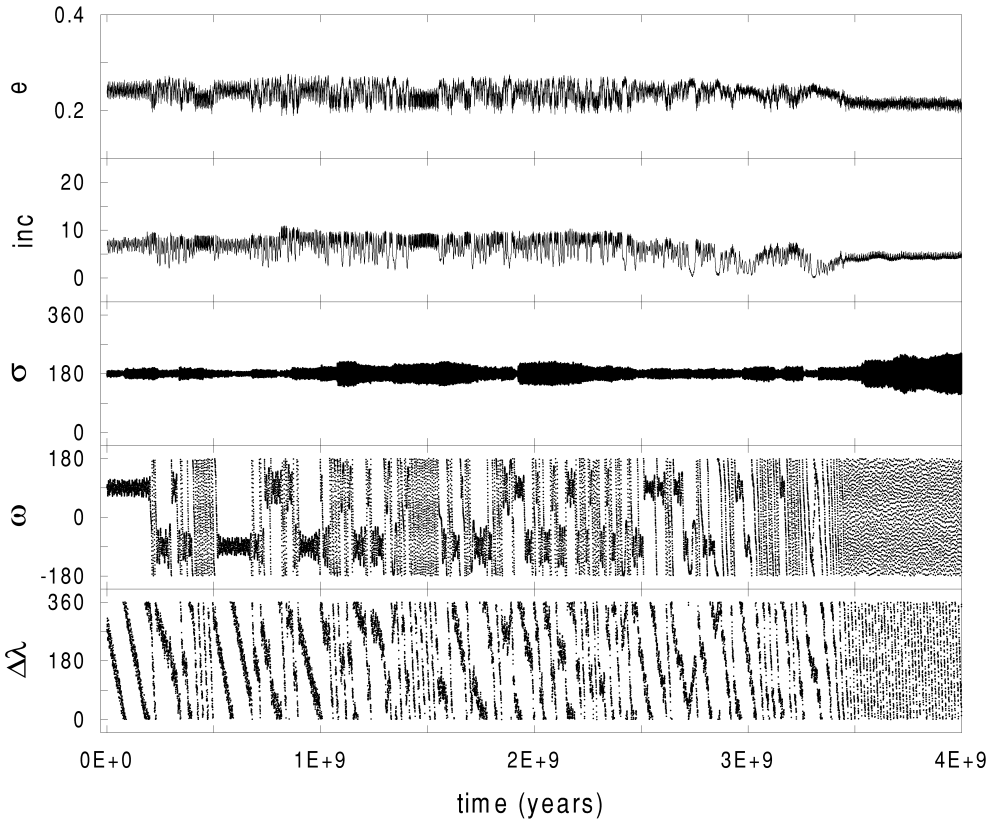

FIG. 6.—Orbit evolution of the test particle starting with $a = 39.2$ AU, $e = 0.25$, and $i = 7°$. $\sigma = 2\lambda_N - 3\lambda + \varpi$ and $\Delta\lambda = \lambda - \lambda_P$. The evolution was characterized by alternations between libration and circulation of ω, only a small excitation of A_σ and prograde circulation of $\lambda - \lambda_P$.

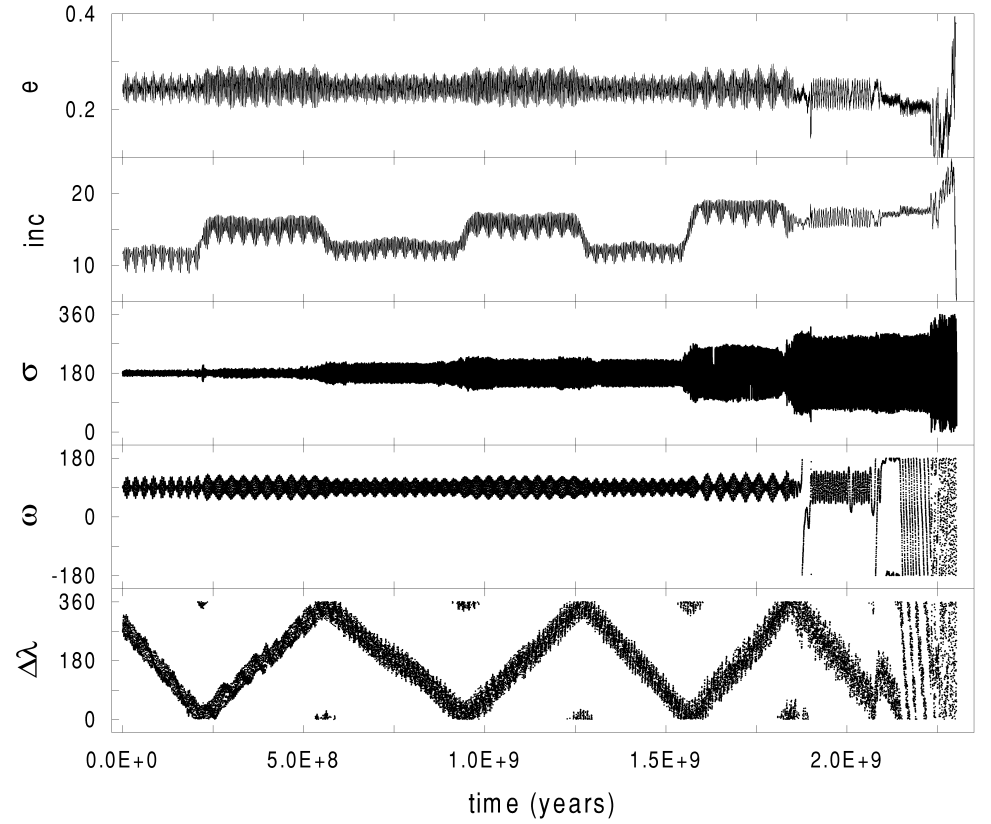

FIG. 7.—Same as Fig. 6 but for the test particle with $i = 11°.8$. The orbital evolution of this test particle was characterized by a horseshoe orbit in the 1:1 mean motion resonance with Pluto. The excitation of A_σ happened when $\lambda - \lambda_P$ reversed its sense of rotation. The perihelion argument librated with a small amplitude up to $t = 1.8 \times 10^9$ yr where A_σ increased to 120°. The particle escaped from the 2:3 resonance at $t = 2.25 \times 10^9$ yr.

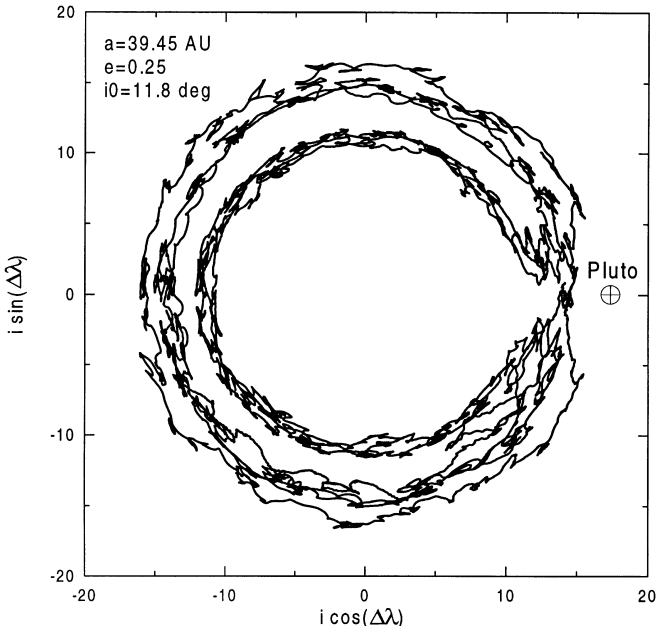

FIG. 8.—Horseshoe orbit of the same particle as in Fig. 7. Inclination and $\Delta\lambda = \lambda - \lambda_P$ are shown in polar coordinates. Unlike an ordinary horseshoe orbit, the action coupled to $\Delta\lambda$ was the inclination and not the semimajor axis or eccentricity. Note also that the mean inclination of this orbit was smaller than the inclination of Pluto.

(n being Pluto's mean motion) along the x-axis of the former and is identical with the former when Pluto is at node. Denote its axes ζ and η. Then, the components of the test particle velocity characterizing encounter in this reference system are $v_\zeta = v[\cos(i - i_P) - 1]$ and $v_\eta = v \sin(i - i_P)$. Moreover, the test particle trajectory intersects the ζ-axis at $\Delta\Omega/3$. From this geometry of the encounter in the Pluto-centric reference frame and under the assumption that the deflection angle is small, it is clear that $|i - i_P|$ will tend to zero if $\Delta\Omega > 0$. This is what happened with inclination of the test particle in Figure 7 at $t = 2 \times 10^8$ yr (see also Fig. 9, where the net effect of Pluto's encounters is shown).

If the differential rotation of nodes were fast so that the epoch of close encounters when $\Omega - \Omega_P \sim 0$ were short, the inclination change would be small, and $\Omega - \Omega_P$ would soon become negative (as for the test particle in Fig. 6—a similar argument holds for the test particle in Fig. 12, where $\Delta\Omega$

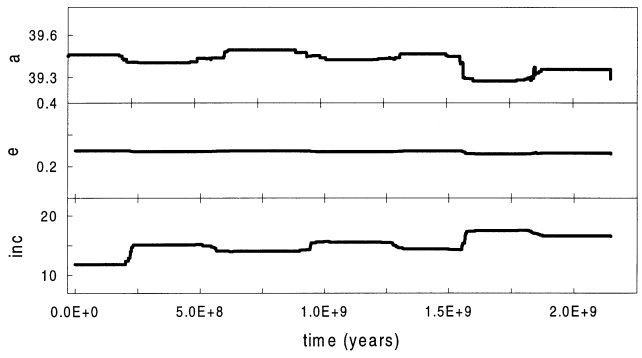

FIG. 9.—Two-body approximation of the dynamics at close encounters with Pluto. See text for details. Compare with Fig. 7 where the orbit evolution of the same test particle was computed by the exact numeric integration.

rotates with positive derivative). However, this was not the case of the test particle in Figure 7, where the inclination due to close encounters with Pluto rapidly grew, and before $\Omega - \Omega_P$ would become negative, i was already close to i_P. It was then important that Pluto (with $A_\sigma = 84°$) have a negative nodal frequency with its absolute value larger than objects with the same orbital parameters but smaller A_σ. This means that when $i = i_P$ for the test particle in Figure 7, both $\Omega - \Omega_P$ and (according to eq. [1]) $\lambda - \lambda_P$ must have had a positive time derivative. This is what we see in Figure 7 in the interval $2.5 < t < 5 \times 10^8$ yr, where Pluto's effect is once again negligible.

The geometry of encounters with $\Delta\Omega < 0$ at $t = 5.5 \times 10^8$ yr is different, and, as an analysis of the encounter in the tangential plane shows, $|\Delta i|$ must increase in this case. Consequently, when i sufficiently decreases in several encounters with Pluto $\Omega - \Omega_P$ reverses its sense of the rotation.

A quantitative computation of the orbital changes in the Öpik approximation of encounters is, however, strongly dependent on the distance R, where one chooses to approximate the motion by the two-body model. For larger values of R the computed change of orbital elements is large, while for small values of R, the computed orbital change is small. The development of a quantitative perturbative model of Neptune-Pluto-Plutino interaction is an interesting area for future research. The circular planar model of Yu & Tremaine (1999) is not realistic enough to account for the real evolution of Plutino orbits.

5.3. $12° < i < 15°$

Several trajectories in the interval $12° < i < 15°$ (Fig. 5*a*—interval 3) were close to the leading or trailing Lagrangian points of the Sun–Pluto–test particle system (tadpole orbits). Pluto's orbit is noncircular, and the triangular Lagrangian points are not necessarily placed at 60° from Pluto. The orbit in Figure 10 (initially $i = 14.°4$) is an example of motion near the trailing stationary point. Most of the time the orbit was protected from close encounters with Pluto, and only a few high-velocity approaches did not enlarge A_σ above the instability limit. The test particle in Figure 10 survived the whole run. The orbits near the Lagrangian points were, however, susceptible to small orbital changes, and they frequently switched to horseshoe orbits in our simulation, where the interaction with Pluto led to the important A_σ excitation.

5.4. $15° < i < 20°$

The initial inclinations in the range $15° < i < 20°$ (Fig. 5*a*) led to a variety of different orbital behaviors. The relative inclinations to Pluto's orbit were small when the nodes became aligned in the simulation and there were more than 15 encounters in 3×10^8 yr with the mutual velocity as low as 0.2 AU yr^{-1} in this interval of initial inclinations (Fig. 5). Large deflection angles (Fig. 4*b*) of the low-velocity encounters caused significant alterations of orbits, excitation of A_σ, and escapes to Neptune–crossing trajectories. The evolution of the test particle in Figure 11 (initial $i = 16.°8$) showed an alternation between all three orbital modes of the 1:1 mean motion resonance with Pluto: the horseshoe orbit and the tadpole orbits near the trailing and leading Lagrangian points. A large excitation of A_σ already occurred for this test trajectory at the beginning of the integration, and the particle escaped from the resonance at

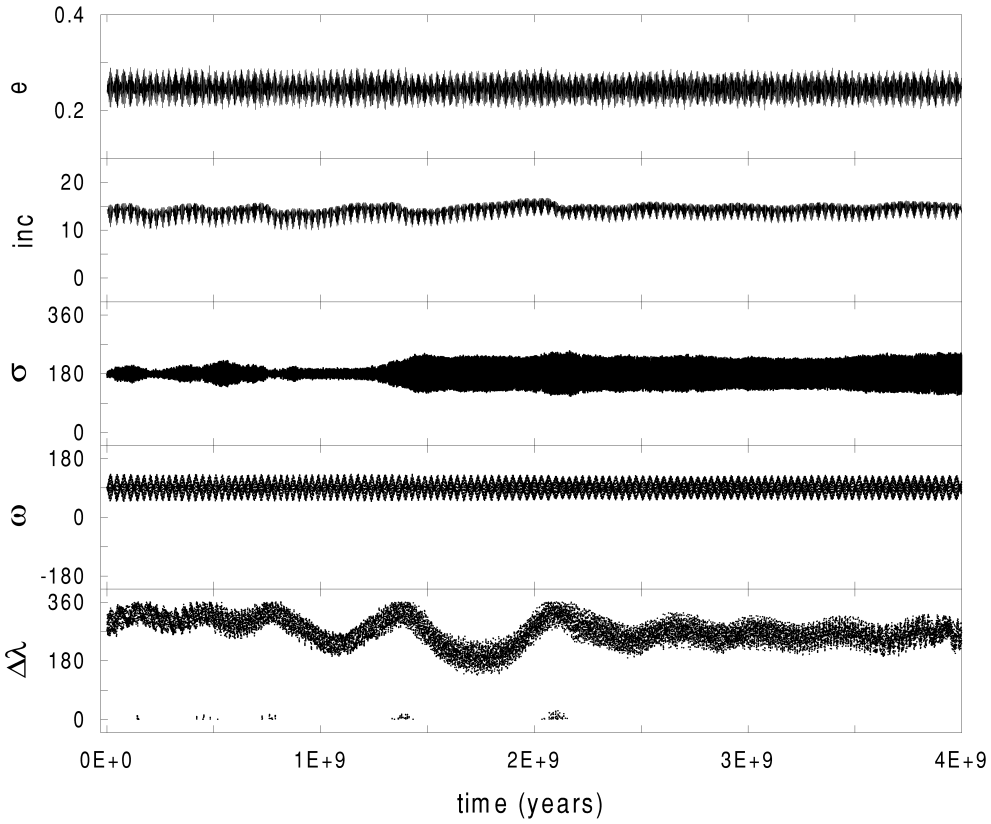

FIG. 10.—Same as Fig. 6 but for the test particle with $i = 14.^{\circ}4$. This trajectory is near the trailing Lagrangian point of the Sun–Pluto–test particle system. Its resonant amplitude was moderately excited at $t = 1.4 \times 10^9$ yr, where $\lambda - \lambda_P$ was close to zero. A_ω of the orbit stayed almost constant, and the test particle survived the whole run in the Kozai resonance.

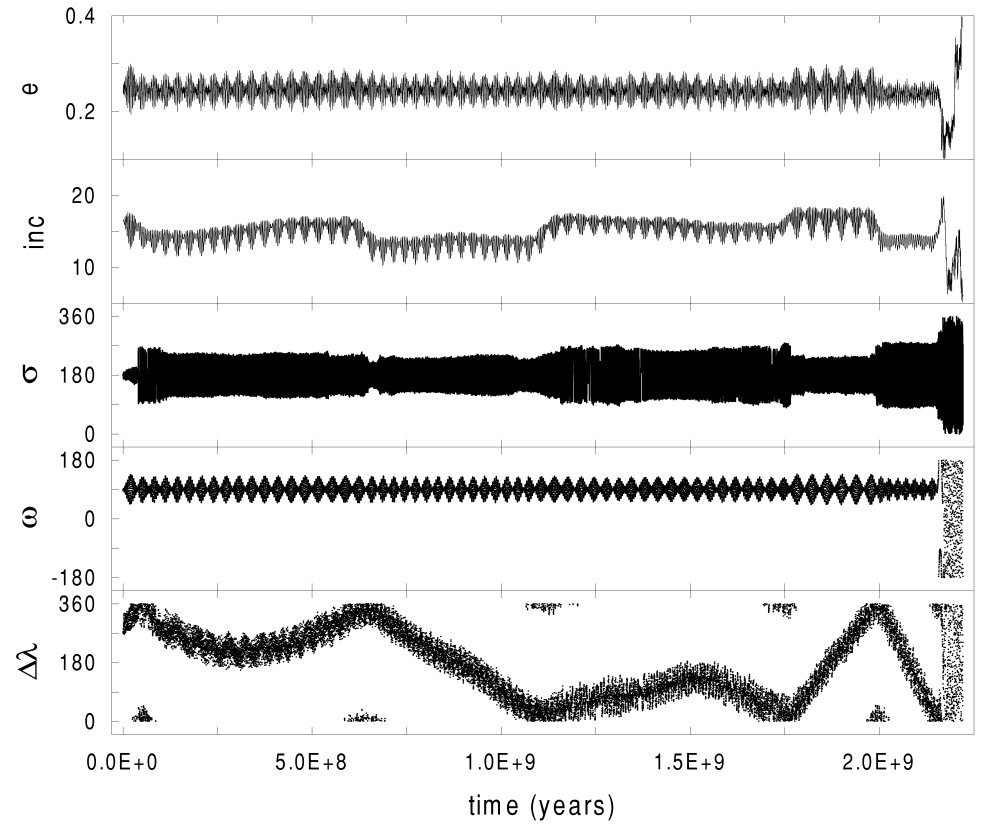

FIG. 11.—Same as Fig. 6 but for the test particle with $i = 16.^{\circ}8$. The trajectory is near the trailing Lagrangian point with respect to Pluto's orbit up to $t = 6 \times 10^8$, where it migrates to the leading point and later performs one cycle of the horseshoe orbit ($1.75 < t < 2.2 \times 10^9$ yr). It escapes from the resonance at 2.2×10^9 yr.

2.2×10^9 yr and was deactivated at 2.25×10^9 yr owing to a very close encounter with Neptune.

5.5. $i > 20°$

The test particles with $i > 20°$ had a prograde circulation of $\lambda - \lambda_P$, and most of them escaped from the 2:3 resonance after their A_σ was significantly excited by close encounters with Pluto. An example of motion is shown in Figure 12 for the test particle with an initial inclination of 23°. Note the large time interval of about 2×10^8 yr that the test particles had passed at the separatrix of the 2:3 resonance ($A_\sigma \sim 180°$). This shows the possible existence of long-lived objects with large A_σ.

6. ORBITAL DISTRIBUTION OF THE SURVIVING POPULATION

Concerning the test particles surviving 4×10^9 yr in the 2:3 resonance in our experiment, we show in Figure 13*a* their smoothed resonant amplitude (averaged over 1° interval of the initial inclination). $A_\sigma(4 \times 10^9$ yr) is denoted by a solid line, and $A_\sigma(0)$ is shown for reference by a dotted line. The excitation of the resonant amplitude is important: the average $A_\sigma(4 \times 10^9$ yr) over all test particles is about 80°. The final resonant amplitude depends on the initial inclination. While for the test particles initially at $i < 10°$ A_σ (4×10^9 yr) is usually smaller than 70°, for a larger initial inclination the excitation is larger. The small depression on the curve of $A_\sigma(4 \times 10^9$ yr) at about 15° is a consequence of the fact that several test particles with this initial inclination passed long time intervals near the Lagrangian points, being phase-protected from close encounters to Pluto.

Another important result of the simulation is that a few test particles were found to be on ω-librating orbits in the Kozai resonance at $t = 4 \times 10^9$ yr. The test particles were chosen so that initially $A_\omega(0) < 25°$ with an average of 10°, and at the end of the run, there were only 14 test particles with $A_\omega < 70°$. Seven of the particles surviving in the Kozai resonance started with inclinations in the interval $12.^\circ5 < i < 16.^\circ5$ and spanned long time intervals on tadpole orbits of the 1:1 mean motion resonance with Pluto. Five other test particles with $A_\omega(4 \times 10^9$ yr) < 70° had an initial inclination larger than 22°. The fact that only 14% of the test particles are found in the Kozai resonance at the end of simulation can be related to the lack of observed Plutinos on orbits similar to Pluto's orbit. We conjecture that the gap observed in the distribution of known Plutinos at the Kozai resonance in Figure 1*b* may be a consequence of Pluto's sweeping effect.

In Figure 13*b* we show the initial (*dashed line*) and final distribution of test particles versus the resonant amplitude A_σ. At $t = 4 \times 10^9$ yr, the number of particles per 10° of A_σ varies between three and eight for $A_\sigma > 25°$ and is zero for $A_\sigma < 25°$. Eleven test particles that have not been deactivated during the run had $130° < A_\sigma(4 \times 10^9$ yr) < 170° in spite of the motion at these resonant amplitudes being chaotic and unstable on at most several 10^8 yr. Consequently, there might be presently many Plutinos on such transitional

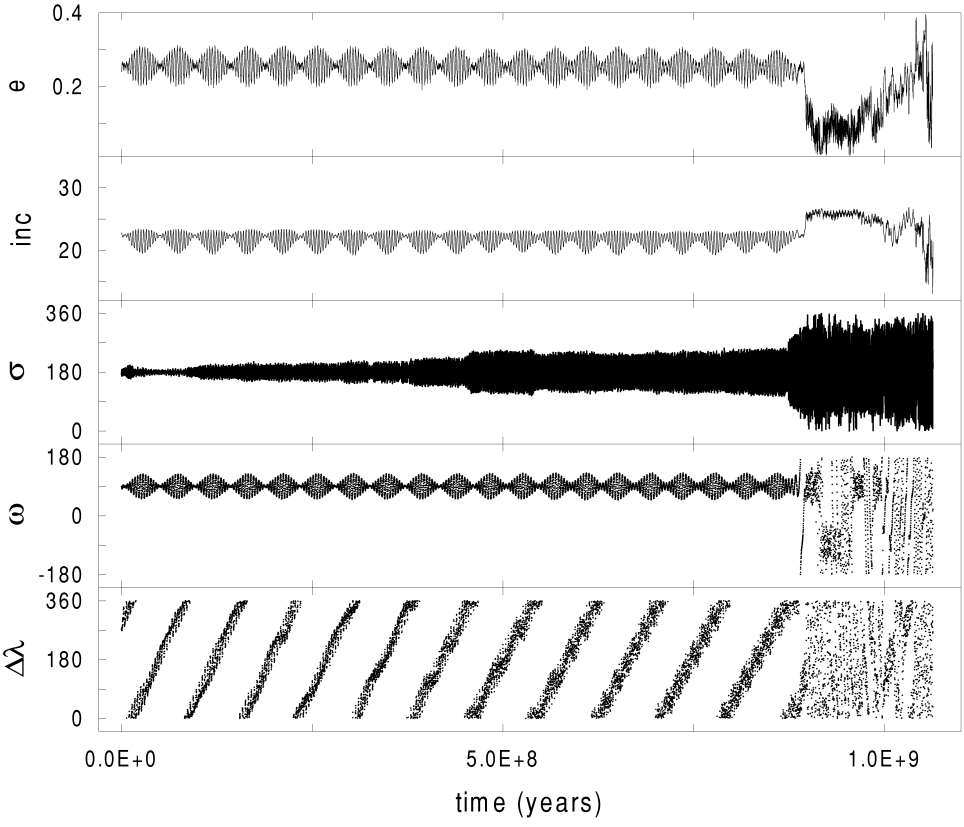

FIG. 12.—Same as Fig. 6 but for the test particle with $i = 24°$. $\lambda - \lambda_P$ evolved with a positive derivative, and each time when $\lambda - \lambda_P = 0$ the resonant amplitude A_σ somewhat increased. The particle was removed from the resonance at 8.7×10^8 yr and was deactivated at 1.07×10^9 yr as its heliocentric distance exceeded 100 AU.

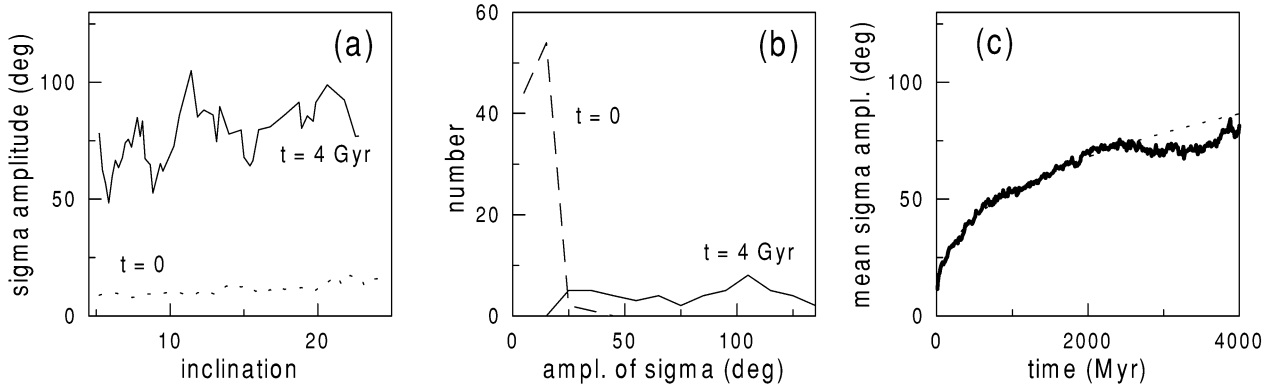

FIG. 13.—(*a*) Mean A_σ (average over a 10° window in inclination) for $t = 0$ (*dotted line*) and $t = 4 \times 10^9$ yr (*solid line*) for the test particles surviving the whole run. (*b*) Distribution of the test particles with respect to their A_σ. The number of test particles within a 10° interval of A_σ is shown for $t = 0$ (*dashed line*) and $t = 4 \times 10^9$ yr (*solid line*). (*c*) Evolution of $A_\sigma(t)$ calculated as average over all surviving particles at time t. The final excitation is about 80°. The dotted line in (*c*) is a least-squares fit. See text for details.

orbits with $A_\sigma > 130°$, and the long-term orbital stability is not a necessary condition of correct orbital elements computation from observations.

Figure 13*c* shows the evolution of the mean libration amplitude of the surviving population with time. The solid line is the average of $A_\sigma(t)$ over the test particles that had survived the integration up to the time t (not considering the test particles that had already escaped from the resonance). The power time dependence αt^β, fitted by the least-squares method to average $A_\sigma(t)$, is defined by $\alpha = 4.83$ and $\beta = 0.344$ (dotted line in Fig. 13*c*). The initially low resonant amplitude increases to about 80° at $t = 4 \times 10^9$ yr.

7. EXPLORING PLUTO'S EFFECT FOR $e \neq 0.25$

The experiment in the previous section has been performed with both initial A_σ and A_ω small choosing the resonant semimajor axis and $e = 0.25$ for the initial orbital elements. Here we explore Pluto's effect in the 2:3 Neptune resonance also for different initial eccentricities.

One-hundred one test particles have been placed at $a = 39.2$ AU, $i = 17°$, and with eccentricity between 0.15 and 0.35 (0.002 step). The initial angles, integration parameters, and integration procedure were exactly the same as in the run in the previous section. The total integration time span was 2×10^9 yr.

Also for these initial conditions, many test particles escaped from the 2:3 resonance. By $t = 2 \times 10^9$ yr, 34 test particles had already left the resonance. A linear extrapolation of a cumulative number of escapes to 4×10^9 yr suggests removal of about 60% of test particles. Recall that also in this case, the escape of test particles must be attributed to the effect of Pluto, as other planets do not cause any secular trends of the resonant orbits with $A_\sigma < 50°$.

Figure 14*a* shows $A_\sigma(0)$ (*solid line*) and $A_\sigma(2 \times 10^9$ yr) (*shadow bars*). Most of the escaping test particles were initially in the interval $0.2 < e < 0.32$, which is the approximate width of Kozai resonance at $i = 17°$ (Morbidelli et al. 1995). For low ($e < 0.2$) and high ($e > 0.32$) eccentricities, the excitation of A_σ was smaller, and fewer test particles leaked from the 2:3 resonance at these eccentricities. The total deflection angle shown in Figure 14*b* is well correlated with the number of escapes. It is larger than 1° for most of the escaping trajectories in the $0.2 < e < 0.32$ interval.

The number of encounters within R_H to Pluto in 3×10^8 yr shows an interesting profile (Fig. 15*a*). There were usually fewer than five encounters for $e < 0.2$ with the mean velocity of 0.4 AU yr^{-1}. At $e > 0.2$, the number of encounters increases with increasing eccentricity up to the peak of about 20 encounters (on average) at $e = 0.25$. This eccentricity coincides with the libration center of the Kozai resonance. The mean encounter velocity is only 0.2 AU yr^{-1} for $e = 0.25$. The relatively large number of encounters combined with low encounter velocity led to large orbital changes of the test particles starting with $0.2 < e < 0.32$ and the excitation of their resonant amplitudes A_σ (Fig. 14*a*). This showed that most orbits in the Kozai resonance (and

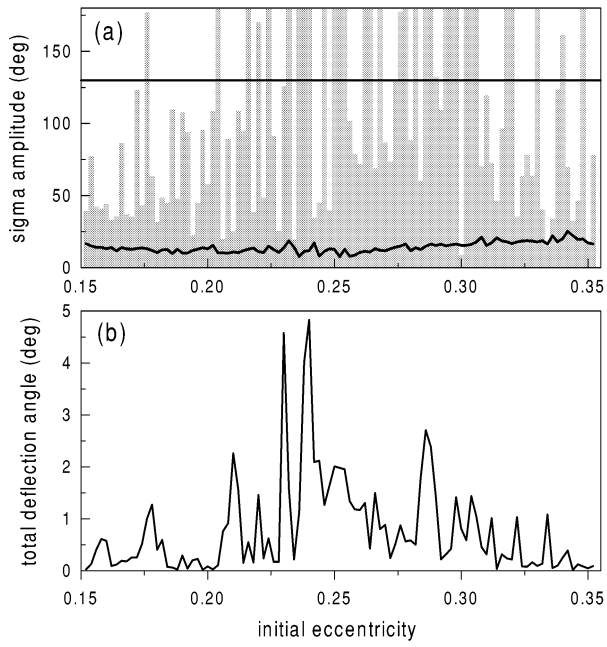

FIG. 14.—Same as Fig. 4 but for the run of 101 test particles initially with $i = 17°$. Most of the escapes happened for $0.2 < e < 0.32$, where also the cumulative deflection angle calculated from encounters with Pluto was large. This region roughly corresponds to the orbits in the Kozai resonance.

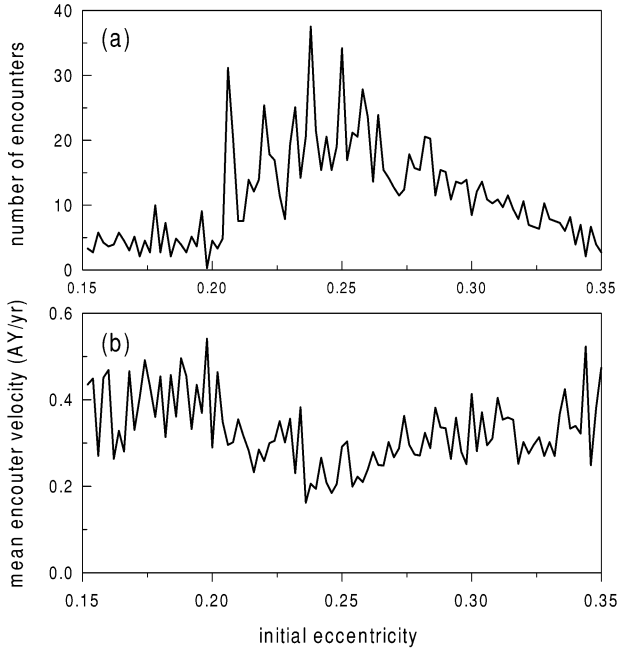

FIG. 15.—Same as Fig. 5 but for the run of 101 test particles initially with $i = 17°$. The number of encounters within R_H to Pluto is the largest at $e = 0.25$, where about 20 encounters happen in 3×10^8 yr. The encounter velocity is about 0.2 AU yr^{-1} for this eccentricity.

not only those at its libration centers) were efficiently modified by Pluto's influence. The gap in the orbital distribution of Plutinos should be roughly of the size of the Kozai resonance.

The surviving 67 test particles at 2×10^9 yr had the mean A_σ as large as 66° (Fig. 16*a*). Initially (dotted line in Fig. 15*a*) the mean A_σ was 14°. The number of test particles in 10° of A_σ versus A_σ is both initially (*dashed line*) and at 2×10^9 yr (*solid line*) shown in Figure 16*b*. There were initially 80 test particles with $10° < i < 20°$. The profile at 2×10^9 yr is characterized by a peak density of test particles at the amplitude of about 45° (mainly formed by the test particles starting with $e < 0.25$ and $e > 0.3$) and a number of orbits with A_σ largely excited. There are about five particles per 10° of A_σ for $70° < A_\sigma < 110°$.

The mean resonant amplitude increased considerably with time (Fig. 16*c*). The solid line in this figure is the average over the surviving particles. The dotted line is the least-squares fit that results in the same power dependence on time as the power fit in Figure 13*c* [$A_\sigma(t) \sim t^{1/3}$]. The extrapolation to 4×10^9 yr shows that the resonant amplitude of the surviving test population at 4×10^9 yr should be about 80°. It could be, however, a little smaller if the deceleration trend observed shortly before 2×10^9 yr would continue also for $t > 2 \times 10^9$ yr. In any case a large excitation of A_σ can be expected also for the orbits with $e \neq 0.25$

8. CONCLUSIONS

Pluto's orbit is locked in the Kozai resonance in contrast with almost all observed Plutinos. According to the analysis in this work, this observation result can be explained by Pluto's effect on Plutinos. The orbits starting with the low amplitude of ω oscillations are, for a wide range of initial inclinations, ejected from the Kozai resonance on the 10^9 yr timescale. As the opposite process (i.e., evolution into the Kozai resonance) is less effective, a gap must have been formed around Pluto's orbit in eccentricity and inclination. This gap is actually observed in the distribution of known Plutinos.[3]

The only objects surviving long time intervals in the Kozai resonance are usually protected from close encoun-

[3] It is certainly a possibility that the lack of Plutinos in the Kozai resonance is related to a slow primordial migration of Neptune's orbit suggested by Malhotra (1996). If the evolution of a captured 2:3 resonant object toward larger eccentricities is envisaged as a consequence of slow outward migration of the 2:3 Neptune resonance, this object encounters the lower separatrix of the Kozai resonance at an eccentricity that depends both on A_σ and inclination (Fig. 1). The theory of adiabatic capture may be applied in this case, and the probability of capture in the Kozai resonance can be computed (a simple numeric experiment can also yield an answer). If the capture probability is near 1, the gap is not primordial. If the probability is near 0, the primordial gap could have been formed, since most bodies should have avoided the Kozai resonance during their migration. We nevertheless believe that collisions (such as the one in which the Pluto-Charon binary has been presumably formed) must have resupplied new objects in the region of the Kozai resonance since then.

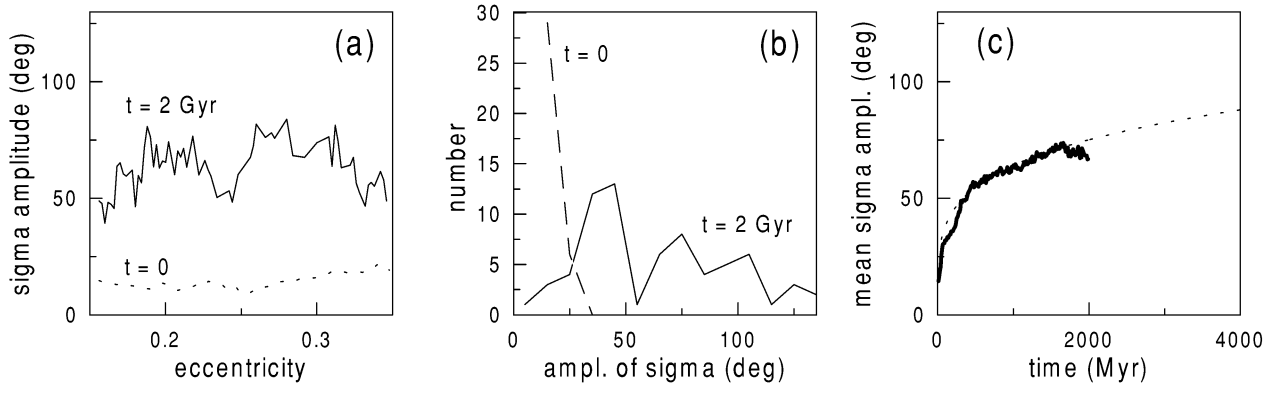

FIG. 16.—(*a*) Mean A_σ (average over a 0.01 window in eccentricity) for $t = 0$ (*dotted line*) and $t = 2 \times 10^9$ yr (*solid line*) for the test particles surviving the whole run. The experiment with $i = 17°$. (*b*) Distribution of the test particles with respect to their A_σ. The number of test particles within a 10° interval of A_σ is shown for $t = 0$ (*dashed line*) and $t = 2 \times 10^9$ yr (*solid line*). In fact all test particles had the initial $A_\sigma < 30°$. (*c*) Evolution of mean $A_\sigma(t)$ calculated as average over all surviving particles at time t. The excitation at 4×10^9 yr suggested by the extrapolation (*dotted line*) is about 80° . The dotted line in (*c*) is a least-squares fit.

ters with Pluto being trapped on tadpole orbits in the 1:1 resonance with the planet. There should be a number of Pluto's Trojans with mean inclinations of about 15°. As we have confirmed by a numeric simulation, 1997 QJ4 is the first observed example of this dynamical class. $\lambda - \lambda_P$ of 1997 QJ4 has been locked at 80° for at least the last 10^9 yr. Such an orbit makes of this object a good candidate for a body dynamically related to the Pluto-Charon binary formation event (Stern, Canupt, & Durda 1999), and the determination of physical properties of its surface by spectral observations would be interesting. Of course, it is equally probable that 1997 QJ4 is just a sample of a dynamically primordial population formed in the Kozai resonance or a collisionally injected body.

Another interesting class of orbital evolution in the 1:1 resonance with Pluto found in our simulations is a horseshoe orbit in which $\lambda - \lambda_P$ is coupled with inclination (Fig. 7). Such orbits are, however, very susceptible to Pluto's perturbation and usually do not survive on the age of the solar system because of the enlargement their resonant amplitude A_σ. The horseshoe orbits present the highest frequency and lowest mutual velocity of encounters with Pluto. Most of the trajectories closely encountering Pluto have the horseshoe dynamics.

An important effect of Pluto is its large excitation of the libration amplitudes in the 2:3 resonance. The surviving population of Plutinos with the primordial inclination larger than 8° should have had its mean A_σ increased to about 80° on the solar system age. The excitation of low-eccentricity orbits is smaller and accounts for an estimated 10° increase of mean A_σ per 10^9 yr. The change of A_σ for a Plutino on the low-inclination orbit can be, however, substantially larger in specific case. The traces of A_σ excitation driven by Pluto can actually be observed in the 2:3 resonance as there exists a lack of observed low-A_σ Plutinos (Fig. 2).

The excitation of A_σ by close encounters with Pluto leads to the escape from the 2:3 Neptune resonance when A_σ increases beyond the instability limit ($\sim$120°). We estimate that about 50% of dynamically primordial objects in the Kozai resonance had been removed from the 2:3 resonance by this mechanism. For $i > 8°$, even more than 70% should have had their A_σ increased above the instability limit after 4×10^9 yr. Consequently, the population of Plutinos must have suffered a significant mass loss in the past.

Pluto-induced excitation of the resonant amplitude and evolution of Plutinos onto Neptune-crossing orbits contributes to the flux of short-period comets from the trans-Neptunian region. We estimate that the flux rate from $i > 8°$ orbits at about 1% of such 2:3 resonant population per 10^8 yr, which is about of the same value as the flux expected from the marginally unstable region without Pluto (Morbidelli 1997). For $i < 8°$, the expected Pluto-induced flux should be a factor of 2–5 smaller. Consequently, the marginally unstable region is continuously resupplied from low-A_σ region, and a large part of the 2:3 resonance is an active source of short period comets.

These were the main conclusions. In the following, we briefly discuss two issues that are related to the work presented here and are of possible interest for future research.

According to Stern & Yelle (1999), *HST* observations had shown that Charon's eccentricity is nonzero, with a best estimated value of 0.0076. The fact that the orbit is not precisely circular indicates some disequilibrium forces have disturbed it from the exact value of zero expected from tidal evolution. It is most likely that the disturbance causing this is generated by occasional close encounters between the Pluto-Charon system and one of the 100 km or larger diameter bodies now known to orbit with Pluto in the Edgeworth-Kuiper belt.

The number of encounters within a distance R to Pluto on time interval t is proportional to $P_i N R^2 t$, where N is the number of bodies ($\sim$10,000 with diameter larger than 100 km according to Jewitt et al. 1998). The intrinsic probability P_i (Davis & Farinella 1997) may be computed from our experiment. As there are on average 10 encounters within R_H to Pluto in 3×10^8 yr, the estimated intrinsic probability is

$$P_i = 5 \times 10^{-22} \text{ km}^{-2} \text{ yr}^{-1} . \quad (6)$$

Setting $R = 40{,}000$ km, which is about double the semimajor axis of Charon's orbit, there is about 1.3 such encounters per 10^8 yr. The possible excitation of Charon's eccentricity by a near fly-by of a 100 km body and the subsequent tidal relaxation of the orbit are surely interesting areas for future studies.

The second interesting issue that emerged with the results presented in this paper is whether the excitation of A_σ works in one direction (i.e., Pluto enlarged A_σ of Plutinos) or whether also the opposite effect (i.e., Plutinos enlarged A_σ of Pluto) might be significant.

Assuming the 7000–14,000 objects with diameters larger than 100 km in the 2:3 Neptune resonance (Jewitt et al. 1998), their total mass (0.01–0.02 of Earth's mass) exceeds Pluto's mass (which is about 0.002 of Earth's mass) by a factor of 5–10. Now, if Pluto has a considerable effect on these bodies in 4×10^9 yr as shown in this paper, the resonant bodies must have at least an equally large effect on Pluto. We conjecture that Pluto's large resonant amplitude ($\sim$80°—equal to the final average excitation observed in our simulations of test particles on initially inclined orbits) resulted—at least partially—from the mutual interaction with resonant bodies.

This subject is closely related to the work of Levison & Stern (1995), but the reasoning is somewhat different. Instead of trying to stabilize Pluto's orbit in the dense primordial Kuiper belt by scattering it to a stable orbit inside the resonance (in time intervals of order of 5×10^7 yr), assume the present Kuiper belt density (which is about 1% of the primordial), and compute the effect of gravitational scattering on Pluto in last 4×10^9 yr. Owing to lower density, the frequency of encounters will be a factor of 100 smaller than in the primordial belt, but the interval is 100 times longer than that in Levison & Stern (1995). Consequently, the net effect in such an interaction can be about the same, and the amplitudes of Pluto's resonant angle and perihelion argument may be expected to change by several to several tens of degrees (as in Fig. 8 of Levison & Stern 1995). Pluto's orbit could well have been different in the past.

Most of the numeric simulations have been performed using the computer resources of the São Paulo University computer center LCCA in the frame of the project "Asteroid Resonant Dynamics and Chaos." This research was sponsored by the São Paulo State Science Foundation FAPESP.

REFERENCES

Brown, E. W., & Shook, C. A. 1966, Planetary Theory (New York: Dover)
Cohen, C. J., & Hubbard, E. C. 1965, AJ, 70, 10
Davis, D. R., & Farinella, P. 1997, Icarus, 125, 50
Duncan, M. J., Levison, H. F., & Budd S. M. 1995, AJ, 110, 3073
Duncan, M. J., Quinn, T., & Tremaine, S. 1988, ApJ, 328, L69
Edgeworth, K. E. 1949, MNRAS, 109, 600
Fernández, J. A. 1980, MNRAS, 192, 481
Henrard, J. 1990, Celest. Mech. Dyn. Astron., 49, 43
Holman, M., & Wisdom, J. 1993, AJ, 105, 1987
Jewitt, D. C., & Luu, J. X. 1993, Nature, 362, 730
Jewitt, D. C., Luu, J. X., & Trujillo, C. 1998, AJ, 115, 2125
Kinoshita, H., & Nakai, H. 1984, Celest. Mech. Dyn. Astron., 34, 203
Knežević, Z., Milani, A., Farinella, P., Froeschle, Ch., & Froeschle, C. 1991, Icarus, 93, 316
Kozai, Y. 1962, AJ, 67, 591
Kuiper, G. P. 1951, in Proc. Astrophysics: A Tropical Symposium, On the Origin of the Solar System, ed. J. A. Hynek (New York: Mc Graw-Hill), 357
Levison, H. F., & Duncan, M. J. 1993, ApJ, 406, L35
———. 1994, Icarus, 108, 18
———. 1997, Icarus, 127, 13
Levison, H. F., & Stern, S. A. 1995, Icarus, 116, 315
Levison, H. F., Stern, S. A., & Duncan, M. J. 1999, Icarus, submitted
Malhotra, R. 1993, Nature, 365, 819
Malhotra, R. 1996, AJ, 111, 504
Milani, A., Nobili A. M., & Carpino, M. 1989, A&A, 96, L1
Morbidelli, A. 1997, Icarus, 127, 1
Morbidelli, A., & Nesvorný, D. 1999, Icarus, 139, 295
Morbidelli, A., Thomas, F., & Moons, M. 1995, Icarus, 118, 322
Nesvorný, D., & Ferraz-Mello, S. 1997, Icarus, 130, 247
Nesvorný, D., & Roig, F. 2000, Icarus, submitted
Öpik, E. J. 1976, in Interplanetary Encounters, ed. Z. Kopal & A. Cameron (New York: Elsevier)
Petit, J. M., Morbidelli, A., & Valsecchi, G. B. 1999, Icarus, 141, 367
Quinlan, G. D., & Tremaine, S. 1990, AJ, 100, 1694
Quinn, T., Tremaine, S., & Duncan, M. 1991, AJ, 101, 2287
Stern, S. A., Canup, R., & Durda, D. D. 1999, preprint
Stern, S. A., & Yelle, R. V. 1999, in The Encyclopedia of the Solar System, ed. T. V. Johnson, P. R. Weissman, & L. A. McFadden (Academic Press), Chapter 22
Sussman, G. J., & Wisdom J. 1988, Science, 241, 433
Thomas, F. 1998, Ph.D. thesis, Observatoire de Paris
Williams, J. G., & Benson, G. S. 1971, AJ, 76, 167
Yu, Q., & Tremaine, S. 1999, AJ, 118, 1873

Anexo:

Mean motion resonances in the trans-Neptunian region. Part II: The 1:2, 3:4 and weaker resonances

Icarus **150**, 104–123 (2001)
doi:10.1006/icar.2000.6568, available online at http://www.idealibrary.com on IDEAL®

Mean Motion Resonances in the Transneptunian Region

Part II: The 1 : 2, 3 : 4, and Weaker Resonances

D. Nesvorný[1] and F. Roig

Institute of Astronomy and Geophysics, São Paulo University, Av. Miguel Stefano 4200, 04301 São Paulo, SP, Brazil
E-mail: david@obs-nice.fr

Received February 16, 2000; revised October 16, 2000

The stability of orbits in the transneptunian region is numerically computed. It is found that, in analogy to the asteroid belt, there exist many chaotic layers associated with thin mean-motion resonances. These are either moderate- and high-order resonances with Neptune or three-body resonances with Neptune and Uranus. The orbital eccentricity chaotically increases at the thin resonances, allowing some Kuiper Belt objects to be slowly transferred to Neptune-crossing orbits. The stability of two large mean-motion resonances with Neptune, the 1 : 2 and 3 : 4, is systematically explored. It is shown that orbits in both resonances, with small resonant amplitudes are stable over the age of the Solar System. The possible role of collisions and dynamical scattering in clearing the resonances is discussed. It is inferred from orbital angles of 1997 SZ10 and 1996 TR66 that these bodies are most probably on stable tadpole orbits in the 1 : 2 Neptune resonance. © 2001 Academic Press

Key Words: **Kuiper Belt; Oort Cloud, celestial mechanics; stellar dynamics.**

1. INTRODUCTION

This paper extends our previous work, in which the regular and chaotic dynamics of the 2 : 3 mean-motion resonance (MMR) with Neptune was studied (Nesvorný and Roig 2000; hereafter N&R00). In N&R00, we calculated the maximum Lyapunov characteristic exponent (LCE) and measures of chaotic evolution of orbital elements (Laskar 1994, Morbidelli 1996) and frequencies (Laskar 1999) for initial conditions on a grid in a, e, i. The first set of initial conditions (1010 orbits) sampled the 2 : 3 resonant orbits at low inclinations and the second set (405 orbits) included large-inclination orbits. We have classified the resonant orbits into three groups: (i) those for which the escape rate to Neptune-crossing orbits at $t = 4$ Byr was more than 1% of the initial population per 1 Byr.[2] We called these orbits the *marginally unstable* orbits. Other orbits, i.e., those for which the escape rate at $t = 4$ Byr was less than 1%, were either (ii) *strongly unstable* orbits, where most of the original population escaped at $t < 4$ Byr, so that at $t = 4$ Byr there were too few surviving bodies to assure the required flux, or (iii) *practically stable* orbits, with the dynamical lifetimes largely exceeding the age of the Solar System and an equally negligible escape rate at $t = 4$ Byr.

The practically stable orbits were characterized by a small LCE and very slow chaotic evolution, and were usually located in the core of the 2 : 3 Neptune MMR. The marginally unstable orbits had larger LCEs (10^{-5}–10^{-6} yr^{-1}) and were initially located at larger resonant amplitudes ($A_\sigma \sim 100^\circ$–120°), where the slow chaotic evolution of A_σ transferred them, after a long time interval, to the strongly unstable region at the resonant borders. The strongly unstable orbits had initially $A_\sigma > 120^\circ$–130° and their A_σ quickly increased, driving them outside the resonance, where bodies lose phase protection against the encounters with Neptune.

This resonant structure has been already known (Duncan *et al.* 1995, Morbidelli 1997, Gallardo and Ferraz-Mello 1998) N&R00 provided an understanding of the 2 : 3 MMR dynamics that is both detailed and global. We identified several secular and other mechanisms present inside the resonance that have a nonnegligible effects on the orbital chaos and instability of resonant objects.

In N&R00, we also discussed the observed population of the 2 : 3 Neptune MMR (Pluto and 15 Plutinos with well-determined orbits) and its relation to the Jupiter-family comets. Assuming that the 2 : 3 MMR supplies 15% of new comets needed to keep the population of the Jupiter-family comets in a steady state, we computed that at most 6×10^8 comets currently exist in the resonance.

[1] Present address: Observatoire de la Côte d'Azur, BP 4229, 06304 Nice Cedex 4, France.

[2] If $P(t)$ is the percentage of test particles escaping from the initial population in the interval $[0, t]$, then by the escape rate at time t we mean the derivative of this function. For practical reasons, we refer here and in the following to the escape rate in units of per billion years.

0019-1035/01 $35.00

In modeling the chaotic dynamics in N&R00 we used special numerical methods. The chaotic evolution (diffusion) was measured by the change of frequencies (frequency analysis) and of actions (determined as extrema of filtered orbital elements on a time-shifting window) over 45 Myr. The algorithms were described in N&R00 and we refer the reader to Section 3.2 of that paper.

One of the recent accomplishments achieved by the application of the above methods was in understanding the fine structure of the asteroid belt. It turned out that, besides the main mean-motion and secular resonances, there exist a large number of thin ($<10^{-2}$ AU) chaotic layers associated with moderate- and high-order MMRs with Jupiter (Holman and Murray 1996), three-body resonances with Jupiter and Saturn (Nesvorný and Morbidelli 1998, 1999), or exterior MMRs with Mars (Morbidelli and Nesvorný 1999). About 40% of asteroids are strongly chaotic and have the Lyapunov time (inverse of the LCE) less than 10^5 yr (Šidlichovský and Nesvorný 1999) because they are located in some thin MMR. Although the chaotic changes of eccentricity that drive resonant asteroids to planet-crossing trajectories happen on much longer time intervals, the stability over the age of the Solar System is not assured for many of them (Murray and Holman 1997, Migliorini *et al.* 1998). As we describe in Section 2, the situation in the Kuiper Belt (KB) is similar.

A detailed account of an extensive literature about the KB dynamics was given in N&R00. In brief, Duncan *et al.* (1995) computed a detailed map of stable/unstable regions in the KB by integrating a large number of orbits in the 32–50 AU semi-major axis interval. The orbits starting at perihelion distances less than 35 AU were found unstable in 4 Byr unless they were associated to some Neptune MMR (Morbidelli *et al.* 1995, Malhotra 1995, Morbidelli 1997). The orbits with the perihelion distances larger than 35 AU were found stable unless they were related to the perihelion or node secular resonances (Knežević *et al.* 1991). These findings determined the stable locations in the KB where real Kuiper Belt objects (KBOs) Could remain today. Indeed, most of the 300 comets detected at present in the KB are located in the stable regions found by Duncan *et al.* (1995). It also turned out that some of the stable regions found by Duncan *et al.* are not populated. This is the main argument that something besides the dynamical sculpting of the planets is responsible for the structure we see. The reader can refer to the review of Morbidelli (1998) for further reading on the Kuiper Belt primordial evolution and its present dynamics.

In this paper we also investigate the regular and chaotic dynamics of two large MMRs. In Section 3 we study the stability of the 1 : 2 MMR with Neptune at 47.8 AU. It is interesting to know whether this resonance is unstable over the age of the Solar System or whether the lack of observed resonant bodies (we discuss the orbits of two possible candidates for 1 : 2 MMR KBOs—1996 TR66 and 1997 SZ10—in Section 3.1) is related to some primordial mechanism. Even if Duncan *et al.* 1995) already showed that there exist some stable 1 : 2 resonant orbits, We believe that a detailed anlysis is needed to answer this question with more confidence.

The 1 : 2 and 2 : 3 Neptune MMRs should have been initially populated by an approximately equal number of objects in the scenario of smooth expansion of the planetary orbits with adiabatic capture of objects into resonances (Malhotra 1995). Hahn and Malhotra (1999) have shown that the above is not necessarily true if the planets interacted with a massive primordial disk ($\sim$50 $M_\oplus$). In this case, the semi-major axis of Neptune was subject to random kicks that made the captures in the 1 : 2 MMR inefficient. Moreover, the scenario of excitation and mass loss in the primordial KB driven by Neptune-scattered planetesimals (Petit *et al.* 1999) does not favor the resonant populations with respect to the nonresonant ones. In Section 3.3, we show what ratio of the 1 : 2 and 2 : 3 MMR populations should be expected from the respective sizes of the stable resonant cores.

In Section 4 we extend the present analysis to the 3 : 4 MMR with Neptune at 36.5 AU, where one KBO—1995 DA2—with well-determined orbit is found. This resonance was proved to be stable over the age of the Solar System by Duncan *et al.* (1995), who also showed that the chaotic evolution on the limit of the stable core of the 3 : 4 MMR mostly affects A_σ.

2. THE FINE RESONANT STRUCTURE OF THE TRANSNEPTUNIAN REGION

The initial conditions of 2800 test particles were chosen equidistantly spaced in semi-major axis ($\Delta a = 0.004$ AU) between 38.8 and 50 AU, fixing $e = 0.1$ and $i = \lambda = \varpi = \Omega = 0$, where λ, ϖ, and Ω are the mean, perihelion and node longitudes, respectively. The initial conditions of four outer planets (Jupiter to Neptune) with respect to the mean ecliptic and equinox J2000 were taken from the JPL DE403 ephemeris for the date 2/21/1997 (JD 2450500.5). The orbital evolution of massive bodies (planets) and massless test particles were computed by the symmetric multistep integrator (Quinlan and Tremaine 1990) for 10^8 yr using a 40-day step for the planets and a 200-day step for the test particles. Additionally, the variational equations were numerically integrated for the purpose of the LCE evaluation of each simulated orbit. This was done by the symmetric multistep method using the same step sizes. The variational vector was periodically renormalized following the algorithm of Benettin *et al.* (1976) in order to avoid computer overflow. The LCE estimate for each surviving test particle was computed as $\ln \Delta(t)/t$, with $t = 10^8$ yr ($\Delta(t)$ is the norm of the variational vector at time t), and is plotted as a function of the initial semi-major axis in Fig. 1c. For the test particles escaping to Neptune-crossing orbits, $\ln \Delta(t)/t$ was plotted at the time of the first Neptune crossing. The minimum value of the LCE that we can detect with the integration time span is about 10^{-7} yr^{-1}. Examples of regular, moderately, and strongly chaotic trajectories as well as the interpretation of the LCE dependence on the semi-major axis were discussed in Morbidelli and Nesvorný (1999).

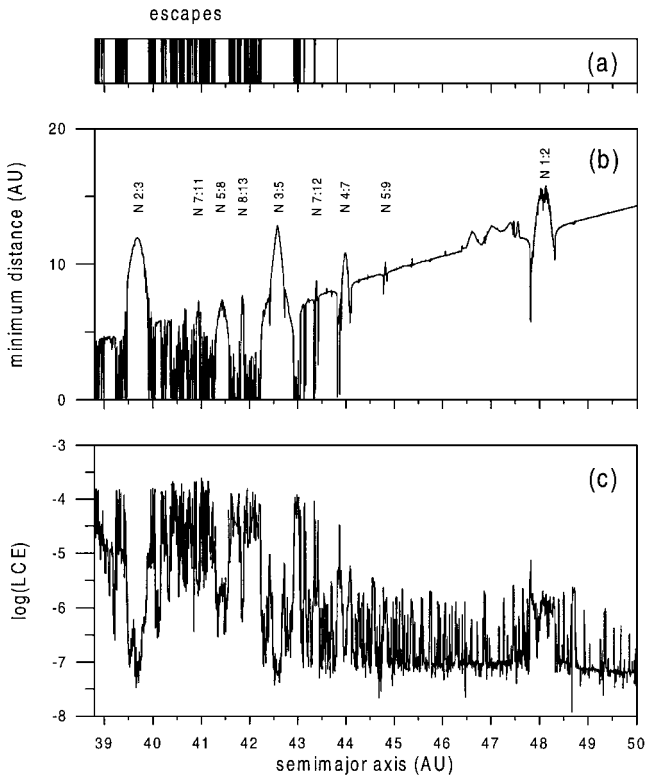

FIG. 1. A survey of LCEs in the transneptunian region: (a) a vertical line was placed at the initial a if the corresponding test particle escaped at $t < 10^8$ yr; (b) minimum distances of test particles to Neptune; and (c) LCE estimates at $t = 10^8$ yr (in logarithmic scale). The initial e and i of the 2800 integrated test particles were 0.1 and 0°, respectively. The test particles at MMRs with Neptune have their minimum distance (b) larger than the test particles in the immediate vicinity due to the resonant phase-protection mechanism. Apart from the main resonances, which may be easily identified in (c) as wide "holes" and "peaks," there are many thin peaks for $a > 44$ AU with the LCE ranging from 10^{-6} to 10^{-7} yr^{-1}. These peaks are related to thin MMRs with Neptune and Uranus. Note the rough background profile of the LCE at about 10^{-7} yr^{-1} for $a > 44$ AU, suggesting the stochasticity of all the integrated trajectories.

2.1. The Phase-Protection Mechanism in MMRs

The minimum-approach distance of each test particle to Neptune in 10^8 yr is plotted in Fig. 1b. The vertical line in Fig. 1a denotes the initial a of test particles that attained the Neptune-crossing orbits in the integrated time span; these orbits were usually ejected to heliocentric distances larger than 100 AU.

More than 50% of test particles with initial $a < 43$ AU escaped to Neptune-crossing orbits. Those that survived in this semi-major axis interval were the test particles that avoided encounters with Neptune, being locked in MMRs (labeled in Fig. 1b). This is easily seen (Fig. 1b) for the 2 : 3, 7 : 11, 5 : 8, 8 : 13, and 3 : 5 MMRs, in which the minimum distance to Neptune is kept larger than in the background.

The phase-protection mechanism is a consequence of resonant dynamics. The resonant angle σ of the $p + q : p$ MMR with Neptune is defined by

$$q\sigma_{p+q:p} = -(p+q)\lambda_{\rm N} + p\lambda + q\varpi, \qquad (1)$$

where p, q are integers and $\lambda_{\rm N}$ is the mean longitude of Neptune. $q \geq 1$ is called the order of the resonance, and the width of the resonance in a is generally proportional to the power $q/2$ of the eccentricity. For the resonances interior to the planet's orbit, $p \geq 1$, and for the outer resonances, $p \leq -2$. With exception of the MMRs with $p + q = -1$ and $p \leq -2$ (i.e., the outer resonances of the type $1 : r, r \geq 2$), which permit asymmetric librations (Beaugé 1994), the angle $q\sigma_{p+q:p}$ oscillates either about 0° (inner resonances with q odd) or 180° (inner resonances with q even, and outer resonances with $p + q \neq -1$).

Assuming a body to be locked in some outer resonance ($p \leq -2$) with the libration center at 180° and a circular orbit for the planet, Eq. (1) shows that in the limit of zero-A_σ librations the conjunctions of this body with the planet ($\lambda = \lambda_{\rm N}$) happen when $q(-\lambda + \varpi) = \pi$. This means that during conjunctions, the mean anomaly $M = (2k+1)\pi/q$, with k being an integer. For first-order resonances ($q = 1$), the true anomaly v is 180° and the object is in the aphelion of its orbit. Consequently, no encounters with the planet occur even on large-e planet-crossing orbits providing they have sufficiently small A_σ.

The minimum distance between Neptune and the low-amplitude 2 : 3 resonant orbits in Fig. 1b is about 12.2 AU. The distance at aphelic conjunctions is $a(1+e) - a_{\rm N}$, where $a = 39.45$ AU. This gives a distance of 13.3 AU for $e = 0.1$, in good agreement with the minimum distance computed in the simulation, the small difference being related to the fact that the angles initially chosen for the simulation did not permit orbits with $A_\sigma < 60°$ in the 2 : 3 resonance.

In general, at outer resonances of order $q > 1$ the resonant angle σ can librate about one of q distinct centers placed at $(2k+1)\pi/q$, k being an integer. If q is odd, then one of the centers is at 180° and the resonant phase-protection mechanism for zero-A_σ librations about this center works in the same way as for first-order resonances ($q = 1$) assuring conjunctions in aphelia. The other $q - 1$ centers are located at $\sigma \neq 180°$ and the zero-A_σ librations about these centers do not have conjunctions at aphelia. If q is even, all centers are at $\sigma \neq 180°$, and again, the conjunctions do not happen at aphelia. The conjunctions condition is $v + \varpi = \lambda_{\rm N}$, and the equation for M at conjunctions can be approximated from $v = M + 2e\cos M + \mathcal{O}(e^2)$, giving

$$M + 2\frac{p+q}{q}e\cos M = -(\sigma_0 + 2k\pi), \qquad (2)$$

where k is an integer and σ_0 is the resonant center under consideration. This equation can be solved for M by iteration, but when the eccentricity is not large, even omission of the first-order term in e gives an acceptable approximation.

In the case of the 3 : 5 MMR at $a = 42.3$ AU, the minimum distance to Neptune in 10^8 yr registered for zero-amplitude librators was 12.6 AU (Fig. 1b). This resonance has two libration centers at $\sigma = 90°$ and 270° and for both of them the conjunctions with Neptune occur at about 90° from perihelia. The distance is $a(1-e^2) - a_{\rm N}$, which for $e = 0.1$ gives 11.7 AU. Equation (2) gives somewhat larger value and still better agreement with the simulation.

In the outer resonances of the type $1:r$, $r \geq 2$, which present asymmetric librations (i.e., $q\sigma_0 \neq 180^\circ$), the phase-protection mechanism is less efficient in separating the orbits from Neptune. For example, in the 1 : 2 Neptune MMR ($a = 47.8$ AU) with $e > 0.3$ the two centers are placed at about $\pm 68^\circ$ (they vary from $\pm 71^\circ$ for $e = 0.3$ to $\pm 66^\circ$ for $e = 0.4$) so that the conjunctions with the planet can happen relatively close to the perihelion. For $e > 0.37$, where the 1 : 2 resonant orbits are Neptune-crossing, the potentially stable orbits must necessarily have the maximum excursions of σ less than 65°.

For $e = 0.1$, the two centers of the 1 : 2 MMR are at $\sigma_0 = \pm 102^\circ$. Assuming that minimum distance happens at conjunction of the two bodies, we compute it by crude approximation of Eq. (2) as $a(1 - e^2)/[1 + e\cos v] - a_N$ with $v = M = 102^\circ$. This gives a minimum distance of 18.2 AU, which is only somewhat larger than the 16 AU determined numerically (Fig. 1b).

2.2. *Taxonomy of MMRs*

None of the test particles starting with $a > 44$ AU escaped to the Neptune-crossing space (Fig. 1a). Having initially larger a and $e = 0.1$ produced sufficiently large perihelion distances (initially >39.6 AU) that even the nonresonant orbits are well separated from Neptune. Test particles initially placed close to the borders of the 1 : 2 MMR ($a = 47.8$ and 48.3 AU) had their minimum distances decreased by as much as 5 AU with respect to the background level; this happened because their e increased by more than 0.1 on 10^8 yr. The chaos near borders of the 5 : 9 and 1 : 2 MMRs destabilized the orbits that, for $e = 0.1$ and $a > 44$ AU, were found unstable on 4×10^9 yr by Duncan *et al.* (1995). As mentioned earlier, the strength of MMRs is proportional to the eccentricity so that at $e = 0.15$, where Duncan *et al.* (1995) identified additional instabilities between the 4 : 7 and 1 : 2 resonances, other MMRs are important (namely 7 : 13, 8 : 15, and 9 : 17).

The LCE estimates (Fig. 1c) show the complex chaotic structure of the transneptunian region. For $a > 44$ AU the plot presents many peaks rising from the background level. We have checked that the main peaks correspond to chaotic regions where the computation of the LCE has converged to a nonzero limit value (see Morbidelli and Nesvorný 1999). The background value of about 10^{-7} yr^{-1} is dictated by the limited integration time span; when the latter is increased, the background level generally decreases. The roughness of the background level in Fig. 1c suggests the general nonintegrability of the motion as discussed for the asteroid belt by Morbidelli and Nesvorný (1999). For $a < 43$ AU, the only orbits with LCE $\sim 10^{-7}$ yr^{-1} are those at centers of the 2 : 3 and 3 : 5 MMRs.

The maximum LCE is nonzero in the 7 : 11 ($10^{-5.6}$ yr^{-1}), 5 : 8 ($10^{-5.8}$ yr^{-1}), and 8 : 13 ($10^{-5.8}$ yr^{-1}) MMRs with Neptune, which appear as holes in the more chaotic background in Fig. 1c. Indeed, most orbits placed with the semi-major axes close to these resonances were found unstable over the age of the Solar System by Duncan *et al.* (1995).

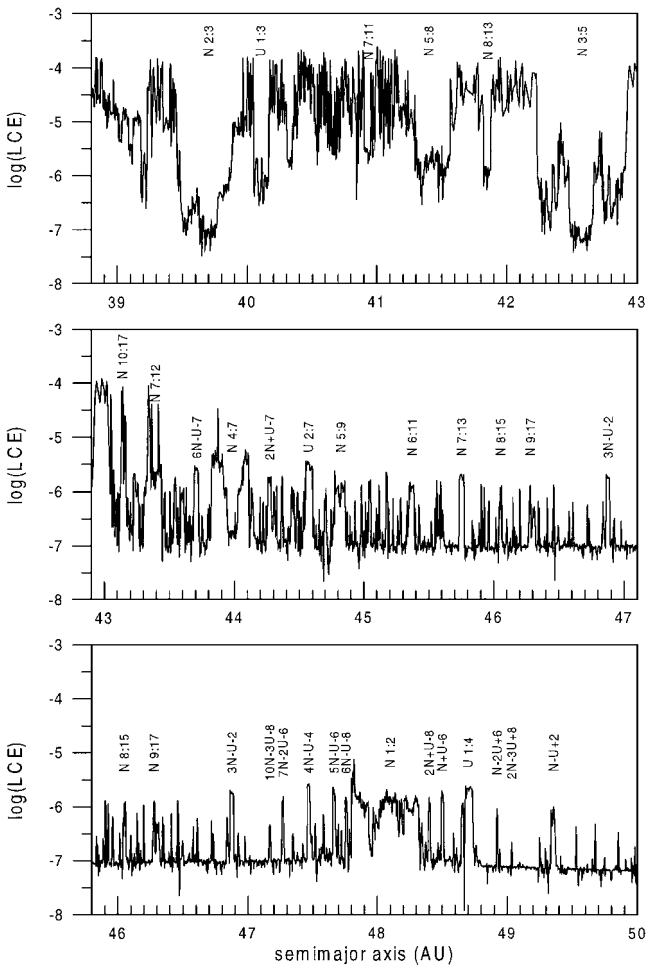

FIG. 2. Enlarged plot of Fig. 1c with the main MMRs being labeled. See text for the notation. Note that the density of resonances increases with decreasing a. Most of the MMRs for $a > 46.5$ AU are the three-body resonances with Neptune and Uranus. The semi-major axis range on the x axis overlaps in the second and third panels.

In analogy to the asteroid belt, most features in the LCE dependence on a observed in Fig. 2 (enlarged from Fig. 1c) are related to MMRs; the secular resonances have lower LCEs due to their longer libration periods. The only exception is the interval 40–42 AU where the three secular resonances (ν_8, ν_{17}, and ν_{18} overlap (Knežević *et al.* 1991), causing escapes in 10^8 yr.

Some of the MMRs are labeled in Fig. 2. These associations[3] were found by short integrations of the test particles having large LCE estimates and by the computation of angles with all resonant combinations that come into question for the given range of semi-major axes. The libration of one resonant angle was usually easily found and the corresponding resonance labeled. The

[3] There is a small shift between the a of the large LCE peaks in Fig. 2 and the mean a of the associated resonances, which is a consequence of short-periodic oscillations in a induced by Jupiter having a 11.8-yr period and a 0.6–0.8 AU amplitude. Consequently, the initial a of a given resonance in our experiment is about 0.25 AU larger than the mean resonant a.

notation in Fig. 2 has the following rules: N$r:s$ is the Neptune resonance with the resonant angle $r\lambda_N - s\lambda + (s-r)\varpi$, where $s > r \geq 1$ are integers; U$r:s$ is the Uranus resonance with the resonant angle $r\lambda_U - s\lambda + (s-r)\varpi$, where λ_U is the mean longitude of Uranus; and the resonances labeled as n_NNn_UUn, with n_N, n_U, and n being integers, are the three-body resonances with the resonant angle $n_N\lambda_N + n_U\lambda_U + n\lambda - (n_N + n_U + n)\varpi$ (Nesvorný and Morbidelli 1998).

While for $a < 46.5$ AU the largest peaks are associated with the MMRs with Neptune, for $a > 46.5$ AU most peaks correspond to the three-body resonances with Neptune and Uranus. We remark that the latter are placed on both sides of the 1 : 2 Neptune MMR according to a peculiar structure, which is a consequence of Uranus and Neptune being close to the mutual 1 : 2 mean-motion resonance: the angle $\lambda_U - 2\lambda_N$ circulates with a negative derivative and a period of about 4230 yr. The sum of a multiple of this angle, $j(\lambda_U - 2\lambda_N)$, j being an integer, with a multiple of the resonant angle of the 1 : 2 Neptune MMR, $k(\lambda_N - 2\lambda)$, k being an integer, gives $(k-2j)\lambda_N + j\lambda_U - 2k\lambda$. This last expression, with appropriate values of k and j, gives the resonant combinations of all 12 labeled MMRs with $a > 46.5$ AU (including the 1 : 4 resonance with Uranus at $a = 48.7$ AU for $k = 2$ and $j = 1$). As the three-body MMRs appear in the perturbation approach at the second order in planetary masses (Nesvorný and Morbidelli 1999), the above observation gives a hint on what combinations of the perturbation harmonics give rise to the identified three-body resonances.

Figure 2 shows that chaotic regions become denser with decreasing a. In fact, the location of MMRs of a given order become denser approaching Neptune, and the sizes of the coefficients of the resonant harmonics increase with decreasing distance from the main perturbing body. This reflects in the number of visible peaks. The height and width of each peak is roughly proportional to the square root of the size of the coefficient of the corresponding resonant harmonic (Murray and Holman 1997, Nesvorný and Morbidelli 1999).

2.3. *The Resonant-Driven Evolution of Eccentricity*

What are the possible dynamical consequences of the complex resonant structure of the transneptunian region revealed by Fig. 2? In analogy to the asteroid belt, each thin MMR represents a track at a given semi-major axis where the eccentricity and inclination chaotically change on long time periods (Murray and Holman 1997). We give an example of this chaotic evolution in Fig. 3.

The numerical simulation was performed with four outer planets (Jupiter to Neptune) and 101 test particles. The initial positions of planets were taken from JPL DE403 ephemeris for the date 1/1/1998 (JD 2450814.5) with respect to the invariable plane of LONGSTOP 1B simulation (Nobili *et al.* 1989). The initial conditions of test particles were chosen as equidistantly spaced in the interval $37 \leq a \leq 39$ AU ($\Delta a = 0.02$ AU), with $e = 0.01$ and $i = 2^\circ$. The initial angles of test particles were

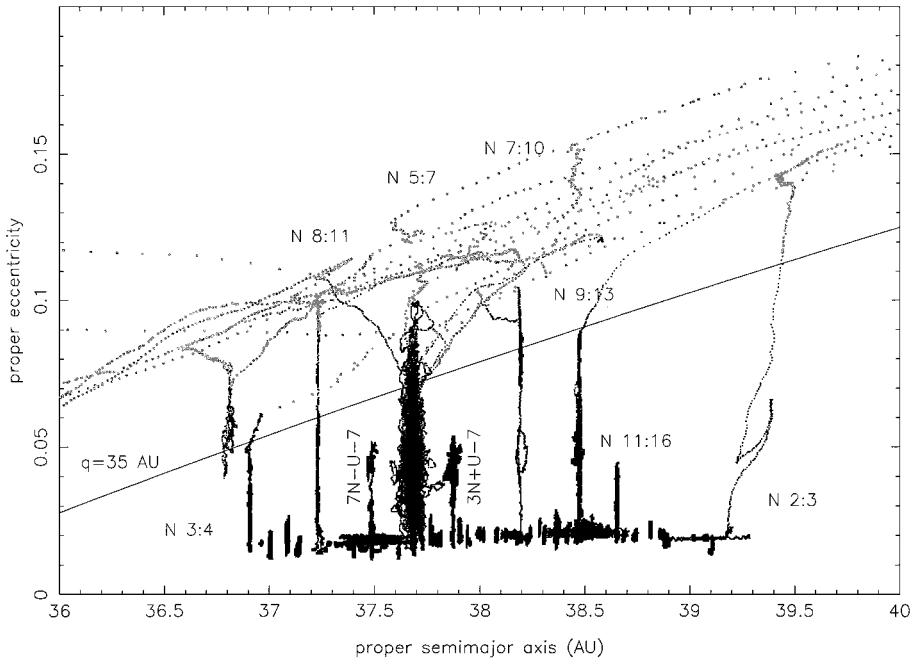

FIG. 3. The chaotic evolution of orbits initially at 37–39 AU with low e and i. The dark points denote the trajectory of a test particle before it first comes to a distance of 2 AU from Neptune's orbit. The large gray symbols show the trajectory after this moment. Sixteen percent of integrated test particles were transferred to Neptune-crossing orbits in 4×10^9 yr. The low-e orbits were modified by slow chaotic diffusion in e driven by labeled MMRs with Neptune (and Uranus). The line of proper $q = 35$ AU is shown for reference. Note that the proper a of all test particles stays almost constant under this line (excluding that at $a > 39$ AU, which started close to the left border of the 2 : 3 MMR). The changes of proper a in the part of the trajectory denoted by gray symbols is due to the effect of close encounters with Neptune.

chosen randomly from a uniform distribution between 0 and 2π. The orbits of planets and test particles were propagated in time using the `swift_rmvs3` integrator (Levison and Duncan 1994) with a 1-yr time step. The total integration time was 4×10^9 yr.

The orbital elements of test particles were averaged over a shifting window of 10 Myr using the same procedure as Morbidelli and Nesvorný (1999, their Eq. (1)). The 10-Myr interval is long enough to cancel out all important quasi-periodic oscillations of orbital elements. Therefore, in the case of local integrability of the equations of motion, the orbital elements defined by the above averaging do not change with time. They are integrals of the motion and are usually called *proper elements*. Conversely, the change of proper elements with time reveals non-quasi-periodic evolution, i.e., *chaotic diffusion*. For purposes of Fig. 3, the proper elements were computed every 10^5 yr.

The dark points in Fig. 3 denote the trajectory before it first became Neptune-grazing (if ever), i.e., before the test particle's osculating perihelion first happened to be close to Neptune's orbit. We choose a threshold distance of 2 AU. Larger gray symbols show the evolution of the trajectory after this instant. The proper perihelion line $q = 35$ AU is shown for reference as an approximate limit above which Neptune dominates the motion. Note however that this is only a rough criterion due to the secular oscillations of osculating eccentricities.

The simulation resulted in 16 escapes to Neptune-crossing orbits. The escapes of two test particles at the extreme left of the integrated a interval happened at the chaotic border of the 3 : 4 Neptune MMR (centered at 36.48 AU). The particle escaping at the extreme right of the integrated interval was initially placed near the chaotic border of the 2 : 3 MMR (centered at 39.45 AU). The remaining 13 particles that became Neptune-crossers during the integration time span evolved from their respective initial locations (initial proper $e < 0.02$) due to a gradual enlargement of the proper e. Such enlargement happened at the positions of second- and higher-order MMRs with Neptune and at locations of three-body resonances with Neptune and Uranus. While the proper a of these particles stayed almost constant at this stage of orbital evolution (dark points), the resonant-driven chaotic diffusion enhanced the objects' proper e; above the line of proper $q = 35$ AU, Neptune close encounters became important. Under the effect of Neptune encounters, these bodies started to random-walk in a, roughly following the curves of invariant Tisserand parameter with respect to Neptune (Valsecchi and Manara 1997). This second stage of orbital evolution was much shorter and the test particles normally reached heliocentric distances larger than 100 AU in a time interval typically not exceeding 10^8 years, at which point they were removed from the simulation. The integration of all 16 particles escaping to Neptune-crossing orbits were stopped before $t = 4 \times 10^9$ yr.

Most of the escaping test particles (9) did so via the 5 : 7 Neptune MMR ($a = 37.68$ AU). In fact, these were all particles that had the initial proper a in the range 37.6–37.75 AU. The size of this interval is about the size of the 5 : 7 MMR determined in the circular planar problem for $e = 0.02$ (=mean initial proper eccentricity of nine escaping particles), which is approximately 0.12 AU. The crossing time (the time elapsed from $t = 0$ to the first crossing of Neptune's orbit) varied between 322 and 1469 Myr with a mean value of 666 Myr. After becoming Neptune grazers, particles were deactivated when some stopping criteria were satisfied (either the heliocentric distance being larger than 100 AU or the test particle being closer than 0.01 Hill radius to any planet), after on average 13 Myr.

Other escapes (one per resonance) occurred at locations of the 8 : 11 ($a = 37.23$ AU, crossing time 641 Myr), 7 : 10 ($a = 38.19$ AU, 620 Myr), and 9 : 13 ($a = 38.47$ AU, 1419 Myr) resonances. The longer crossing time at the 9 : 13 MMR is due to its higher order (4) and smaller chaotic diffusion rate. (See references below). The eccentricity was significantly excited at the 11 : 16 Neptune MMR ($a = 38.654$ AU) and also at the three-body resonances with Neptune and Uranus: $7\mathrm{N} - \mathrm{U} - 7$ (resonant angle, $7\lambda_\mathrm{N} - \lambda_\mathrm{U} - 7\lambda + \varpi$) and $3\mathrm{N} + \mathrm{U} - 7$ ($3\lambda_\mathrm{N} + \lambda_\mathrm{U} - 7\lambda + 3\varpi$). These latter resonances are placed at 37.487 and 37.878 AU, respectively.

The escape mechanisms from the low-e region 37–39 AU shown in Fig. 3 are analogous to those of inner belt asteroids to Mars-crossing orbits (Migliorini *et al.* 1998, Morbidelli and Nesvorný 1999). The analytic estimates of the resonant size, LCE, and diffusion rate at the MMRs in the asteroid belt (Murray and Holman 1997, Murray *et al.* 1998, Nesvorný and Morbidelli 1999) apply also to the KB.

The speed of chaotic evolution at a MMR depends on its strength (Murray and Holman 1997): for some resonances (e.g., on the borders of the 7 : 12 Neptune MMR located at about 43.4 AU) the speed of the chaotic diffusion is enough to enlarge the initial e to the critical value above which the orbit becomes Neptune grazing and the body escapes in 10^8 yr (Fig. 1). There thus must be many test particles escaping from weaker MMRs on longer time intervals. Hence we believe that the thin MMRs are responsible for escapes in many narrow regions in a found by Duncan *et al.* (1995) for $45 < a < 47$ AU. Moreover, this also means that if there were not not enough new bodies injected into the resonances (by collisions or mutual interaction between the KBOs), escaping bodies must open narrow gaps or at least cause local density reductions at the resonant semi-major axes.

For a weak MMR and the resonant body with initially small e, the process of slow chaotic diffusion normally results only in a moderate change of e (and i) over the age of the Solar System. Consequently, this could have caused a chaotic "processing" of KBOs in e (and i) and an alteration of the original characteristics of the KB. By this we mean that the KB is not dynamically "frozen." Whatever structures has been formed in it (collisional families, for example) have dispersed with time and should have depended with other slowly diffusing (in e and i) resonant bodies. The first traces of such a process are being recently revealed on the much better known distribution of asteroids in the main belt (Milani and Nobili 1992, Morbidelli and Nesvorný 1999).

Assuming a uniform distribution of KBOs in the interval $45 < a < 47$ AU and $e = 0.1$, the number of *resonant* objects must be proportional to the total phase space volume occupied by

resonances. In Fig. 2 we can identify about 80 peaks with LCE $> 10^{-6.8}$ yr^{-1} in this interval. These peaks have a total width of about 0.512 AU, which means that about 26% of KBOs at $45 < a < 47$ AU and $e = 0.1$ must be chaotic with LCE $> 10^{-6.8}$ yr^{-1}. Therefore, a significant chaotic evolution in e (and i) may be expected for this part of the KB.

Outside the MMRs (Fig. 3), the proper elements of test particles almost do not change. The small variation of proper a and e for nonresonant orbits validates our calculation of proper elements as 10-Myr averages; these orbits are expected to be close to regular. Note that there is no tendency to alter the proper a, and thus it is practically impossible for the initially nonresonant particles to reach one of the diffusion tracks at resonances.

This result confirms the conclusion of Duncan *et al.* (1995) that under the perturbations of four outer planets most low-e orbits with initial a between the outer edge of the 3 : 4 Neptune MMR (37 AU) and the inner edge of the 2 : 3 MMR (39 AU) are stable over 4×10^9 yr. Because of this orbital stability, one would expect that there exist KBOs with $37 < a < 39$ AU, $q > 35$ AU, and $i < 10^\circ$. Nevertheless, observations have not provided a single object (among 63 known KBOs with good orbits in September 1999) with orbital elements in this interval.[4] Duncan *et al.* (1995) suggested that some mechanism other than the long-term gravitational effects of four outer planets must have cleared it. The effect of Neptune-scattered large planetesimals (Petit *et al.* 1999), sweeping MMRs (Malhotra 1995), or sweeping secular resonances (H. F. Levison *et al.* 1999, preprint) are three different possibilities of how this might have been achieved during the primordial stage of the KB formation.[5]

[4] The recent recovery of 1998 SN165 (Gladman *et al.* 2000b) suggests that this object has the orbital elements $a = 38.1$ AU, $e = 0.05$, and $i = 5^\circ$. This indicates that the concerned region is not completely void of objects and probably hosts a considerable number of KBOs. Still, based on the discovery rate, the region is underpopulated in comparision with other stable places in the KB.

[5] We have also checked another possibility and in this context recall the particular geometry of Pluto's orbit: the argument of Pluto's perihelion oscillates around 90° with an amplitude of 22°. This, together with the equation of ellipse,

$$r = \frac{a(1-e^2)}{1+e\cos v}, \tag{3}$$

where r and v are the heliocentric distance and true anomaly of Pluto, $a = 39.45$ AU and $e = 0.25$, shows that Pluto intersects the ecliptic plane close to $v = \pm 90^\circ$ at a heliocentric distance of about 37 AU. Consequently, the low-e and low-i objects with $a \sim 37$ AU may encounter Pluto when it passes through ecliptic whenever the phasing of orbital revolutions is correct. However, the numerical simulation with five planets (Jupiter to Pluto) showed that Pluto's effect over the age of the Solar System is almost negligible in the interval 37–39 AU, the escape rate being the same as in the simulation with four planets. This is due to the fact that Pluto's inclination (17.2°) and eccentricity (0.25) determine a relatively high velocity at intersection with the orbit at $a = 37$ AU and $e = i = 0$:

$$V = 2\pi\sqrt{2\frac{1-\cos i_{\rm P}}{a}} = 0.3 \text{ AU/yr} = 1.5 \text{ km/s}, \tag{4}$$

and the deflection of passing trajectories—proportional to V^{-2}—is small. In fact, Pluto gravitational sweeping has a negligible effect on the distribution of objects in the KB (Gladman *et al.* 2000a), with the exception of moderately and high-inclined Plutinos (Nesvorný *et al.* 2000).

3. THE 1 : 2 MMR WITH NEPTUNE

The 1 : 2 resonant angle $\sigma_{1:2} = \lambda_{\rm N} - 2\lambda + \varpi$ oscillates—unlike in the case of most other MMRs—around a center that is neither 0° nor 180°. Such a case is usually referred to as an *asymmetric* libration, and is found exclusively in the 1 : 1 MMRs (tadpole orbits) and the MMRs exterior to a planet of the type 1 : 2, 1 : 3, 1 : 4, etc. (Beaugé 1994, Morbidelli *et al.* 1995). Consequently, the range of A_σ accessible to stable resonant librations in the 1 : 2 MMR with Neptune is smaller.

In the following experiment, the initial angles of test particles were chosen so that $\sigma_{1:2} = \sigma_0(e)$, $\varpi = \varpi_{\rm N}$, and $\Omega = \Omega_{\rm N}$, where $\sigma_0(e)$ is the asymmetric libration center for given e. Figure 4a shows $\sigma_0(e)$ computed by a semi-numerical method in the restricted three-body model with Neptune on a circular and planar orbit. Figure 4b shows an analytically computed maximum possible $A_\sigma(e)$ of tadpole orbits. For A_σ exceeding this value, the motion happens on horseshoe trajectories.

We have run simulations for two sets of initial conditions:

(1) 707 test particles with $47.5 \le a \le 48.5$ AU ($\Delta a = 0.01$ AU), $e = 0.04$, 0.1, 0.2, 0.25, 0.3, 0.35, 0.4 (101 test particles at each e) and $i = 5^\circ$;

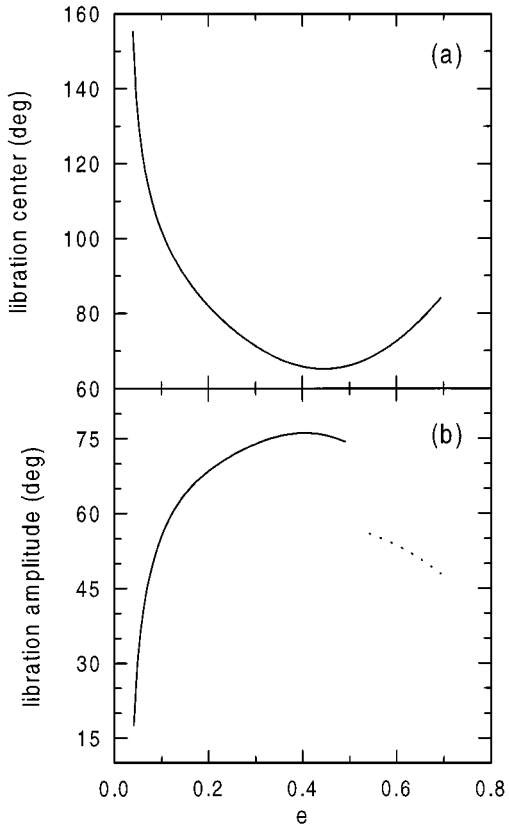

FIG. 4. (a) The asymmetric center (σ_0) of the 1 : 2 MMR as a function of eccentricity. The other center is placed symmetrically in the interval $[-\pi, 0]$. (b) The maximum amplitude of tadpole orbits determined as half-width of the libration island enclosed by separatrices. The discontinuity at $e = 0.5$ is due to the change in the resonant topology introduced by collisions with Neptune. The dashed line approximates the half-width of the tadpole island for $e > 0.5$.

(2) 606 test particles with $a = 47.95$ AU, $0 \le e \le 0.4$ ($\Delta e = 0.004$) and $5 \le i \le 30^\circ$ ($\Delta i = 5^\circ$, 101 test particles at each i).

In the first set we sampled the resonant orbits with small i; the dynamics at larger i was explored in the second set.

As in N&R00, test particles were numerically integrated with four outer planets (Jupiter to Neptune) for 10^8 yr by the symmetric multistep integrator. The initial conditions of the planets were taken from JPL DE403 ephemeris for the date JD 2449700.5 with respect to the mean ecliptic and equinox J2000. The time steps of 40 days for the planets and 200 days for the test particles were used. A smoothing filter was applied to $a \exp \iota\sigma$, $e \exp \iota\varpi$ and $i \exp \iota\Omega$ ($\iota = \sqrt{-1}$). This procedure suppressed periods smaller than 5000 yr. See N&R00 for a more detailed description of the experimental setup.

3.1. Regular and Chaotic Dynamics for Small e

Estimate of the maximum LCE and the minimum distance to Neptune in 10^8 yr are plotted as the set (1) of initial conditions in Fig. 5. The color coding in Fig. 5a is the same as that used in N&R00: test particles escaping within the integration time span are shown in yellow while test particles with smallest LCE are shown in blue. In Fig. 5, we have compensated the scale on the x axis for the short-periodic variations of the semi-major axis with a shift of 0.18 AU in a, so that the test particles with $A_\sigma \sim 0$ are near the true resonant center at 47.8 AU.

In Fig. 5a, we plot the libration centers and separatrices of tadpole orbits (bold vertical line at 47.8 AU and bold lines joining each other at $e = 0.04$ and delimiting the "V"-shaped resonant region). The exterior bold lines are the limits of horseshoe orbits. The Kozai resonance is shown by the thin full line. We have computed its location from $f_\varpi - f_\Omega = 0$, where $f_\varpi(a, e)$ and $f_\Omega(a, e)$ were numerically computed in our experiment. The Kozai resonance intersects the libration center of the 1 : 2 Neptune MMR at $e \sim 0.38$, but we were unable to plot its location at $0.35 < e \le 0.38$, because our initial conditions did not sample this interval.

The dashed line in Fig. 5a shows the 5 : 1 commensurability between the resonant frequency and the frequency of the angle $\lambda_U - 2\lambda_N$. The 4 : 1 commensurability between the same angles is at larger eccentricities and its location at $e = 0.35$ is indicated by two arrows. The 4 : 1 three-body resonance has the same "U"-shaped form as the 5 : 1 resonance and intersects the libration centers of the 1 : 2 Neptune MMR at $e \sim 0.32$.

From 191 KBOs currently registered in the Asteroid Orbital Elements Database of the Lowell Observatory (ftp://ftp.lowell.edu/pub/elgb/astorb.html), six objects are close to the 1 : 2 Neptune MMR ($46.5 < a < 49$ AU). Computing the smoothed orbital elements (i.e., the orbital elements from which the short periodic variations has been removed—see N&R00) of these objects, we find that only one object—1997 SZ10—falls within the interval of a and e shown in Fig. 5. A pair of two-headed vertical arrows has been placed in this figure, indicating the extrema of filtered a and e of 1997 SZ10 (determined from a numerical integration of its orbit over 10^7 yr). This figure indicates that this object is on a horseshoe orbit with $A_\sigma \sim 150^\circ$, which is unstable on 10^8 yr. However, there is a large uncertainty in the semi-major axes of this and the other five bodies that were computed from small observational arcs, so that conclusions would be premature. In contrast, we believe from the following reasons that two of the above six objects are on stable resonant orbits.

Our argument is based on the orbital angles of 1997 SZ10 and 1996 TR66, which according to E. Bowell (personal communication) are quite determinate,[6] conversely to the semi-major axes, which have 1-σ uncertainties of $\sim$0.07 and $\sim$0.31 AU, respectively. It is interesting to note that the present value of $\sigma_{1:2}$ of 1997 SZ10 (at JD 2449700.5) is -69°, which is almost exactly the value of the second resonant center $\sigma_0(e) \sim -67^\circ$ at $e = 0.36$ (Fig. 4a). This coincidence is quite surprising because the orbital angles were not deliberately chosen to put 1997 SZ10 close to the libration center. This shows that it is quite possible that this object is in fact a stable resonant body with the semi-major axis erroneously (by some 0.2–0.3 AU) determined from observations. Moreover, the second object—1996 TR66—which falls close to the 1 : 2 Neptune MMR has $\sigma_{1:2} = -62^\circ$, again very close to the corresponding $\sigma_0(e)$ for $e \sim 0.38$.[7] This should not be a mere coincidence because the probability that $\sigma_{1:2}$ of a discovered object is within 5° from to one of the libration centers (as it happens for both 1997 SZ10 and 1996 TR66) is 1 in 18. Indeed, for nonresonant objects, $\sigma_{1:2}$ circulates and receives values between 0° and 360° with equal probability. Consequently, at the time of observation, the nonresonant bodies would be uniformly spread in $\sigma_{1:2}$ between 0° and 360°.

As we will show in Section 3.3, the stable resonant objects with $e \sim 0.3$ are expected to move within $\pm 30^\circ$ from $\sigma_0(e = 0.3)$. At $e \sim 0.36$–0.38, where the limit of the stable tadpole motion is smaller than at $e = 0.3$ (Fig. 5), the stable resonant objects must always stay closer than 10°–20° to σ_0, exactly at a place where 1997 SZ10 and 1996 TR66 are currently located. Moreover, if both objects are resonant bodies, they probably also fall into the Kozai resonance since, at present, $\omega = 341^\circ$ for 1997 SZ10 and $\omega = 311^\circ$ for 1996 TR66, and for $e = 0.38$ the stable ω libration happens around $\omega_0 = 325^\circ$ (Section 3.4).

On the other hand, we still cannot exclude the possibility that 1997 SZ10 and 1996 TR66 are captured scattered disk objects

[6] The assumed orbital elements of 1997 SZ10 and 1996 TR66 on 8/10/1999 (JD 2451400.5) are $a = 48.6752$ AU, $e = 0.37419$, $i = 11.768^\circ$, $M = 11.393^\circ$, $\omega = 341.122^\circ$, $\Omega = 9.422^\circ$, and $a = 47.3227$ AU, $e = 0.38081$, $i = 12.3906^\circ$, $M = 35.732^\circ$, $\omega = 311.325^\circ$, $\Omega = 342.993^\circ$, respectively. Note also that B. Marsden give similar solutions for the orbital angles of 1997 SZ10 and 1996 TR66.

[7] The uncertainty domains of the orbital elements are such that the true semi-major axes of 1997 SZ10 and 1996 TR66 may be as far as 0.4 and 2 AU from their current nominal orbits, respectively, without significantly alternating their orbital angles (J. Virtanen and K. Muinonen, personal communication).

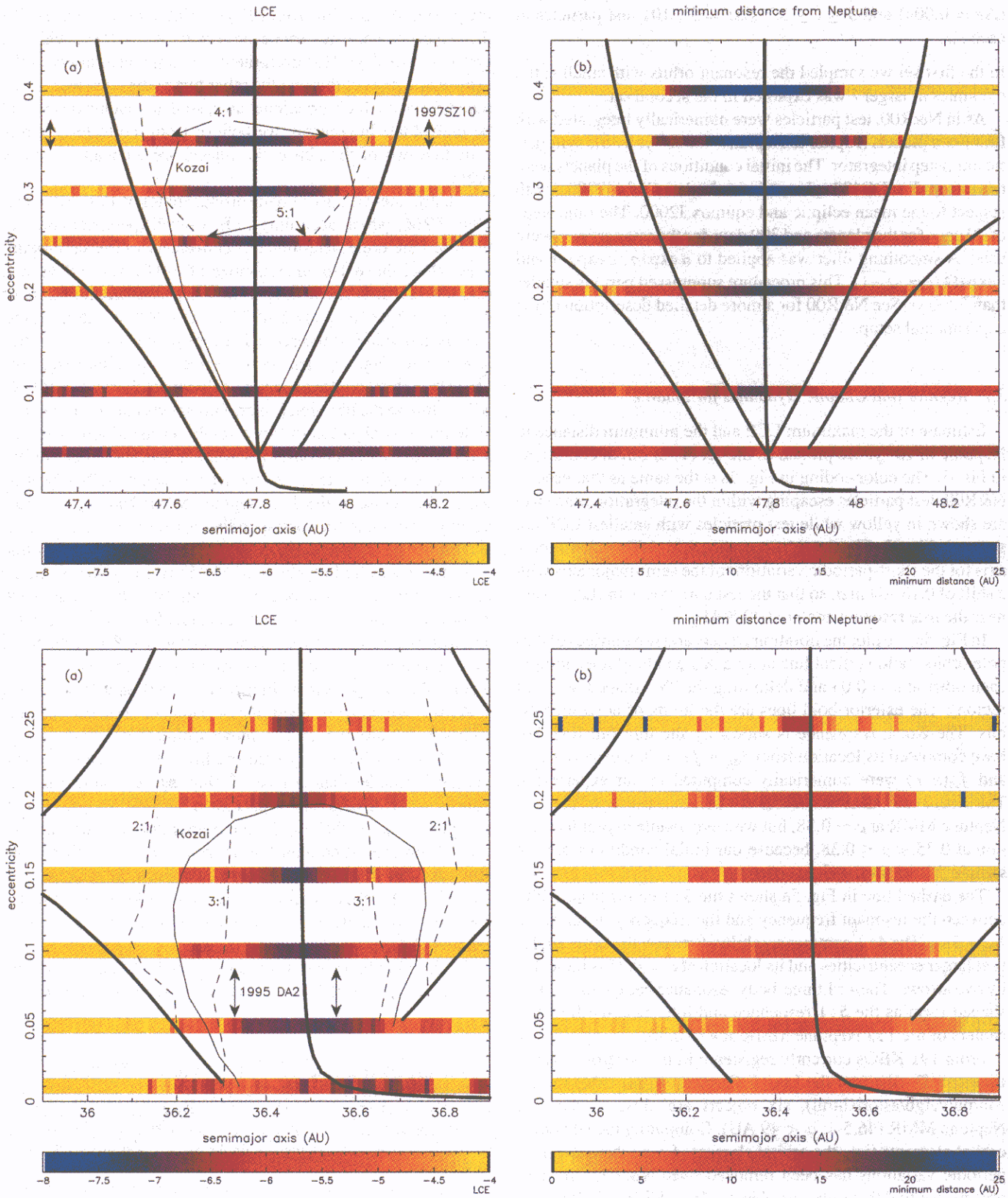
LCE
minimum distance from Neptune
(a)
(b)
4:1
1997SZ10
Kozai
5:1
eccentricity
semimajor axis (AU)
LCE
minimum distance (AU)
2:1
3:1
1995 DA2

(Duncan and Levison 1997). Such bodies spend about 20% of their lifetimes within 5° from σ_0 (H. Levison, personal communication). So, the probability of seeing captured objects where 1997 SZ10 and 1996 TR66 are currently located is small but not completely negligible.

In Fig. 5a, the LCE is smaller than $\sim 10^{-7}$ yr^{-1} in the central region of the 1 : 2 MMR, which shows orbital regularity comparable to that of the central region of the 2 : 3 MMR (N&R00, their Fig. 2). The central region is the widest for $e = 0.3$, where it accounts for almost 0.4 AU in a. This is much less than the resonant size computed by Malhotra (1996) for the same e in the circular and planar model with Neptune. Our computation shows that the central region of the 1 : 2 MMR at $e = 0.3$ is similar in size to the stable region of the 2 : 3 MMR.

For smaller and larger e, the region of small LCE of the 1 : 2 MMR shrinks. There is a large gradient of the period of σ with respect to e so that at $e = 0.1$, the libration frequency is comparable to the perihelion and node frequencies. For $e < \sim 0.1$, the tadpole region is very narrow and the $A_\sigma \sim 0$ tadpole orbits are destabilized on short time scales. These orbits later evolve alternating between circulation and horseshoe regimes, with short intermittences of tadpole librations. The resonant motion at $e \sim 0.4$ and small A_σ is moderately chaotic (LCE $\sim 10^{-6.5}$ yr^{-1}). This is not because of the effect of Neptune encounters (Fig. 5b) but rather an influence of the Kozai resonance. In Section 3.4, we show by long-term numerical simulation that the resonant motion is unstable over 4×10^9 yr when $e > \sim 0.4$.

One can also note in Fig. 5a that the chaos is enhanced at the 4 : 1 and 5 : 1 three-body resonances, where LCE $\sim 10^{-5.8}$ and $\sim 10^{-6.2}$ yr^{-1}, respectively. These values are similar to those found at the same three-body resonances in the 2 : 3 Neptune MMR (N&R00, their Fig. 2a). Here however, the resonant positions are quite different (4 : 1 resonance is "inner" to 5 : 1 resonance), with a shape following convex lines (5 : 1 is shown by dashed line in Fig. 5a). This particular configuration is related to the fact that inside the asymmetric island of the 1 : 2 MMR, the libration period increases when approaching the separatrices while at the 2 : 3 MMR, the libration period decreases when approaching to the separatrices.

The horseshoe orbits in the 1 : 2 MMR are generally chaotic ($\ln \Delta(t)/t = 10^{-5}$–$10^{-6}$ yr^{-1} with $t = 10^8$ yr). Although we have not investigated the sources of this chaos in detail, one reason could be the large period of σ for horseshoe orbits (roughly double of the period for tadpole orbits for the same e). Thomas and Ferraz-Mello (2000, in preparation) have shown that the secondary and secular resonances are frequently present in the horseshoe regime of the 1 : 1 MMR with a planet.

Figure 6 shows the measures of chaotic evolution of the orbital elements, δA_σ (a), δe (b), and δi (c), and of frequencies, δf_σ (d), δf_ϖ (e), and δf_Ω (f). These quantities have been determined in the same way as in N&R00 (their Eqs. (2)–(4)). δA_σ, δe, and δi are the chaotic changes of orbital elements over 45 Myr. δf_σ, δf_ϖ, and δf_Ω are the relative changes of frequencies over the same time interval.

Comparing Figs. 5 and 6, one can see the correlation between the values of the LCE and the measures of chaotic evolution of orbital elements. For example, the orbits are very stable in the core of the 1 : 2 MMR where the LCE is small. Figure 6 is nevertheless more rigorous concerning the orbital stability/instability, specifically:

(1) The most stable place in the 1 : 2 MMR is at $e = 0.3$, where $\delta A_\sigma = 0.1°$ per 45 Myr for $A_\sigma < 30°$ (Fig. 6a). There the expected change of A_σ over 4.5 Byr is 1°. Even if $e = 0.3$, the maximum A_σ available for tadpole orbits is 70° (Fig. 4b), for $A_\sigma > 30°$, such orbits are already unstable and escape from the resonance.

(2) Stable tadpole motion practically does not exist for $e < 0.1$ and for $e > 0.4$, where $\delta A_\sigma > 1°$ per 45 Myr. While in the former case, the test particles may still survive several billion years on horseshoe orbits, because their e is small, in the latter case, the test particles are efficiently removed from the resonance by encounters with Neptune.

(3) The chaotic structure of the resonant region at intermediate eccentricities ($0.1 < e < 0.4$) is complex. Apart from the resonances shown in Fig. 5a, there are the $2(g - s_8) = 0$ secular resonance at $e \sim 0.2$ and the $2g - s - s_8 = 0$ secular resonance at $e \sim 0.3$, for $A_\sigma \sim 0$ (g and s are the perihelion and nodal frequencies of test particle, and $g_8 = 0.673$ arcsec yr^{-1} and $s_8 = -0.691$ arcsec yr^{-1} are the perihelion and nodal frequencies of Neptune).

(4) The horseshoe orbits for $e > \sim 0.3$ are generally unstable on 10^8 yr (yellow in Figs. 5a and 6a–6c). Also for $e < 0.3$, the chaotic evolution of horseshoe orbits is large (Figs. 6a–6c) and many objects are expected to escape from the resonance by increasing their orbital e.

FIG. 5. The maximum LCE (a) and minimum distance to Neptune (b) computed for $i = 5°$ and several a, e in the 1 : 2 MMR with Neptune (set (1) of initial conditions). The x-axis scale was corrected for the difference between initial osculating and mean resonant semi-major axis due to short-period perturbations. The resonant center and the limits of tadpole and horseshoe orbits are shown by bold lines. Inner resonances are denoted by thin lines (the location of the 4 : 1 three-body resonance is indicated only for $e = 0.35$). The current orbital elements of 1997 SZ10 would indicate a horseshoe orbit unstable on 10^8 yr (the two-headed vertical arrows delimit the maximum and minimum values of its a and e on 10^7 yr, but see the discussion in text). In the central resonant space, LCE $< 10^{-7}$ yr^{-1}. The minimum distance to Neptune is larger than 20 AU for $A_\sigma \sim 0$ and $e > 0.25$.

FIG. 12. The maximum LCE (a) and minimum distance to Neptune (b) computed for $i = 5°$ and several a, e in the 3 : 4 MMR with Neptune (set (1) of initial conditions). The x-axis scale was corrected for the difference between initial osculating and mean-resonant semi-major axis due to short-period perturbations. The resonant centers and separatrices are shown by bold lines. Inner resonances are denoted by thin lines. The KBO 1995 DA2 has a stable orbit (the two-headed vertical arrows delimit the maximum and minimum values of its filtered a and e on 10^7 yr). In the central resonant space, LCE $< 10^{-7}$ yr^{-1} and the minimum distance to Neptune does not exceed 15 AU and is less than 10 AU for $e < 0.1$.

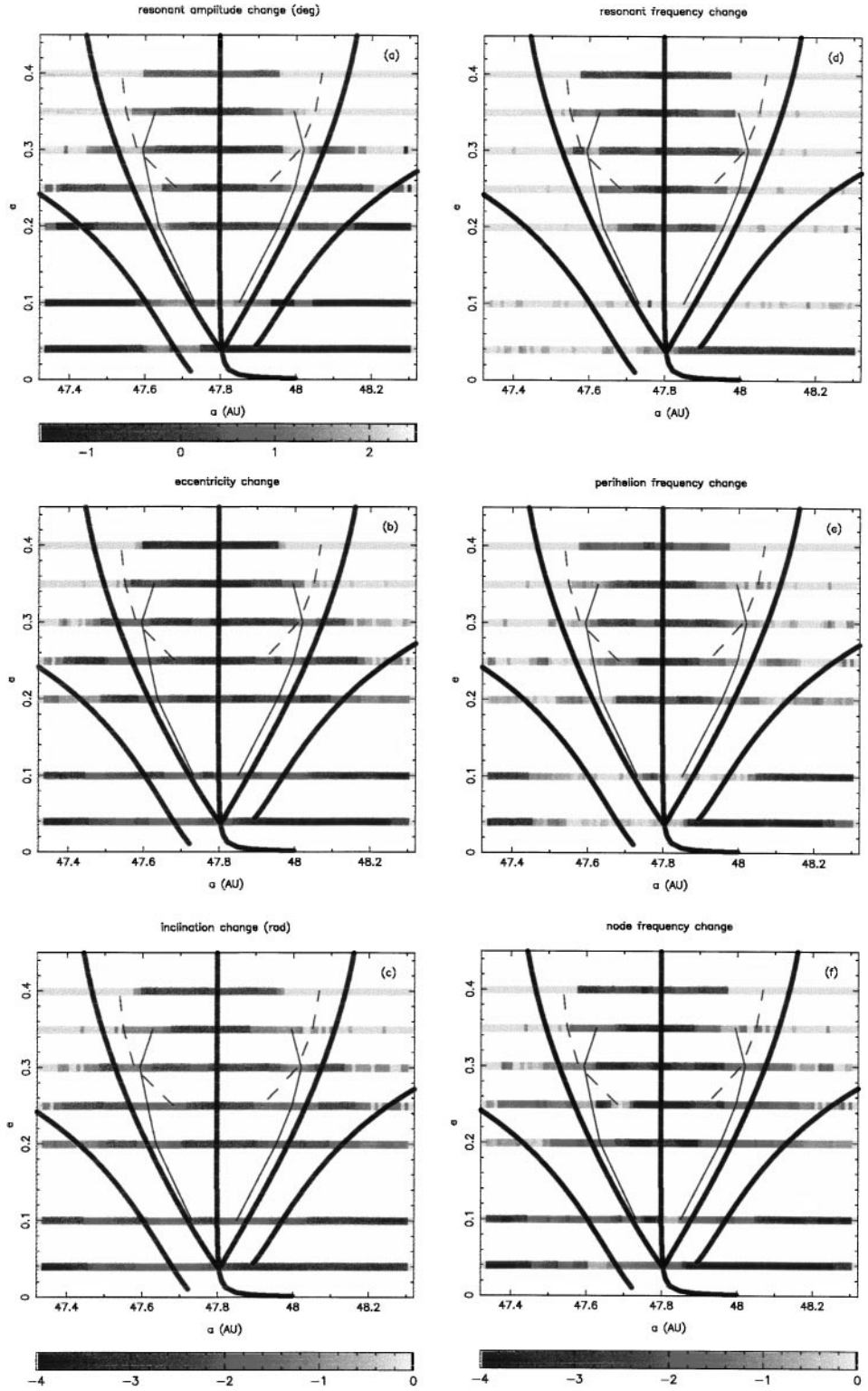

FIG. 6. The changes of orbital elements, δA_σ (a), δe (b), and δi (c), and of the frequencies, δf_σ (d), δf_{ϖ} (e), and δf_Ω (f), measured per 45 Myr, for the set (1) of initial conditions in the 1 : 2 Neptune MMR. The color coding is the same in all panels but (a). The low-A_σ tadpole orbits are stable over the age of the Solar System because the chaotic evolution of orbital elements/frequencies is small there. Apart from the resonances shown in these figures, there are the $2(g - s_8)$ and $2g - s - s_8$ secular resonances located at $e \sim 0.2$ and ~ 0.3 near $A_\sigma \sim 0$, respectively. The horseshoe orbits are generally unstable with ejection times indirectly proportional to the initial e.

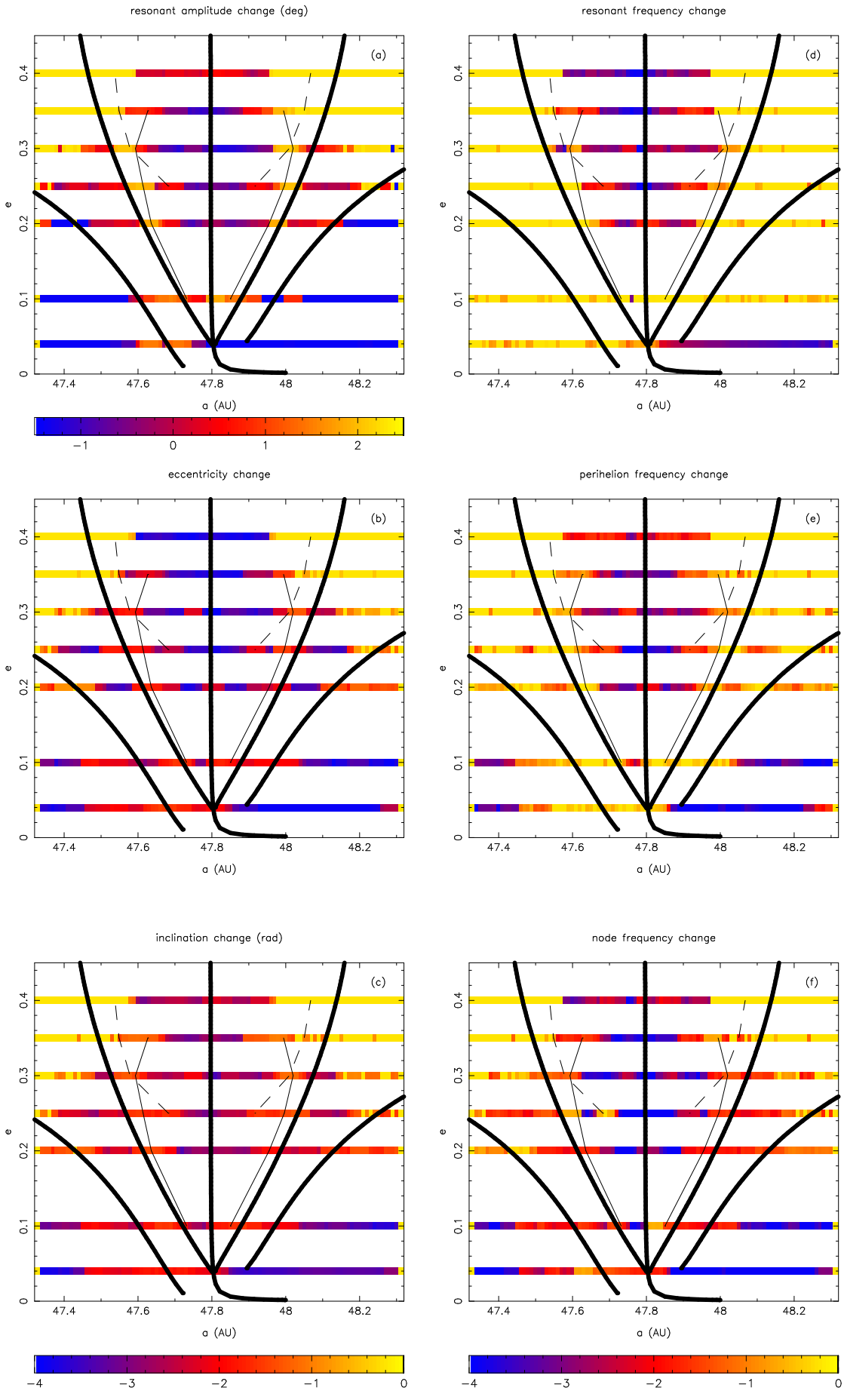
resonant amplitude change (deg)
(a)
resonant frequency change
(d)
eccentricity change
(b)
perihelion frequency change
(e)
inclination change (rad)
(c)
node frequency change
(f)
e
a (AU)
0
0.1
0.2
0.3
0.4
47.4
47.6
47.8
48
48.2
−1
0
1
2
−4
−3
−2
−1
0

3.2. *The Dynamics at $A_\sigma \sim 0$ and Larger i*

The set (2) of initial conditions was designed to study the orbital dynamics near the libration centers. Indeed, the test particles with $a = 47.95$ AU had initially $A_\sigma < 20^\circ$ for $e > 0.1$ (this lower e limit depends on i). For $e < 0.1$, where the tadpole orbits practically do not exist, the studied orbits move in a horseshoe regime. Figure 7a shows the maximum LCE. Figure 7b shows the minimum distance from Neptune over 10^8 years for $i = 10^\circ$.

The particles on the left side of the full thick line in Fig. 7a are chaotic with LCE $\sim 10^{-5.5}$–$10^{-6.5}$ yr^{-1}. The full thick line was empirically traced through LCE $= 10^{-6.5}$ yr^{-1}. On the right side of this line, $\log(\ln \Delta(t)/t)$ almost linearly decreases with $\log t$ and the minimum value of the LCE in Fig. 7a ($\sim 10^{-7}$ yr^{-1}) is dictated by the integration time span. There is only one well-determined structure visible in the plot: for $e > 0.36$ and $i > 15^\circ$, $\ln \Delta(t)/t$ converges to $\sim 10^{-6.5}$ yr^{-1}, where the Kozai resonance is located. The minimum distance from Neptune smoothly decreases with e in the regular region and drops to 15 AU in the chaotic low-e region (Fig. 7b).

Measures of chaotic diffusion (Fig. 8) reveal two secular resonances in the "regular" region. The $2(g - s_8)$ secular resonance is at $e = 0.185$ and the $2g - s - s_8$ resonance is at $e \sim 0.3$. The full thin lines in Fig. 8 were plotted at $2(f_{\varpi} - s_8) = 0$ (denoted by $2(g - s8)$) and $2f_{\varpi} - f_{\Omega} - s_8 = 0$ (denoted by $2g - s - s8$), respectively, where $f_{\varpi}(e, i)$ and $f_{\Omega}(e, i)$ were determined numerically in our experiment. The dashed lines were empirically traced at approximate positions of separatrices of the $2g - s - s_8$ secular resonance. This resonance overlaps with the Kozai resonance for $i > \sim 20^\circ$. The resonant angles, $2(\varpi - \Omega_N)$ of the former and $2\varpi - \Omega - \Omega_N$ of the latter, clearly librate for test particles in these resonances. Figure 9 shows the time evolution of $2\varpi - \Omega - \Omega_N$ (9a) and of e (9b) for the test particle with initial conditions: $a = 47.95$ AU, $e = 0.304$ and $i = 10^\circ$. The evolutions are correlated as it is expected for pendulum-like coupled motion of the action and resonant angle.

The total variations of e and i in the "chaotic" region, extrapolated to 4.5 Byr, are 0.2° and 10°, respectively. This suggests a prevailing stability of primordial bodies since the motion in horseshoe regime gets strongly unstable only for $e > 0.3$. The "regular" region at small A_σ is generally stable for $e < 0.35$ and $i < 25^\circ$. The secular resonances may potentially destabilize only the orbits with $i > 25^\circ$. This instability limit of i is about the same as found by Duncan *et al.* (1995) for other resonances.

3.3. *A Simple Model of Chaotic Diffusion*

A one-dimensional random-walk model of chaotic diffusion in the 2 : 3 Neptune MMR was described in N&R00 (see their Section 4 for details). Here, we use the same model for the 1 : 2 MMR.

For a given initial value of A_σ, 1000 test particles were simulated with $e = 0.3$ and $i = 5^\circ$. Assuming a random walk in A_σ, we advanced the orbits of these test particles by applying random kicks of the size of δA_σ (taken from Fig. 6a) to their

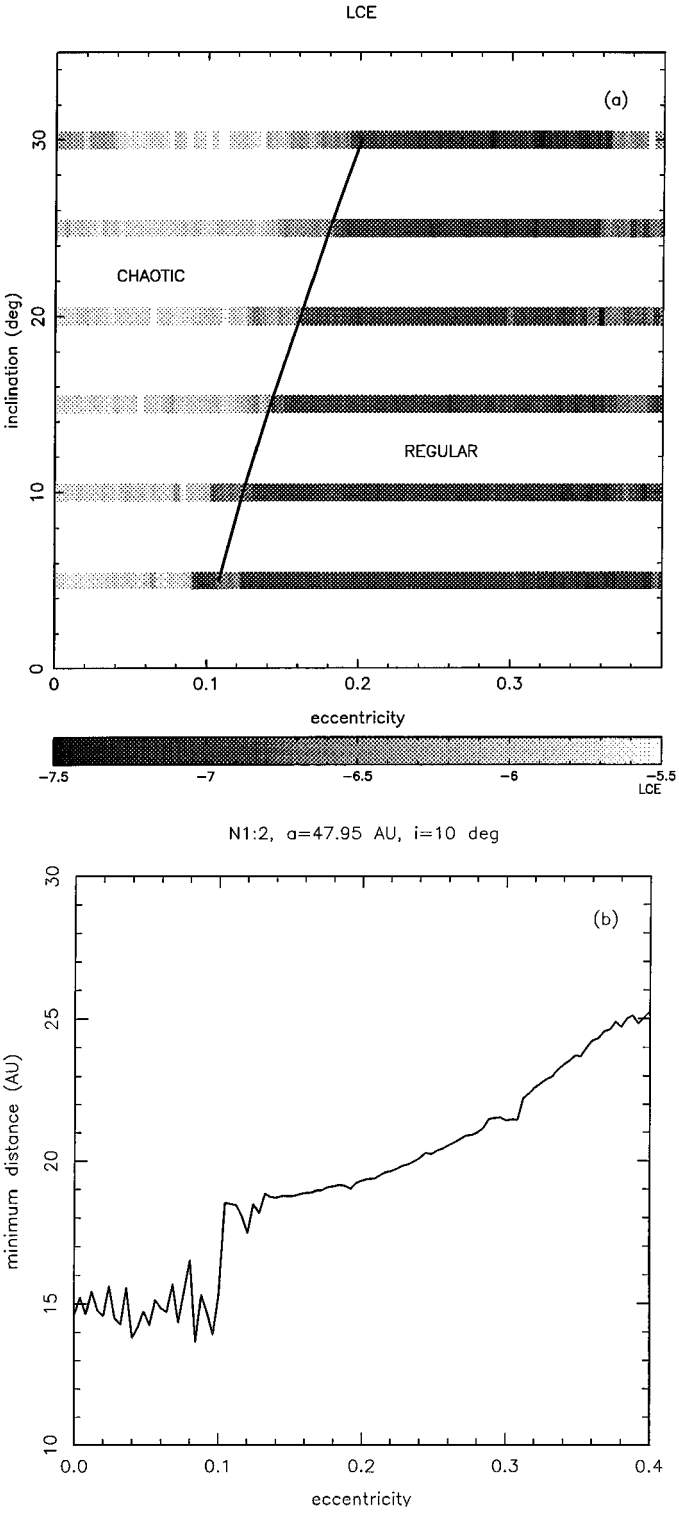

FIG. 7. The maximum LCE (a) and the minimum distance to Neptune (b) for the set (2) of initial conditions in the 1 : 2 Neptune MMR (initial $a =$ 47.95 AU). The bold line in (a) schematically separates two regions with different strengths of chaos. For test particles in the large-e region (denoted by "regular"), $\ln \Delta(t)/t$ does not converge to a limit value on the integration time span. Conversely, in the low–e region (denoted by "chaotic"), LCE $> 10^{-6}$ yr^{-1}.

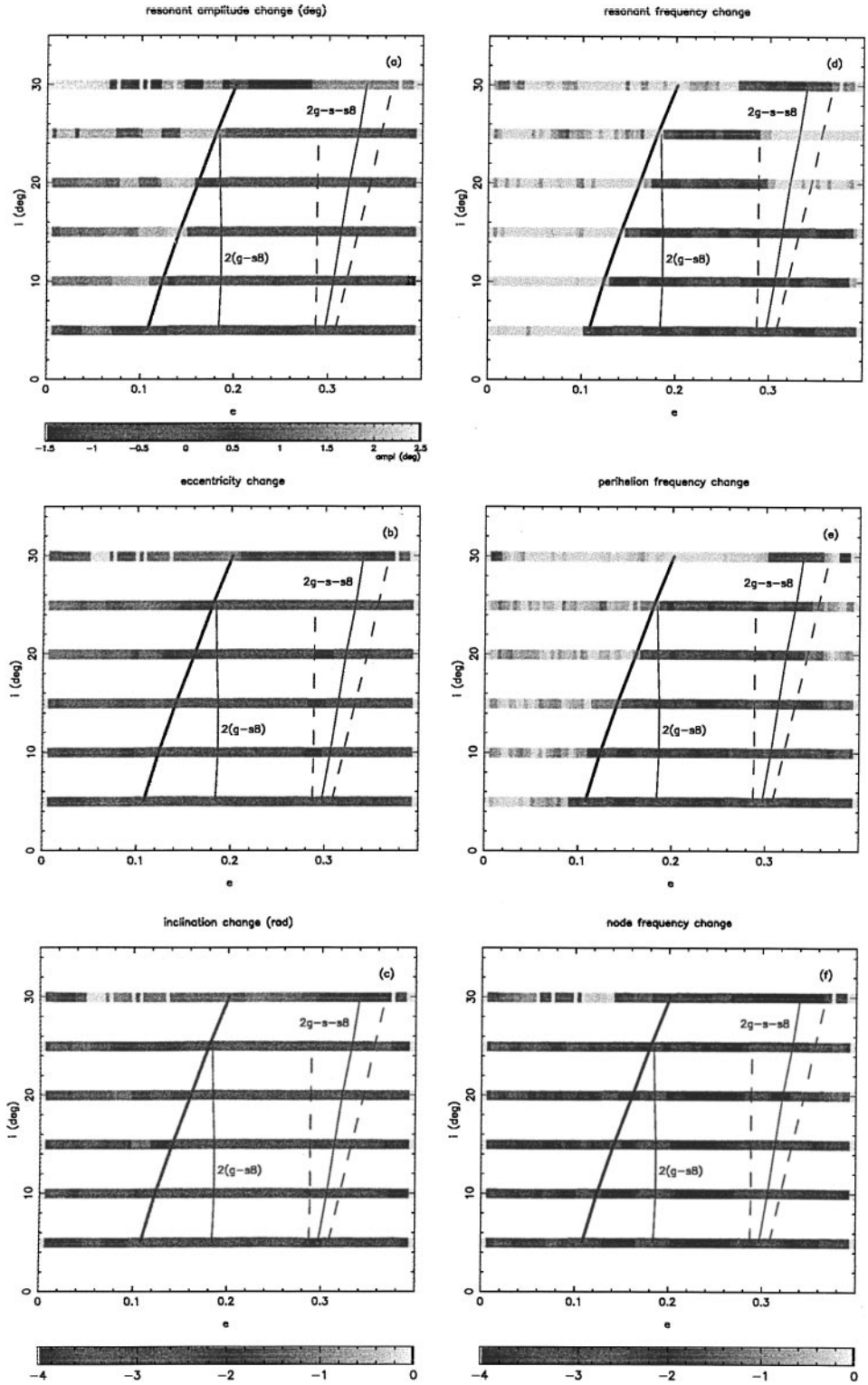

FIG. 8. The changes of orbital elements, δA_σ (a), δe (b), and δi (c), and of frequencies, δf_σ (d), δf_{ϖ} (e), and δf_Ω (f), measured per 45 Myr, for the set (2) of initial conditions in the 1 : 2 Neptune MMR (initial $a = 47.95$ AU). The color coding is the same for all panels but (a). The $2(g - s_8)$ secular resonance is shown by the thin line at $e = 0.185$. The center (full thin line) and approximate positions of the separatrices (dashed thin lines) of the $2g - s - s_8$ secular resonance are shown near $e = 0.3$. The Kozai resonance is at $e \sim 0.38$ and overlaps with $2g - s - s_8$ for $i > 20^\circ$.

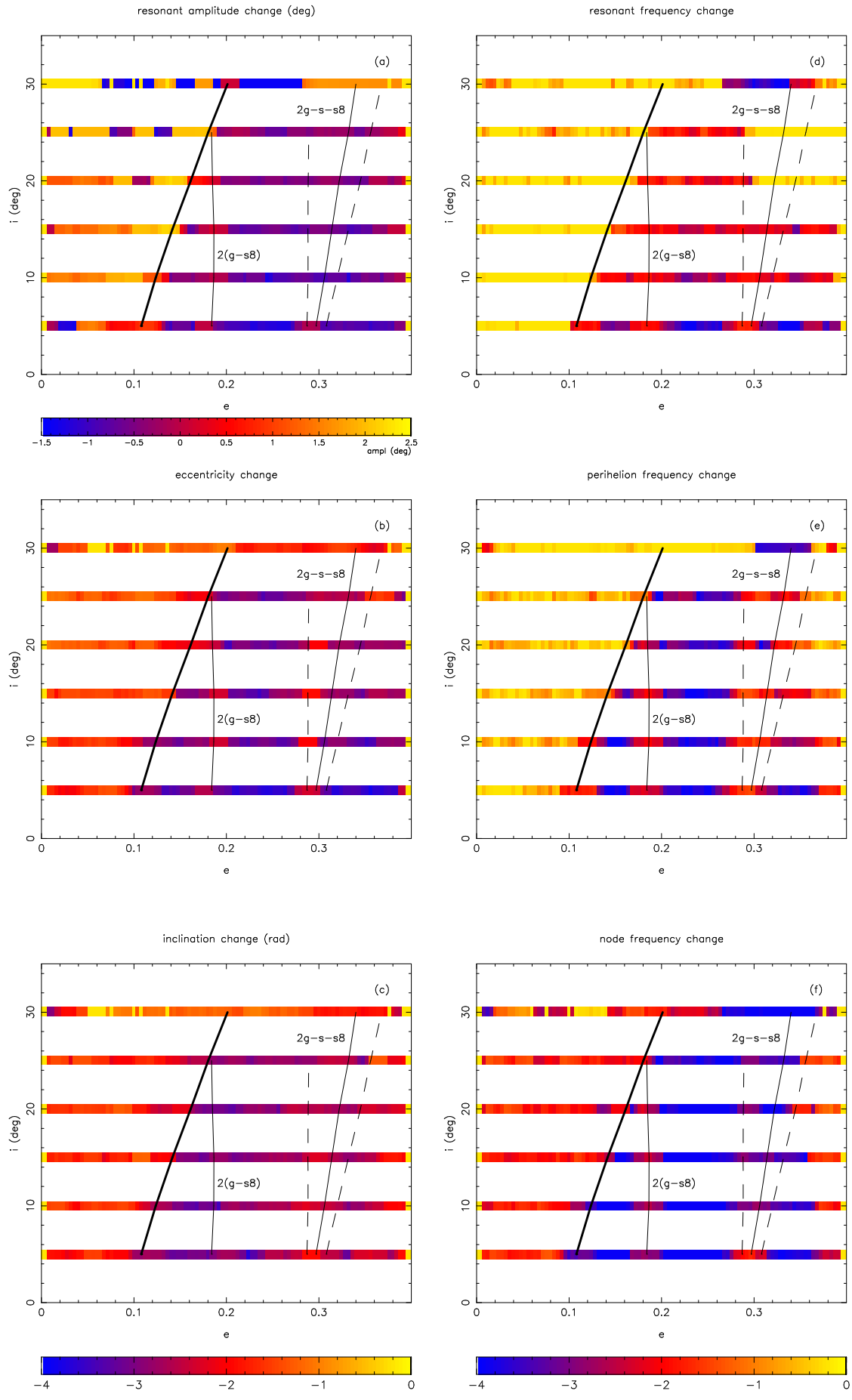
resonant amplitude change (deg)
(a)
2g−s−s8
2(g−s8)
i (deg)
e
ampl (deg)
resonant frequency change
(d)
eccentricity change
(b)
perihelion frequency change
(e)
inclination change (rad)
(c)
node frequency change
(f)

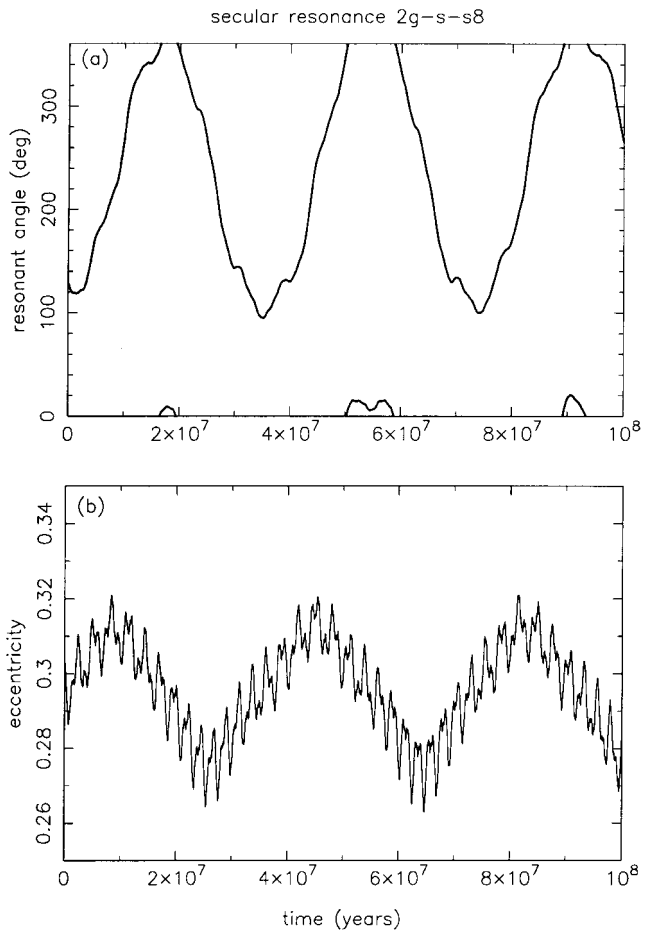

FIG. 9. The evolution of $2\varpi - \Omega - \Omega_N$ (a) and e (b) for a test particle starting with $a = 47.95$ AU, $e = 0.304$, and $i = 10^\circ$. Note that the libration of the angle with a period of ∼40 Myr is correlated with oscillations of e. This particle is in the $2g - s - s_8$ secular resonance.

A_σ. A test particle was deactivated if $A_\sigma > 85^\circ$. This simulation was repeated for 51 different values of A_σ regularly spaced between 0 and 50°. The total volume $V(50^\circ)$ occupied by these orbits is 36.1 AU × deg. The number of surviving test particles was then rescaled to a total number of 1000 particles initially placed in the interval $0 \le A_\sigma \le 50^\circ$, and uniformly distributed in a, λ, ϖ, and Ω.

Figure 10 shows the initial density profile of test particles (dashed line) and the eroded density profile at $t = 4$ Byr (bold line denoted by "+0"). Sixty-four percent of the test particles survived 4 Byr. Most of the escapes happened for $A_\sigma > 30^\circ$, and for $A_\sigma > 50^\circ$ more than 90% of test particles left the resonance. According to Fig. 10, and assuming that only the dynamical diffusion was acting on resonant bodies, the maximum density of the current resonant population should be at $A_\sigma \sim 30^\circ$.[8]

[8] We show in Fig. 10 the distribution of surviving particles vs the *initial* A_σ, which is not much different from the distribution of surviving particles vs the *final* A_σ. The density is still peaked at $A_\sigma \sim 30^\circ$ and decreases somewhat more steeply to larger A_σ than is shown in Fig. 10.

The following qualification is in order. We have assumed in the model that the resonant population was initially uniform in the semi-major axis and angles. This implies that the number of initial objects at A_σ was proportional to the volume in the phase space occupied by orbits with A_σ (see N&R00, Section 4). The initial density has an increasing trend with A_σ (dashed line in Fig. 10), simply because the resonant orbits with larger A_σ occupy larger volume in the phase space and are more frequently sampled. It is generally believed that the model of sweeping resonances and the resonant capture in MMRs in the primordial KB (Malhotra 1995) should have produced a nonuniform distribution in A_σ of the initial population of the 1 : 2 MMR. As discussed in N&R00, this is not a result of the process of resonant capture, but mainly a consequence of the smaller volume of small-A_σ orbits and the dynamical instability at larger A_σ. This is the reason why Malhotra's captured population is peaked at moderate amplitudes. In general terms, we would expect that if the capture simulation carried out by Malhotra (1997) for the 2 : 3 MMR were repeated also for the 1 : 2 MMR, the maximum resonant density of captured KBOs would be at slightly larger A_σ than that in our Fig. 10 (for $e = 0.3$) because of the short time span used in Malhotra's capture simulations for which orbits at large A_σ are still stable. For this reason, our assumption of

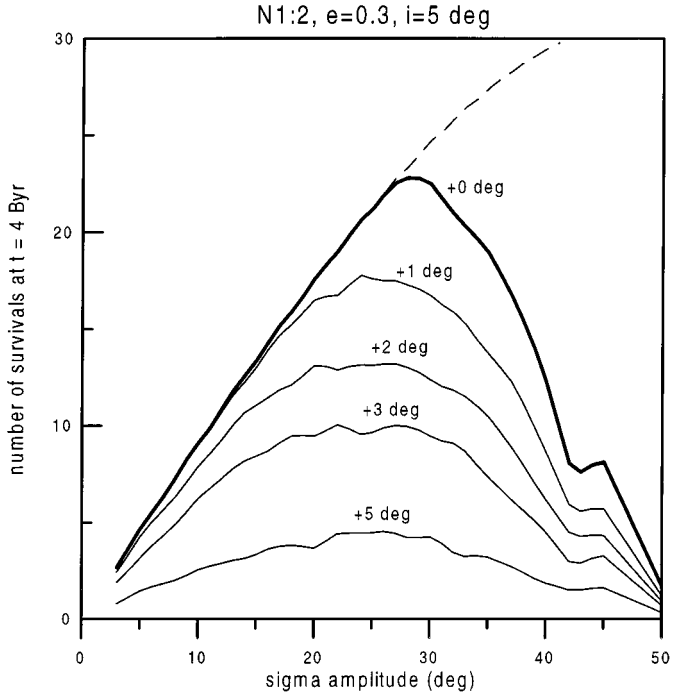

FIG. 10. The number of surviving particles at $t = 4$ Byr in the 1 : 2 MMR ($e = 0.3$ and $i = 5^\circ$) vs initial A_σ. Dashed line shows the initial density distribution in number of particles per 1°. The other lines show the eroded density distributions assuming a random walk at $0 < t < 4$ Byr with a local rate given by $\delta A_\sigma + \delta A_\sigma^{\rm kick}$ (see text). The value of δA_σ is shown in Fig. 6a. The bold line denoted "+0 deg" corresponds to $\delta A_\sigma^{\rm kick} = 0$. The thin lines correspond to values of $\delta A_\sigma^{\rm kick}$ ranging between 1° per 45 Myr (denoted "+1 deg") and 5° per 45 Myr (denoted "+5 deg").

initially uniform semi-major axes and angles is approximately valid for the resonance sweeping scenario.

The other curves in Fig. 10 show the results of additional experiments adding to δA_σ (which is the chaotic diffusion induced by gravitational perturbations of four major planets only), the evolution of A_σ due to random kicks produced by mutual collisions or dynamical scattering: $\delta A_\sigma^{\rm kick} = 1^\circ$ per 45 Myr (53% particles survived), 2° per 45 Myr (41%), 3° per 45 Myr (31%), and 5° per 45 Myr (13%) (see Section 4 in N&R00). The last value shows that $\delta A_\sigma^{\rm kick} > 5^\circ$ per 45 Myr is needed in order to reduce the original population to 1/10.

Of course, this is a very rough model of the real collision dynamics in the 1 : 2 MMR because it does not account for the disruption of bodies and for the resulting changes in the size distribution. In such a case, the loss of resonant KBOs of a given size may have been partially compensated from disrupted larger bodies.

Assuming that the dependence of the primordial KBO density on heliocentric distance r was proportional to $\sim r^{-2}$ (Tremaine 1990) and that the primordial excitation in the 2 : 3 and 1 : 2 MMRs efficiently randomized orbital eccentricities in the interval $0 < e < 0.35$, the ratio between current populations of the most stable places in the resonances ($e = 0.2$ in 2 : 3 and $e = 0.3$ in 1 : 2) is

$$\frac{1}{2}\frac{V(A^*_{2:3})}{V(A^*_{1:2})}\frac{P^{2:3}_{\rm surv}}{P^{1:2}_{\rm surv}}\left(\frac{a_{1:2}}{a_{2:3}}\right)^2, \qquad (5)$$

where $V(A^*_{2:3}) = V(127^\circ) = 116.6$ AU × deg (N&R00), $V(A^*_{1:2}) = V(50^\circ) = 36.1$ AU × deg, $P^{2:3}_{\rm surv} = 0.81$, $P^{1:2}_{\rm surv} = 0.64$, $a_{2:3} = 39.5$ AU, and $a_{1:2} = 47.8$ AU. $P_{\rm surv} = N_{\rm surv}/N_{\rm prim}$ is the relative fraction of objects surviving at $t = 4$ Byr with respect to the number of primordial objects. The factor 2 in the denominator is a result of two asymmetric libration centers in the 1 : 2 MMR against one center in the 2 : 3 MMR.

Evaluating Eq. (5) indicates that there should currently exist three times more objects with $e = 0.2$ in the 2 : 3 MMR than with $e = 0.3$ in the 1 : 2 MMR. The same calculation with survival percentages $P^{2:3}_{\rm surv}$ and $P^{1:2}_{\rm surv}$ evaluated in the experiments with $\delta A_\sigma^{\rm kick} = 3^\circ$ per 45 Myr results in the ratio of 4.25.

There are ∼15 KBOs and Pluto observed at present on stable orbits in the 2 : 3 MMR (N&R00) and two likely candidates for the 1 : 2 MMR resonant bodies (1997 SZ10 and 1996 TR66—Section 3.1). The apparent observational ratio between the 2 : 3 and 1 : 2 MMR populations is thus 8. As the selection observational effect probably contributes by a factor of 0.3 (Jewitt *et al.* 1998), the intrinsic (real) ratio between these two populations should be about 2.5, in a reasonable agreement with the ratio predicted by Eq. (5) with $\delta A_\sigma^{\rm kick} = 0$.

3.4. A Long-Term Simulation of the 1 : 2 Resonant Orbits

In order to verify the long-term stability of orbits in the central region of the 1 : 2 MMR we simulated 40 test particles with initially small A_σ over 4 Byr. We used the `swift_rmvs3` integrator (Levison and Duncan 1994) with a time step of 0.8 yr and included the perturbations of four major planets. The planetary initial conditions were taken from the JPL DE403 ephemeris at JD 2450814.5, with respect to the invariable plane of the LONGSTOP 1B simulation. The initial conditions of test particles were $a = 47.5$ AU, $i = 2^\circ$, and e ranging from 0.04 to 0.45 ($\Delta e \simeq 0.01$). We set initially $\varpi - \varpi_{\rm N} = 0$, $\Omega - \Omega_{\rm N} = 0$, and chose the value of the initial mean anomaly in order to have $\sigma_{1:2} = \sigma_0(e)$, where σ_0 stands for the asymmetric center located between 0° and 180° for the corresponding e (Fig. 4a). This choice of initial conditions implies that all particles with $e > 0.13$ have $A_\sigma < 30^\circ$.

Most simulated orbits with small A_σ survived over the age of the Solar System without any significant change of their mean (A_σ, e, i). The only particles with initially small A_σ that escaped during the simulation were those initially located at $e > 0.41$. At these eccentricities, the overlap of inner resonances (as the 4 : 1 three-body and Kozai resonances) generates a strong chaos, driving particles to the Neptune-crossing orbits.

For $0.37 < e < 0.40$, orbits are affected by the Kozai resonance. In contrast with the classical Kozai resonance, the ω librations do not occur around 90° or 270°, but rather around $\sim 140^\circ$ or $\sim 320^\circ$ (Fig. 11). This is a consequence of the asymmetric libration of $\sigma_{1:2}$. For $0.37 < e < 0.40$, σ librates around $\sigma_0 \sim 65^\circ$.

The shift of the equilibrium points of the Kozai resonance in the 1 : 2 resonance can be explained on the basis of a simple model. Consider the Hamiltonian $\mathcal{H}_{\rm res}$ of the averaged restricted three-body problem, with the massive body on a circular and

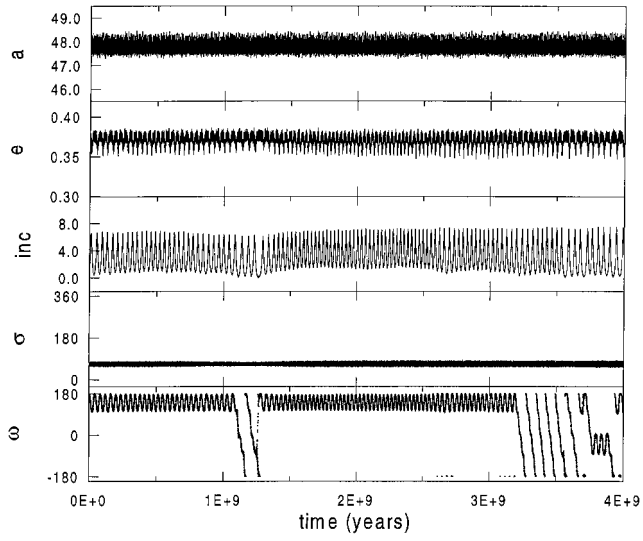

FIG. 11. Evolution of a test particle in the 1 : 2 Neptune MMR. The initial conditions (initial $e = 0.3778$) were chosen so that the orbit of this particle is characterized by small-A_σ libration around $\sigma_0 = 65^\circ$. This particle evolves in the Kozai resonance with ω libration around $\sim 140^\circ$. This libration is correlated with coupled oscillations of e and i.

planar orbit. Expanding its Keplerian part around the resonant semi-major axis a_0, and the perturbing function up to the second degree in inclination, we can write

$$\mathcal{H}_{\rm res} = -\frac{3}{2L_0^2}L^2 - m_1 \times \left[R_0 + \frac{\eta^2}{2}\left(R_1 + R_2\cos 2\sigma_z + R_3 \sin 2\sigma_z\right)\right], \quad (6)$$

where m_1 is the mass of the perturbing body, $L_0 = \sqrt{a_0}$, $L \propto S_z$, $\eta = \sin i/2 \propto \sqrt{S_z}$, and S_z is the action conjugated to $\sigma_z = \sigma + \omega$. The coefficients R_i are functions of a, e, σ and we evaluate them at the MMR's libration center: $R_i = R_i(a_0, e_0, \sigma_0)$ (Roig *et al.* 1998).

This one degree of freedom Hamiltonian can be written as

$$\mathcal{H}_{\rm res} = -\left(\frac{3}{2L_0^2}L^2 + m_1\frac{\eta^2}{2}R_1\right) + m_1\frac{\eta^2}{2}R\cos(2\sigma_z + 2\phi), \quad (7)$$

with

$$R = \pm\sqrt{R_2^2 + R_3^2} \quad (8)$$

$$\tan 2\phi = -\frac{R_3}{R_2}\ . \quad (9)$$

The choice between the plus and minus signs of R is arbitrary. The signs of R_2 and R_3 determine two complementary values of 2ϕ. After fixing η, the resonant Hamiltonian has the form of the harmonic oscillator

$$\mathcal{H} = \alpha J^2 + \beta\cos\psi, \quad (10)$$

with $J \propto S_z$, $\psi = 2\sigma_z + 2\phi$, and $\alpha \simeq -3L_0^{-2}/2 < 0$.

The location of stable equilibrium points depends on the sign of β. If $\beta > 0$, the stable point is at $\psi = 0$, while if $\beta < 0$, the stable point is located at $\psi = \pi$. This means that

$$\begin{aligned} R > 0 &\Rightarrow \omega = k\pi - \phi - \sigma_0 \\ R < 0 &\Rightarrow \omega = \frac{2k+1}{2}\pi - \phi - \sigma_0\ , \end{aligned} \quad (11)$$

where k is integer.

When $\sigma_0 = \pi$, as in the case of the 2 : 3 MMR with Neptune, then $R_2 > 0$ and $R_3 = 0$. In this case, $R > 0$ implies that $\phi = \pm\pi/2$, which gives $\omega = (2k-1)\pi/2$. If, on the other hand, $R < 0$ then $\phi = 0$ and once again $\omega = (2k-1)\pi/2$. These constitute the common libration centers of the Kozai resonance at 90° and 270° (the same result holds for the MMRs with $\sigma_0 = 0$).

If however σ_0 of a MMR is neither 0 nor π, the Kozai resonance does not have libration centers at 90° and 270°. As an example, consider the asymmetric libration center of the 1 : 2 MMR located at $a_0 = 47.797$ AU, $e_0 = 0.383$, and $\sigma_0 = 66.4°$. In this case, $R_2 < 0$ and $R_3 < 0$. If $R > 0$ then $\phi = 329°$ and $\omega = 180k - 35.4°$, while if $R < 0$ then $\phi = 59°$ and $\omega = 90(2k+1) - 125.4°$. The stable centers of the Kozai resonance are at 144.6° and 324.6°, respectively, in good agreement with values observed numerically (Fig. 11).

The choice of initial conditions in our simulation did not guarantee the occurrence of asymmetric librations for $e < 0.13$. The width of the asymmetric island is narrow for small e and all nine particles in the run were initially librating with large A_σ around the symmetric saddle point at 180° (horseshoe orbits). The amplitudes of horseshoe orbits were chaotically changing between 120° and 180°, and only rarely (and for at most several 10^6 yr) did temporary captures in the asymmetric islands occur.

We have performed additional simulations with orbits starting at small e. First, we have found by several trials that permanent tadpole orbits do not exist in practice for $e < 0.07$ (for $e > 0.07$ it is possible to find tadpole orbits that are stable over 4 Byr). Next, we simulated several test particles with initial $e = 0.01$ and 0.05. For each value of e, we have obtained 10 objects showing a resonant behavior, typically alternating between horseshoe orbits and circulation. Their e and i irregularly evolve in the intervals 0–0.2 and 0°–10°, respectively. Interestingly, the irregular motion of some of these test particles was stabilized in a horseshoe regime at $e \sim 0.15$–0.2, $i \sim 5°$–$7°$, and $A_\sigma \sim 100°$. From the test particles with initial $e = 0.01$, only one escaped, while for $e = 0.05$ three particles escaped. This corresponds to the general fact that the orbits starting with initially larger e get destabilized faster by the chaotic eccentricity drift. We estimate that the median lifetime of orbits at $e = 0.05$ in the 1 : 2 MMR is slightly larger than the age of the Solar System. In summary, we found that the resonant space at low e in the 1 : 2 MMR a accounts for about 0.3 AU in a. From 47 resonant test particles simulated with $e < 0.12$ only 8 escaped in 4 Byr, and in this sense, the 1 : 2 MMR is stable in small e. This finding confirms the results of Duncan *et al.* (1995).

4. THE 3 : 4 MMR WITH NEPTUNE

4.1. A Portrait of Regular and Chaotic Dynamics

The only known object in the 3 : 4 MMR with Neptune is 1995 DA2. We have taken this KBO's orbital elements from the Asteroid Orbital Elements Database of the Lowell Observatory.[9] They are reasonably well determined for our purposes because of a relatively large observational arc for this KBO. 1995 DA2 is a counterpart of the asteroid 279 Thule, which is the only stable asteroid discovered until now in the 4 : 3 MMR with Jupiter in the outer asteroid belt. The presence of only one large body in the 4 : 3 Jupiter MMR is puzzling (the diameter of 279 Thule is 135 km), because if the size distribution were similar to the main asteroid belt, there would exist also many small bodies in the resonance (Nesvorný and Ferraz-Mello 1997). On the other hand, the KB is less well known than the asteroid belt and new bodies in the 3 : 4 Neptune MMR may be discovered soon.

[9] The assumed orbital elements of 1995 DA2 on 8/10/1999 (JD 2451400.5) are $a = 36.3396$ AU, $e = 0.074684$, $i = 6.5585°$, $M = 31.836°$, $\omega = 332.008°$, and $\Omega = 127.485°$.

The stability test of the 3 : 4 MMR was performed by the same means as for the 1 : 2 MMR in Section 3. The initial angles of test particles were chosen so that $\sigma_{3:4} = 3\lambda_N - 4\lambda + \varpi = 180^\circ$, $\omega = 90^\circ$, and $\Omega = \Omega_N$. Two sets of initial conditions have been simulated:

(1) 606 test particles with $36 \le a \le 37$ AU ($\Delta a = 0.01$ AU), $e = 0.001$, 0.05, 0.1, 0.15, 0.2, 0.25 (101 test particles for each e), and $i = 5^\circ$; and

(2) 202 test particles with $a = 36.57$ AU, $0 \le e \le 0.3$ ($\Delta e = 0.003$), and $i = 10^\circ$ and 30°. The integration over 10^8 yr was performed by the symmetric multistep method. The planetary configuration, parameters of the simulation, and smoothing routine were the same as for the experiment in the 1 : 2 MMR.

For set (1) of initial conditions, the estimate of the LCE and the minimum distance to Neptune are plotted in Fig. 12. The color coding in Fig. 12 is the same as that used in Fig. 5. Again, we have compensated the scale on the x axes for short-periodic variations of the semi-major axis by a shift of 0.1 AU in a, so that the test particles with the smallest A_σ are near the true resonant center at 36.48 AU.

In Fig. 12, we plot the libration centers and separatrices of the 3 : 4 MMR (bold lines). The Kozai resonance is shown by a thin line (Fig. 12a). We have computed its location from $\dot\varpi - \dot\Omega = 0$, where the frequencies $\dot\varpi$ and $\dot\Omega$ were determined as functions of e and a by the semi-numerical method of Henrard (1990). The dashed lines in Fig. 12 show the the 2 : 1 and 3 : 1 commensurabilities between the resonant frequency and the frequency of $\lambda_U - 2\lambda_N$. A pair of two-headed vertical arrows indicates the extrema of the filtered a and e of 1995 DA2 over 10^7 yr (its inclination varies between 1.5° and 8.4°). 1995 DA2 has a resonant orbit with $A_\sigma = 76^\circ$, which is stable on 10^8 yr.

There is a slight asymmetry in the maximum and minimum values of a of 1995 DA2 with respect to the resonant center, which typically happens in the MMRs close to a planet, where the real dynamics differs somewhat from the averaged circular approximation. Nevertheless, the resonant amplitude of 1995 DA2 is clearly small and this object is located in the central regular region of the resonance.

The maximum LCE in the central region of the 3 : 4 MMR is smaller than $\sim 10^{-7}$ yr^{-1} in the interval of 0.3 AU for $e = 0.05$ and of 0.2 AU for $e = 0.1$. The region of small LCE has the size of 0.1 AU for $e = 0.15$, and $\ln \Delta(t)/t$ visibly converges to a nonzero value ($\sim 10^{-6.5}$ yr^{-1}) at $A_\sigma = 0$ for $e \ge 0.2$. The size of the central region we determine here is smaller than that determined by Malhotra (1996) as an extent of regular resonant orbits in a model with Neptune on a circular orbit ($\sim$0.8 AU for $e = 0.1$).

The 3 : 1 three-body resonance is at intermediate A_σ. The corresponding region is clearly chaotic with LCE $\sim 10^{-5.5}$ yr^{-1}. Chaos with the similar LCE value was found in the 4 : 1 three-body resonance inside the 2 : 3 Neptune MMR in N&R00, and it was shown in that paper that moderate chaos generates a slow random walk in A_σ, which in turn can lead to late escapes from the resonance. In this analogy, the orbits in 3 : 1 three-body resonance inside the 3 : 4 Neptune MMR are also potentially unstable. The 3 : 1 resonance should approximately delimit the 30°–40° interval in A_σ of marginally unstable region in the 3 : 4 Neptune MMR.

The minimum distance to Neptune is smaller in the 3 : 4 than in the 1 : 2 (Fig. 5b) and 2 : 3 MMRs (N&R00, their Fig. 2b). It is typically between 5 and 13 AU for the surviving particles. Most particles that approached Neptune at less than $\sim$4 AU subsequently escaped from the resonance.

The determination of δA_σ, δe, and δi shows that the most stable place in the 3 : 4 MMR is at $e = 0.05$, where $\delta A_\sigma = 0.6^\circ$ per 45 Myr for $A_\sigma < 120^\circ$. The expected change of A_σ over 4.5 Byr is 6°. In order to estimate the fraction of objects surviving at $t = 4$ Byr vs A_σ at this eccentricity, we have performed the same experiment as in Section 3.3, modeling the chaotic diffusion as a random walk.

1000 test particles were simulated for each A_σ, and the simulation was repeated for 136 values of A_σ regularly spaced between 0° and 135° for $e = 0.05$ and $i = 5^\circ$. The volume $V(135^\circ)$ occupied by these orbits is 91.4 AU × deg. Assuming the random walk in A_σ, we advanced the orbits of test particles by applying random kicks of the size of δA_σ to their resonant amplitudes. A test particle was removed from the simulation if $A_\sigma > 170^\circ$.

Figure 13 shows the initial density of test particles (dashed line) and the eroded density profile at $t = 4$ Byr (bold line denoted by "+0"). Sixty-eight percent of test particles survived at $t = 4$ Byr. Most escapes occurred for $A_\sigma > 90^\circ$, and for $A_\sigma > 135^\circ$ more than 99% of test particles left the resonance. According to Fig. 13, the maximum density of the current the 3 : 4 MMR population should be at about $A_\sigma \sim 90^\circ$.

The other curves in Fig. 13 show the results of additional experiments adding to δA_σ the evolution of A_σ due to random kicks produced by mutual collisions and dynamical scattering: $\delta A_\sigma^{\rm kick} = 1^\circ$ per 45 Myr (63.5% particles survived), 2° per 45 Myr (58%), and 3° per 45 Myr (53%). The last value shows that $\delta A_\sigma^{\rm kick} > 3^\circ$ per 45 Myr is needed in order to reduce the original population to one-half.

The same reasoning as in Section 3.3 allows us to estimate the ratios of the current numbers of KBOs in the 3 : 4 MMR to those in the 2 : 3 and 1 : 2 MMRs (Eq. (5)). Using $a_{3:4} = 36.48$ AU, $V(135^\circ) = 91.4$ AU × deg, and $P_{\rm surv}^{3:4} = 0.68$, the present number of objects in the 3 : 4 MMR (at $e = 0.05$) should be 77% of the number of the 2 : 3 resonant objects (at $e = 0.2$)[10] and 2.3 times the number of the 1 : 2 resonant objects (at $e = 0.3$). Both of these percentages are in clear contradiction to the observed abundance of the resonant KBOs, implying that the 3 : 4 resonant KBOs must have been efficiently depleted in the early stages of Solar System evolution.

Figure 14 shows the LCEs for set (2) of initial conditions: $i = 10^\circ$ in (a) and $i = 30^\circ$ in (b). The distinctive features are the chaos at $e < 0.05$ (LCE > $\sim 10^{-6}$ yr^{-1}) and regular-like motion

[10] According to Jewitt *et al.* (1996), the observational selection effect is about the same for the 2 : 3 and 3 : 4 MMRs.

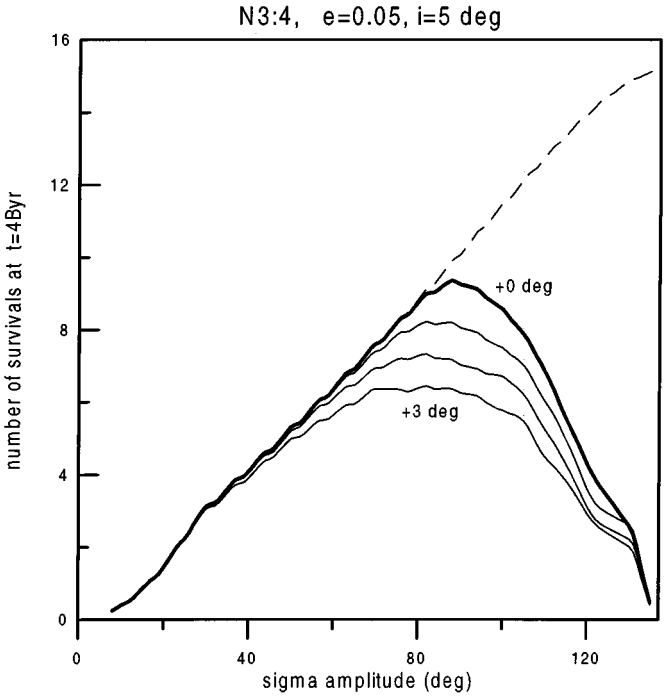

FIG. 13. The number of surviving particles at $t = 4$ Byr in the 3 : 4 MMR ($e = 0.05$ and $i = 5^\circ$) vs initial A_σ. Dashed line shows the initial density distribution. The other lines show the eroded density distributions assuming a random walk at $0 < t < 4$ Byr at a local rate given by $\delta A_\sigma + \delta A_\sigma^{\rm kick}$. The bold line denoted "+0 deg" corresponds to $\delta A_\sigma^{\rm kick} = 0$. The thin lines correspond to values of $\delta A_\sigma^{\rm kick}$ ranging between 1° per 45 Myr and 3° per 45 Myr (denoted "+3 deg").

inside the Kozai resonance ($0.18 < e < 0.23$ for $i = 10^\circ$ and $0.15 < e < 0.25$ for $i = 30^\circ$).

The orbits with small and moderate amplitudes in the Kozai resonance are stable even at large i over the age of the Solar System: $\delta A_\sigma = 0.5^\circ$ per 45 Myr, $\delta e = 0.001$ per 45 Myr, and $\delta i < \sim 1^\circ$ per 45 Myr. Such orbits represent an exception from the general rule found by Duncan *et al.* (1995) that the low-order MMRs in the Kuiper Belt are unstable for $i > 25^\circ$.

4.2. The Long-Term Integration of the 3:4 Resonant Orbits

We performed a long-term integration of 27 test particles initially located in the 3 : 4 MMR. The simulation with `swift_rmvs3` and a time step of 0.5 yr spanned 4 Byr. We have included the perturbations of four major planets with the same initial conditions as in Section 3.4. The test particles initially had $a = 36.735$ AU, $i = 2^\circ$, $0 \le e \le 0.26$ ($\Delta e = 0.01$), $\omega = 90^\circ$, $\Omega - \Omega_{\rm N} = 0$, and $\sigma_{3:4} = 180^\circ$.

For the test particles with $0.02 \le e \le 0.08$, the initial A_σ varied between 20° and 60° (the lower the e, the larger the initial A_σ). These particles move in the ν_{18} secular resonance: the angle $\Omega - \Omega_{\rm N}$ librates around 0 with an amplitude <60°. The amplitude reaches a minimum (30°) for $e \sim 0.06$, which shall correspond to the center of ν_{18} for $i = 2^\circ$ and $A_\sigma \sim 0$. All particles in the interval $0.02 \le e \le 0.08$ survive 4 Byr.

For $e < 0.02$, $\sigma_{3:4}$ alternates between libration with large A_σ and circulation. These orbits are usually unstable over 4 Byr, although they can survive for 2–3 Byr in the resonance before their eccentricities are driven to Neptune-crossing values.

For $e \ge 0.09$ all particles have $A_\sigma < 25^\circ$. These small-A_σ orbits are stable over the age of the Solar System, and most test particles survive the whole simulation without any significant change in their mean A_σ, e, and i. The only exceptions are four particles with initial $e \ge 0.23$, which are ejected from the resonance at $t < 2$ Byr due to close encounters with Neptune. The test particles with $0.19 \le e \le 0.22$ are in the Kozai resonance. The Kozai resonance is narrow for small i and the test particles integrated in this region do not show stable ω librations, but rather alternate between the two centers of the Kozai resonance (90° and 270°) on <∼100 Myr. Stable librations in the Kozai resonance happen at larger i.

The results of this simulation are in general agreement with the resonant portrait presented in the last section. In particular,

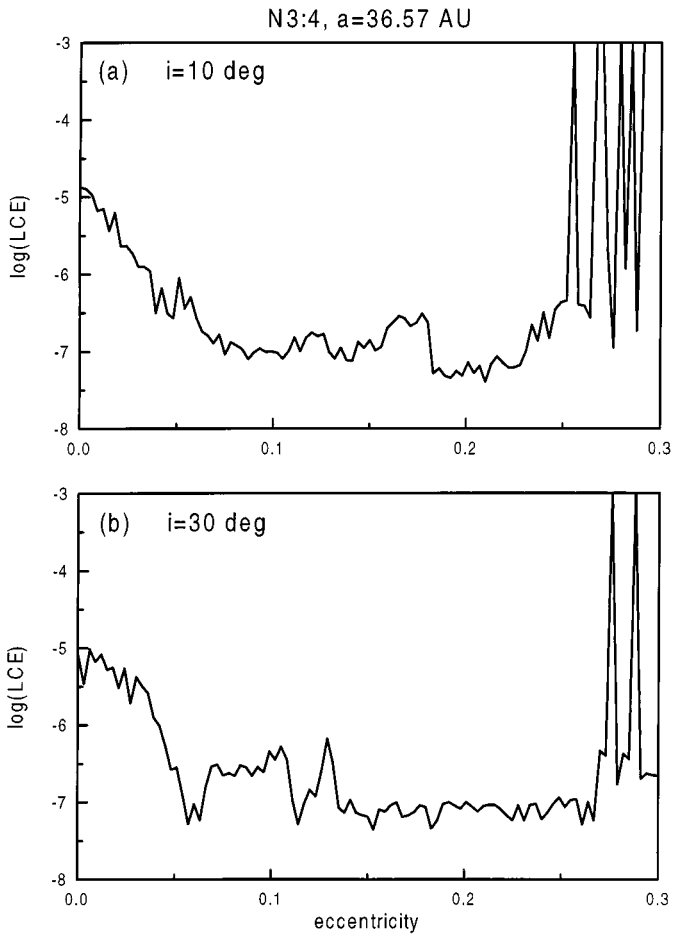

FIG. 14. The LCE for $i = 10^\circ$ (a) and 30° (b) in the 3 : 4 Neptune MMR for $A_\sigma \sim 0$ (set (2) of initial conditions). The largest region with small LCE ($<10^{-7}$ yr^{-1}) is near $e = 0.2$, inside the Kozai resonance. The Kozai resonance enlarges with increasing i, and for $i = 30^\circ$ the interval $0.15 < e < 0.25$ corresponds to practically regular motion.

they verify the existence and extent of the stable core of the 3 : 4 MMR.

5. CONCLUSIONS

We have shown that most chaotic structures in the Kuiper Belt are related to the MMRs with Neptune, three-body resonances with Neptune and Uranus, and MMRs with Uranus (in descending order of importance).

The chaotic evolution of orbits at thin resonances is easy to understand due to its "one-dimensionality": numerical experiments show that orbits evolve in e at almost fixed resonant a, while i changes moderately. The speed of the random walk in e is determined in a complex way by the structure of overlapping resonant multiplets (Nesvorný and Morbidelli 1999) and developing a satisfactory theoretical model is an issue for future studies.

The existence of a resonant-driven random walk in e changes the common view that the minor body belts are "frozen" in regions sufficiently distant from the main MMRs and secular resonances, and suggests that the structure of these belts is time-dependent, with substantial eccentricity evolution. Apart from widely discussed consequences—as the mechanism of supply of transient populations of planets-crossers (ecliptic comets from the KB and Earth-crossers from the inner asteroid belt)—we believe that thin MMRs are ideal places for testing today's models of collisional, scattering, and dissipative evolution in the belts. Indeed, a large percentage of the current population at thin MMRs should have been collisionally injected, and the detection of "mini-gaps" (or failure to detect them) at thin MMRs can provide constraints on the injection probabilities. Such a study is more appropriate for asteroids, whose orbital distribution is better known.

The chaotic evolution in large MMRs is more complex and is determined by the structure of inner secular, secondary, and three-body resonances. We have investigated the first-order 1 : 2, 2 : 3 (in N&R00), and 3 : 4 MMRs with Neptune. This study has confirmed the findings of Duncan *et al.* (1995) and Morbidelli (1997) that the chaotic evolution in MMRs dominantly affects A_σ (or equivalently, the amplitude of a) and that the above resonances have stable "cores" for small A_σ, where all orbits survive 4×10^9 yr. This stable core is substantially smaller in the 1 : 2 than in the other two MMRs. The approximate limits of stable motion at small i are $0.15 < e < 0.35$ and $A_\sigma < 30^\circ$ in the 1 : 2 MMR, $0.05 < e < 0.25$ and $A_\sigma < 100^\circ$ ($A_\sigma < 50^\circ$ for $e = 0.3$) in the 2 : 3 MMR, and $0.03 < e < 0.2$ and $A_\sigma < 80^\circ$ in the 3 : 4 MMR. The most regular motion for large inclinations occurs inside the Kozai resonance at $e \sim 0.25$ in the 2 : 3 MMR, at $e \sim 0.2$ in the 3 : 4 MMR, and in the interval $0.2 < e < 0.27$ in the 1 : 2 MMR. These orbits are stable over the age of the Solar System.

The stable resonant cores are enclosed by the marginally unstable regions where a percentage of objects escape from resonances over the age of the Solar System (Duncan *et al.* 1995, Morbidelli 1997). This region is typically 20°–40° wide in A_σ. In the case of the 2 : 3 resonance, the marginally unstable region is at the place of the 4 : 1 three-body resonance. In addition to thin MMRs outside the 2 : 3 MMR, it is this 4 : 1 three-body resonance that generates a significant number of the present Neptune-crossers. The marginally unstable region in the 3 : 4 MMR with Neptune generated by the 3 : 1 three-body resonance.

The evolution of e is important in the strongly unstable region at large A_σ. The alternation between resonant libration and circulation produces a fast random walk of e. It takes at most several 10^8 yr to drive an orbit from the small e to Neptune-crossing orbit by this mechanism.

We have determined the number of currently known KBOs on resonant orbits stable over 4 Byr. There is 1 such body in the 3 : 4 MMR (1995 DA2), 15 bodies and Pluto in the 2 : 3 MMR, and probably 2 objects in the 1 : 2 MMR.

The current best-fit orbital elements of 1997 SZ10 and 1996 TR66 do not correspond to the stable resonant motion in the 1 : 2 Neptune MMR. While for 1997 SZ10 they indicate an unstable horseshoe orbit, the current orbital elements of 1996 TR66 place this object on a nonresonant orbit. Conversely, the orbital angles of these KBOs suggest they are resonant bodies. Indeed, the angles $\sigma_{1:2}$ of 1997 SZ10 (-69°) and 1996 TR66 (-62°) are surprisingly close to the center of the asymmetric librations for $e = 0.37$: $\sigma_0 \sim 67^\circ$, which is likely not a mere coincidence. 1997 SZ10 and 1996 TR66 are most probably dynamically primordial objects in the 1 : 2 MMR that currently librate with small A_σ on stable orbits. We believe that future improvement of their orbital elements will confirm this conjecture. Neverthless, as we have discussed in Section 2.1, our probabilistic argument in favor of this hypothesis cannot completely exclude the possibility that 1997 SZ10 and 1996 TR66 are temporarily captured objects from the scattered disk.

We have estimated that, if eccentricities have been efficiently uniformized by the primordial excitation at resonances, then the current number of objects at the most stable places the resonances ($e = 0.3$ for 1 : 2, $e = 0.2$ for 2 : 3, and $e = 0.05$ for 3 : 4) shall be roughly in the ratio $N_{1:2} : N_{2:3} : N_{3:4} = 2 : 6 : 5$, while the observed apparent ratio is 2 : 16 : 1. Correcting the apparent ratio for the observational selection effects (Jewitt *et al.* 1998), the estimated current population of the 2 : 3 and 1 : 2 MMRs agrees roughly with the above theoretical prediction. Conversely, the 3 : 4 MMR with Neptune must have been significantly depleted in the early phases of the Solar System evolution.

ACKNOWLEDGMENTS

This research was sponsored by the São Paulo State Science Foundation FAPESP. Some of the numerical simulations were performed using the facilities of the São Paulo University computer center LCCA in the frame of the project "Asteroid resonant dynamics and chaos." We are indebted to Harold Levison for a very helpful referee report. We thank Brett Gladman for language corrections.

Note added in revisions. We recently learned about the recovery of 1997 SZ10 (B. Gladman, personal communication), which allowed for better determination of its orbit (B. Marsden, personal communication). While the eccentricity and the angular orbital elements stayed basically unchanged with respect to the previous determination (eccentricity changes by 0.005 and angles by less than 1.5°), the semi-major axis came down to 48.411 AU. This is exactly what we

have anticipated in this work. The 0.26-AU change of the semi-major axis places 1997 SZ10 very close to the libration center of the 1 : 2 MMR. We found in an additional simulation that these new orbital elements of 1997 SZ10 correspond to an initially resonant orbit starting with $A_\sigma \sim 30^\circ$ in the tadpole regime. In the meantime, 1996 TR66 still awaits for a recovery that would improve its orbital determination.

REFERENCES

Beaugé, C. 1994. Asymmetric librations in exterior resonances. *Celest. Mech. Dynam. Astron.* **60**, 225–248.

Benettin, G., L. Galgani, and J. M. Strelcyn 1976. Kolmogorov entropy and numerical experiments. *Phys. Rev. A* **14**, 2338–2345.

Duncan, M. J., and H. F. Levison 1997. A disk of scattered icy objects and the origin of Jupiter-family comets. *Science* **276**, 1670–1672.

Duncan, M. J., H. F. Levison, and S. M. Budd 1995. The dynamical structure of the Kuiper belt. *Astron. J.* **110**, 3073–3081.

Gallardo, T., and S. Ferraz-Mello 1998. Dynamics in the exterior 2 : 3 resonance with Neptune. *Planet. Space Sci.* **46**, 945–965.

Gladman, B., J. J. Kavelaars, J.-M. Petit, A. Morbidelli, M. J. Holman, and T. Loredo 2000b. The structure of the Kuiper belt: Size distribution and the radial extent. *Astron. J.*, submitted for publication.

Gladman, B., J.-M. Petit, and M. Duncan 2000a. Does Pluto affect the trans-neptunian region? In *Minor Bodies in the Outer Solar System* (R. West, Ed.). Kluwer Academic, Dordrecht, in press.

Hahn, J. M., and R. Malhotra 1999. Orbital evolution of planets embedded in a planetesimal disk. *Astron. J.* **117**, 3041–3053.

Henrard, J. 1990. A semi-numerical perturbation method for separable Hamiltonian systems. *Celest. Mech. Dynam. Astron.* **49**, 43–67.

Holman, M., and N. Murray 1996. Chaos in high-order mean resonances in the outer asteroid belt. *Astron. J.* **112**, 1278–1293.

Jewitt, D., J. Luu, and J. Chen 1996. The Mauna Kea–Cerro Tololo (MKCT) Kuiper belt and Centaur survey. *Astron. J.* **112**, 1225–1238.

Jewitt, D., J. Luu, and C. Trujillo 1998. Large Kuiper belt objects: The Mauna Kea 8K CCD survey. *Astron. J.* **115**, 2125–2135.

Knežević, Z., A. Milani, P. Farinella, Ch. Froeschlé, and C. Froeschlé 1991. Secular resonances from 2 to 50 AU. *Icarus* **93**, 316–330.

Laskar, J. 1994. Large-scale chaos in the Solar System. *Astron. Astrophys.* **287**, L9–L12.

Laskar, J. 1999. Introduction to frequency map analysis. In *Hamiltonian Systems with Three or More Degrees of Freedom* (C. Simó, Ed.), pp. 134–150. Kluwer, Dordrecht.

Levison, H. F., and M. Duncan 1994. The long term behavior of short-period comets. *Icarus* **108**, 18–36.

Malhotra, R. 1995. The origin of Pluto's orbit: Implications for the Solar System beyond Neptune. *Astron. J.* **110**, 420–429.

Malhotra, R. 1996. The phase space structure near Neptune resonances in the Kuiper belt. *Astron. J.* **111**, 504–516.

Malhotra, R. 1997. Implications of the Kuiper belt structure for the Solar System. In *ACM Conference 1996, Versailles, France.* Unpublished.

Migliorini, F., P. Michel, A. Morbidelli, D. Nesvorný, and V. Zappalà 1998. Origin of Earth-crossing asteroids: A quantitative simulation. *Science* **281**, 2022–2024.

Milani, A., and A. Nobili 1992. An example of stable chaos in the Solar System. *Nature* **357**, 569–571.

Morbidelli, A. 1996. The Kirkwood gap at the 2/1 commensurability with Jupiter: New numerical results. *Astron. J.* **111**, 2453–2461.

Morbidelli, A. 1997. Chaotic diffusion and the origin of comets from the 2/3 resonance in the Kuiper belt. *Icarus* **127**, 1–12.

Morbidelli, A. 1998. The structure of the Kuiper belt and the origin of Jupiter-family comets. In *Solar System Formation and Evolution* (D. Lazzaro, R. Vieira Martins, S. Ferraz-Mello, and C. Beaugé, Eds.), pp. 83–105. ASP Conference Series 149, San Francisco.

Morbidelli, A., and D. Nesvorný 1999. Numerous weak resonances drive asteroids toward terrestrial planets orbits. *Icarus* **139**, 295–308.

Morbidelli, A., F. Thomas, and M. Moons 1995. The resonant structure of the Kuiper belt and the dynamics of the first five trans-neptunian objects. *Icarus* **118**, 322–340.

Murray, N., and M. Holman 1997. Diffusive chaos in the outer asteroid belt. *Astron. J.* **114**, 1246–1259.

Murray, N., M. Holman, and M. Potter 1998. On the origin of chaos in the asteroid belt. *Astron. J.* **116**, 2583–2589.

Nesvorný, D., and S. Ferraz-Mello 1997. On the asteroidal population of the first-order jovian resonances. *Icarus* **130**, 247–258.

Nesvorný, D., and A. Morbidelli 1998. Three-body mean motion resonances and the chaotic structure of the asteroid belt. *Astron. J.* **116**, 3029–3037.

Nesvorný, D., and A. Morbidelli 1999. An analytic model of three-body mean motion resonances. *Celest. Mech. Dynam. Astron.* **71**, 243–271.

Nesvorný, D., and F. Roig 2000. Mean motion resonances in the trans-neptunian region. I. The 2 : 3 resonance with Neptune. *Icarus* **148**, 000–000.

Nesvorny, D., F. Roig, and S. Ferraz-Mello 2000. Close approaches of transneptunian objects to Pluto have left observable signatures on their orbital distribution. *Astron. J.* **119**, 953–969.

Nobili, A., A. Milani, and M. Carpino 1989. Fundamental frequencies and small divisors in the orbits of the outer planets. *Astron. Astrophys.* **210**, 313–336.

Petit, J. M., A. Morbidelli, and G. Valsecchi 1999. Large scattered planetesimals and the excitation of the small body belts. *Icarus* **141**, 367–387.

Quinlan, G., and S. Tremaine 1990. Symmetric multistep methods for the numerical integration of planetary orbits. *Astron. J.* **100**, 1694–1700.

Roig, F., A. Simula, S. Ferraz-Mello, and M. Tsuchida 1998. The high-eccentricity asymmetric expansion of the disturbing function for non-planar resonant problems. *Astron. Astrophys.* **329**, 339–349.

Šidlichovský, M., and D. Nesvorný 1999. A study of chaos in the asteroid belt. In *The Dynamics of Small Bodies in the Solar System: A Major Key to Solar System Studies* (B. Steves and A. E. Roy, Eds.), pp. 31–36. Kluwer, Dordrecht.

Tremaine, S. 1990. Dark matter in the Solar System. In *Baryonic Dark Matter* (D. Lynden-Bell and G. Gilmore, Eds.), pp. 37–65. Kluwer, Norwell, MA.

Valsecchi, G., and A. Manara 1997. Dynamics of comets in the outer planetary region II. Enhanced planetary masses and orbital evolutionary paths. *Astron. Astrophys.* **323**, 986–998.